Design and Development of an Elastin Mimetic Stent with Therapeutic Delivery Potential

A Dissertation

Presented to

The Academic Faculty

By

Adam W. Martinez

In Partial Fulfillment
Of the Requirements for the Degree
Doctor of Philosophy in Biomedical Engineering

Georgia Institute of Technology
December 2011

Design and Development of an Elastin Mimetic Stent with Therapeutic Delivery Potential

Approved by:

Elliot Chaikof, M.D.,Ph.D., Advisor
Dept. of Biomedical Engineering
Georgia Institute of Technology
Dept. of Surgery
Harvard Medical School

Mark Allen, Ph.D.
Dept. of Electrical and Computer Engineering
Georgia Institute of Technology

Rudy Gleason, Ph.D.
Dept. of Biomedical Engineering
Georgia Institute of Technology

David Harrison, M.D.
Dept. of Medicine
Vanderbilt University

Mark Prausnitz, Ph.D.
Dept. of Chemical & Biomolecular Engineering
Georgia Institute of Technology

Date Approved: October 21, 201

Acknowledgements

I have been blessed to have an abundance of colleagues, family, and friends that have assisted me on my path to complete a PhD in biomedical engineering. I would first and foremost like to thank my research advisor, Dr. Elliot Chaikof, for his support and guidance throughout my time as a graduate student in his lab. I would also like to thank Dr. Mark Allen for his support and guidance, especially over the last year. I am also appreciative of the insight and input my thesis committee, Dr. Mark Prausnitz, Dr. Rudy Gleason, and Dr. David Harrison, has given me over the years. I would also like to thank the members of the Chaikof and Allen groups for their advice, assistance, and camaraderie. I would especially like to thank Dr. Jeff Caves for being a sounding board and a great collaborator and Dr. John Wilson for being someone I could talk to all matters lab-related and not. I also want to thank Vivek, John Q, and Julie for being there to make the lab a better place. In addition to my labmates, I would especially like to thank my BME friends for the fond memories and being there when times were tough.

Obviously, this journey would not have been possible without the unconditional love and support of my family. In particular, I would like to thank Marly who has been a source of strength in this entire process and transitioned from a loving girlfriend to a dedicated wife. I would like to thank my mom for her reassuring phone calls and faith in my abilities, and my dad for being an inspiration of what is possible. I would also like to thank my brother who was always there when I needed him. Finally, I would like to thank all of my other family members for their assistance on this journey.

I would also like to acknowledge the National Science Foundation and TI:GER program for financial support received through graduate fellowships.

Table of Contents

List of Tables

List of Figures

Summary

Stenting remains a common treatment option for atherosclerotic arteries. A stent is a thin walled tube with fenestrations capable of being delivered to and expanded in a section of a vessel that has been narrowed or blocked with atherosclerotic plaque to open and maintain the patency of the vessel. The main drawback of early stent platforms was restenosis which has been combated by drug eluting stents (DESs). The current limitation facing these DESs is late stage thrombosis. The major research focuses in this field has been the development of the next generation of DESs and first generation bioabsorbable stents to combat current stenting limitations.

The main objective of this proposed research was the design and development of a new class of bioabsorbable stents composed of elastin mimetic protein polymers. The initial work focused on the ability to process these protein polymers into stents and ensure they possess the necessary mechanical strength to serve as stents. Once that endpoint was achieved optimization of both the stent design and fabrication process were explored. Preliminary investigations have demonstrated the ability of elastin mimetic materials to have the mechanical integrity to serve as a material for stent development. These materials have been fabricated into stents through the use of molding and laser ablation. The drug loading capacity of these elastin mimetics were explored to allow for the inhibition of restenosis. The ability of the elastin mimetics to recruit and promote the endothelialization of the stent lumen was also explored. Finally, the capacity of these elastin mimetics to overcome the current limitations of current stent platforms was explored in vivo.

Chapter 1:
Introduction

1.1 Motivation and Rationale

Stenting is a billion dollar industry that is still limited by restenosis and late stage thrombosis(LST). The development and acceptance of drug eluting stents(DESs) has allowed for dramatic reductions in restenosis. However, DESs have led to a rise in LST caused by a reduction and delay of endothelial coverage. We believe that our protein polymer technology will allow us to overcome the limitations of current stent platforms through the implementation of advanced bioabsorbable thromboresistant materials and sustained local delivery of therapeutics.

1.2 Central Hypothesis and Specific Aims

The central hypothesis encompassing this dissertation is that recombinant elastin mimetic proteins can be used to create stents that provide a scaffold for remodeling of the vascular wall after angioplasty while inhibiting restenosis and thrombosis formation by local delivery of anti-restenotic agents and facilitating accelerated endothelialization. The overall objectives of the work detailed in this dissertation were i) the fabrication of a vascular stent from an elastin mimetic protein polymer with targeted mechanical properties, conformability, and deformability, ii) devise general fabrication strategies for the fabrication of fenestrations in protein polymer films, iii) tailor the recombinant elastin mimetics to allow for delayed drug delivery and endothelialization, and iv) combine this knowledge to implant a stent in vivo.

1.3 Significance and Scientific Contribution

The clinical efficacy of endovascular therapy, including stent placement, remains limited by restenosis and thrombosis. The proposed research is significant because it represents a unique approach for improving stent performance with the establishment of a new paradigm in medical device development in which a device is constructed from a non-thrombogenic structural protein that contains therapeutic agents. In the development of this device, we have developed fabrication strategies that are being used by collaborators to fabricate constructs from biological tissue. We have also developed crosslinking techniques that can enhance protein polymer performance without reengineering the sequence.

1.4 Background

Vascular stenting is a common procedure used to treat atherosclerotic vessels.

Cardiovascular disease continues to be the leading cause of death in the US and the rest of the western world. In the US, cardiovascular disease accounts for one in three deaths. One of the most pressing areas in cardiovascular disease is the narrowing and occlusion of vessels with atherosclerotic plaque, which limits and ultimately prevents blood flow to the heart and other organs. Vessels with severe atherosclerotic plaque can be treated with an open procedure where the vessel with the plaque is replaced or a minimally invasive procedure where the vessel is opened from the inside. Over the past twenty years, vascular stenting has become the most common minimally invasive procedure for treating atherosclerotic plaque because of its capacity to reduce recovery times and decrease surgical expense. The procedure alleviates the blockage

in a vessel by cracking the plaque with an angioplasty balloon. Then an angioplasty balloon with a mounted stent is inserted and guided to the site of the previous blockage, and the stent and balloon are expanded to completely reopen the vessel. The balloon and catheter are removed leaving the stent behind to provide a scaffolding to keep the vessel patent as the vessel remodels. Stents have shown promise as a successful minimally invasive approach to treating atherosclerosis. However, the increased usage of stents has highlighted the serious shortcomings of the currently approved stent designs and platforms.

Stents are currently plagued by two major complications.

Stent restenosis and thrombosis are the major causes of stent failure today. Restenosis is the formation of new blockages at the site of angioplasty or stent placement, resulting from tissue growth at the site of treatment caused by an over proliferation of the smooth muscle cells (SMCs). Restenosis tends to occur during the first 3 to 6 months after the procedure, and the incidence rate has been decreased by the development of drug eluting stents (DESs). DESs seem to provide a solution to one of the problems that affected stents, but in so doing have created another, as they lead to an increased rate of thrombosis, especially LST. The risk of thrombosis is the greatest immediately after angioplasty because the resultant tissue trauma tends to trigger blood clotting; however, this type of thrombosis formation has been greatly reduced by using antiplatelet drugs during and after the procedure. However, LST is more complicated to treat as it can occur at unpredictable time points despite the use of antiplatelet therapy as illustrated in a 3 year follow up study [1]. Future stent designs

must minimize the risk of these complications through careful consideration of stent design and deployment.

Approved and Developing Stent Platforms

Extensive clinical trials have examined the viability of different stent designs, material choices, and coatings. In the field of stenting, there have been incremental improvements to stents. Bare Metal Stents (BMSs) were initially used in the treatment of atherosclerosis. The next improvement was the addition of a therapeutic in the form of DESs. The next frontier appears to be bioabsorbable stents which have the potential to revolutionize the stent field and are currently under development in both industrial and academic settings. Bioabsorbable stents have the potential to perform their function and then absorb into the vessel leaving behind no permanent foreign body. There are currently several bioabsorbable stents in the development stages for different companies. In addition to bioabsorbable stent platforms, significant research expenditures from both commercial and academic researchers are focusing on advanced coatings for approved platforms to decrease platelet formation and enhance drug delivery and endothelialization. Researchers are attempting to achieve these ends via extremely varied thin coatings on proven platforms, discussed in the following sections. The following three sections will discuss the emerging technology in the three specific areas: stent platform, drug release, and endothelialization.

Stent Platforms Currently Used and Under Investigation

The most important choice in stent design is the material selection. The material selection is critical because this decision dictates stent design and function. Most of today's stents are made from 316L stainless steel, nitinol, or cobalt chromium. These

metals have been carefully chosen over the years for their mechanical properties. In the mid 90's, there was an unsuccessful push for polymer stents. There were several reasons for the demise of this idea, such as, thrombogenicity and improper degradation kinetics. Today polymeric stent research has been revived because of new polymers and their versatility in manufacturing, drug delivery and degradation. Since we are mainly focused on the polymer side, the literature will focus on the progress in that field. However, I will discuss some of the leading principles behind the highly successful metallic stents.

The suitability of a new material must be considered on several fronts such as machinability, mechanical properties, and biocompatibility. Elastic materials can provide a challenge as they have a large amount of recoil. This is why some polymeric stents depend on elastic recoil or ratcheting mechanisms to keep them open. However, when designed properly the recoil can be eliminated, and elastic materials have the ability to return to their deployed form after a crushing injury which prevents permanent collapse.

Drug Eluting Stents (DES) and current work to address their shortcomings

DESs typically consist of a BMS, a therapeutic, and a polymeric drug delivery system. Drug eluting stents have shown great potential in preventing restenosis; however, they come with side effects discussed above. These side effects have been linked to both the drug and the coating aspects of DESs. This has led researchers to look at new coating options and explore different types of therapeutics.

To overcome the polymer coating issues, researchers have experimented with various families of biocompatible polymers as well as polymer free stents. These polymer free

stents have been able to circumvent the need for polymer delivery systems by incorporating drug releasing reservoirs into stents, fabricating porous surfaces, and applying novel coating strategies to existing stent platforms. An example of a stent that contains a microporous coating include the Corel-C™ stent that is fabricated from CoCr with a carbon nanoparticle coating (Relysis Medical, India) [2]. Microporous surfaces have also been incorporated into polymer based bioabsorbable stents [3]. As noted, sandblasting has been used to create pores between 1 to 100 μm on the surface of stainless steel stents, an example of which is the Yukon™ stent platform(Translumina, Hechingen, Germany) [4]. Adsorption of rapamycin along with other drugs has proven feasible and showed a dose-dependent efficacy in prevention of restenosis [5]. However, the rapamycin eluting Yukon™ stent was found to be clinically inferior to the Cypher™ stent, as well as a version of the Yukon™ stent coated in a drug containing bioabsorbable polymer [6]. At least two examples exist of nanoporous stent surfaces. The Jomed™ coating consists of a thin aluminum base layer, which is then subjected to an acidic solution that converts the aluminum into a thin ceramic nanoporous aluminum oxide[7]. A recent report suggests that particle debris may be released from the stent surface [8]. MIV Therapeutics, Inc. has developed a stent with a hydroxyapatite coating that is 0.30 to 1μm in thickness with a porosity of 40-60% in volume [9]. This stent has shown promising responses in both animal studies and in an initial clinical study after adsorption of sirolimus[10]. The therapeutics that DESs release has also been extensively researched. The majority of the early therapeutics used were antiproliferative drugs such as sirolimus and paclitaxel. Recently novel therapeutics have been introduced to target specific cells of interest.

Biopharmaceuticals have also seen great use in the academic arena as a more tunable system that could speed vascular wall remodelling. Peptides [11], DNA [12], and heparin [13], as well as anti-platelet agents, such as abciximab [14], growth factors and integrin binding sequences have been incorporated onto stents to reduce thrombosis or increase endothelial migration. An enzymatic release system for releasing RGD as the therapeutic from a stent surface was also researched. RGD was shown to be eluted in an enzyme concentration dependent manner by an exogenous enzyme given systemically. The researchers have identified other peptides that adsorb strongly to an array of stent materials which allows for beneficial uniform application and active delivery of a large range of peptides[15]. RGD-containing peptides have also been shown to be effective inhibitors of platelet aggregation and smooth muscle cell migration, by the prevention of certain ligand binding activities leading to a reduction in neointima formation[16].

Enhancing Endothelialization

The improvement of stent lumen endothelialization has been looked at on two main fronts: increasing endothelial cell migration and recruitment of circulating endothelial cells. To this end researchers have focused on the physical and chemical properties of a stent's surface and the integration of biopharmaceuticals on to stent surfaces.

Topologically rough surfaces have been created via microblasting and reactive ion etching leading to improved cell attachment [17]. Nanoscale surface features produced by polishing have influenced endothelial cell proliferation and protein

expression. Patterned Ti with grooves ranging from 750nm to 200μm have also shown enhanced endothelial coverage on nanometer scale patterns compared to micron scale patterns or random nanostructured surfaces[18]. Nanometer patterns can also be produced in a manner that leads to endothelial cell alignment that mimics native endothelium[19]. Of note, surfaces with a defined nanopatterned grid demonstrated a greater degree of endothelial cell adhesion, as compared to responses observed on random nanostructured surfaces[20]. Nanostructured surfaces, when compared to microstrutured surfaces, appear to afford greater adhesion of endothelial cells than smooth cells [21], lead to higher cell densities [22], and enhanced adhesion and spreading[23]. Interestingly, features between 100nm and 1μm have yielded greater cell adhesion densities than those less than 100nm[24]. The molecular mechanisms of these effects have not been well defined, but may be related, in part, to changes in protein adsorption profiles.

Surface modifications that alter surface chemistry can influence protein and cell adhesion leading to enhanced endothelial cell growth and proliferation[25, 26]. Recent examples include sputtering TiO2 onto 316L stainless steel [27] and binding tropoelastin to plasma treated metal surfaces, which enhanced cell attachment and proliferation [28]. Also cold plasma grafting of polypeptides that mimic mussel adhesive have imparted improved EC adhesion and accelerated growth, while maintaining favorable blood contacting properties[29].

In the biopharmaceutical space researchers have looked at enhancing enothelialization through the delivery and adsorption of both plasmids coding for vascular endothelial growth factor (VEGF) [30] and VEGF [31]. Cyclic Arg-Gly-Asp

(cRGD), as well as anti-CD34 and anti-kinase insert domain antibodies have been applied to increase the recruitment and retention of endothelial progenitor cells[11] and have shown initial success [32]; however, the latest research has shown some concerns[33].

Elastin mimetic protein polymers have been known to possess advantageous blood contacting properties, tailorable mechanical properties, and drug delivery potential which makes them an ideal stent material.

Genetic engineering has provided researchers a method to design and synthesize a wide variety of polypeptides. These polypeptides are able to have precisely controlled molecular architectures, amino acid sequence, and size that can be easily manipulated by altering the sequence and length of the encoding DNA. A common family of recombinant polypeptides is elastin analogs that are derived from the native elastin repeat found in human elastin. A large portion of our lab's focus has revolved around the design and development of several classes of elastin mimetic analogs. These have been built on the foundation of synthesizing elastin mimetic analogs with additional amino acid residues and/or certain cell recognition sequences. These large multiblock protein polymers offer a unique opportunity to systematically modify material microstructure to generate materials with a wide array of mechanical properties, drug delivery potential, and advanced surface properties. While these complex material compositions have been looked at in some detail for other applications, this is the first time they have been used in the development of a stand alone protein device. This foray into stent development is logically based on the scientific benchmarks that this material has cleared. These benchmarks include the

ability of these material to have mechanical properties that can be tailored to provide a wide range of elastic moduli, the ability to encapsulate drugs, advanced blood contacting properties, and the ability to enhance endothelialization.

Tailorable Mechanical Properties

The mechanical and biological properties of elastin mimetic proteins can be modulated by different processing solvents, protein concentrations, crosslinkers, and the addition and deletion of certain amino acid residues. While the basic processing conditions have been well documented, there is a lack of data on the processing techniques and fabrication modalities capable of being used. Therefore, all fabrication techniques used in the development of medical devices from elastin mimetics have the potential to unsuspectingly change the physical and biological attributes of these materials. The ability to tailor the mechanical properties and degree of swelling of elastin like protein gels and films has been shown with changes in protein concentration, crosslinker concentration, lysine content, and molecular weight[34-38]. Some of the crosslinking agents used were tris-succinimidyl aminotriacetate [34], glutaraldehyde [35], hexamethylene diisocyanate [36], bissulfosuccinimidyl suberate [37], and disuccinimidyl suberate [37]. On a more specific, note hexamethylene diisocyanate crosslinking provided a higher elastic moduli than glutaraldehyde [36], and a mechanical difference was noted when two different crosslinking strategies, a crosslinked solution and a solvent cast film setup, were used [37]. In our lab it has been shown that our elastin mimetic materials can have their properties tailored with judicious selection of both solvents and processing conditions as these control the meso- and nanoscale structure of the proteins [38].

Drug Release Potential

Drug release from elastin like materials and other protein coatings has been utilized in the stenting field, but more thoroughly in the tissue engineering space. Previously, gelatinous [39, 40] and collagenous [41, 42]materials have been used to create therapeutic eluting protein stent coatings. Of specific note was the ability to control sirolimus release via a topcoat of genipin crosslinked collagen [41]. Also of note is the development of a stent coating created from a thin collagenous tissue inoculated with EPCs that were able to migrate and proliferate forming a completely endothelialized lumen in vitro [42]. Elastin like proteins, similar to the ones used in this proposal, were capable encapsulating and delivering drugs in solution form [43] and in the form of micro- and nano-particles [44].

Valuable Blood Contacting Properties and Endothelialization Potential

Elastin is considered to have advantageous blood contacting properties due to the fact that elastin is a structural protein found in native vessels and induces minimal amounts of platelet adhesion and aggregation [45]. Researchers in our lab have also shown that a recombinant elastin mimetic protein polymer coated on 4mm grafts in an acute primate ex vivo shunt model induces minimal thrombogenicity [46]. Other researchers have also found that recombinant elastin polypeptides passively adsorbed onto synthetic surfaces can decrease platelet deposition and activation in vitro [47]. Additionally increases in the degree of crosslinking via genipin have shown the ability to increase the hemocompatibility of some proteins [41].

Elastin mimetics can be altered to allow for an enhanced rate of endothelialization capable of preventing LST and recapitulating the native lumen environment preventing further stenting complications. Incorporation of cell binding sequences and/or biopharmaceuticals have allowed for enhanced endothelialization through the recruitment and adhesion of endothelial cells. As alluded to earlier, the fact that elastin mimetic materials are made through recombinant means allows researchers to splice cell binding motifs into the native elastin repeat sequences. The addition of cell binding sequences allows for tailored cell responses based on the cell binding sequences chosen. Researchers constructed elastin like proteins with fibronectin CS5 domains [37, 48, 49] of note was the ability of HUVECs to adhere and remain on this modified elastin surface after being subjected to physiologically relevant stresses [49]. The addition of an RGD sequence to a specific protein has been shown to be superior in terms of binding endothelial cells more strongly and inducing faster cell spreading than a CS5 cell binding sequence[50]. Elastin like proteins with RGD present in the structure were capable of being coated on different materials with complex geometries via adsorption and imparted enhanced surface properties for cells to these materials [51]. Increasing the density of RGD domains in crosslinked films showed the ability to modulate cell adhesion and spreading [52]. The crosslinking of these films via lysine residues, which is required for the mechanical properties we need, can affect the cell binding sequences. Lysine residues were shown to have an affect on the efficacy of cell binding sequences when placed within or near the binding sequence; however, lysine residues on the end of the protein sequence do not affect the degree to which HUVECS were able to adhere and spread[53]. It has also been shown that altering a

cell binding sequences can prevent HUVEC spreading [54]. These studies show that the addition of RGD can provide a surface capable of enhanced endothelialization, but steps in the fabrication process could ultimately have a significant impact on HUVEC spreading and adhesion by altering the conformation of the protein or the binding site. While elastin can be tailored to increase endothelialization, it should be noted that elastin coatings have also been reported to inhibit smooth muscle cell migration without affecting endothelial cell migration[55].

Mechanical Thresholds

The mechanical properties of commercially available stents have been tested using several methods with the most widely accepted test being the collapse pressure test. This setup will allow us to determine the mechanical potential of new stent designs and material composition. While it would be beneficial to create a formula that could be predictive of the mechanical strength without having to make and test the stent, this is a near impossible goal given the ever changing mechanical properties of the elastin mimetic material. There are some groups that have created finite element analyses of stents, based on commercially available stents and assumptions on things such as vessel properties[56-58]. However, the challenge with our work is the material properties are not standard, which creates an enormous hurdle when devising an analysis. Therefore, we have chosen to ascertain the collapse pressure of our material in several designs and analyze the trends. The number one hurdle was ensuring our stent design has a sufficient collapse pressure. This leads to the question what is the minimum value of collapse pressure needed? Agrawal et al. came up with a minimum acceptable collapse pressure of 300mmHg. This was ascertained by assuming that the

average intraluminal pressures in an artery to be stented were on the order of 100 mmHg. If this is assumed and a stent is designed to withstand the difference between the transluminal and intraluminal pressures or pressures up to 175 mmHg, and a factor of safety is added then a calculated minimum acceptable collapse pressure for stents is 300 mmHg or 40 kPa [59].

Discussed below are some of the collapse pressure trends found in the literature. Although most of the data is on older stent designs and SS and nitnol stents, the trends are valuable for both the differences in stent design and material choice. PLLA stents with diameters ranging from 1.6 to 2.4 mm were fully expanded to 2.3–4.7 mm and were shown to have a collapse pressures ranging from 40-240 kPa, depending on the thickness and other design parameters [60]. The collapse pressure of PLLA stents has been shown to be in excess of 40kPa [61] and in the case of the Duke stent, 100 kPa. In another study on PLLA stents, researchers discovered that collapse pressures were molecular weight dependent, with a range of 180-250 kPa, and design dependent, helical stents have a collapse pressure 100kPa lower then their tubular counterparts, and the addition of drugs, especially at higher amounts, decreased the collapse pressure of the stents [62]. A look at 3mm SS stents showed a collapse pressures ranging from 65.86 - 71.94 kPa with a high outlier of 106.39 kPa; after these stents reached their collapse pressure they collapsed abruptly [63]. Other tests revealed that most nitinol stents with a diameter of 3.5mm had a collapse pressure ranging from 53-80kPa. It also showed that stents without struts in the longitudinal direction connecting radial segments had lower collapse pressures [64]. A study of peripheral stents, with a diameter of 8mm and a length of 37-40mm, showed self expanding stents had collapse

pressures around 20kPa and balloon expandable stents had collapse pressures around 90kpa [65].

A process needed to be determined to allow us to calculate the collapse pressure for future designs based on the experimental results of previous designs. There are some basic equations that allow us to elucidate the most important strength factors for stent viability before the fabrication process. In looking at the collapse pressure and the necessary radial forces there seem to be two main things that need to be focused on. The first is when does a stent fail which is different for balloon expandable and shape memory stents. When balloon expandable stents collapse they do not return to their previous shape where as shape memory stents return to their initial starting diameter. In the elastin mimetic stents shape recovery occurs so they can be considered with the shape memory stents. The other point necessary is when does ovalization begin because once this happens the extra force applied rapidly collapses the stents. The term ovalize is simply the process of an object losing round. Even in the commercially available stents this ovalization usually occurs because the forces while uniform never exert the necessary axi-symmetric forces needed to cause the stent to close its cells. Elastic ovalization was described by Timoshenko and Geere for thin walled shells which are similar to the stents we are researching. They derived an elastic ovalization pressure equation that can be found in support documents. Thin wall tubes, however, become harder to calculate if slots are placed in them. Also in commercially available stents the open area increases as the stent is expanded. However, in our testing the slotted area versus the material area is known based on the design used. This ovalization point is also critical during stent fabrication and deployment because the

degree to which the stent is out of round can have a large impact on its ability to support extra weight.

Determine Drug Delivery Thresholds, Release Profiles and Delivery Modes.

Currently there is not an optimal drug or release profile for DESs. This is a result of several confounding factors ranging from limited release of proprietary data, failures of current designs, variations in current release technology, and an ever evolving knowledge of drug kinetics in the vessel. In FDA disclosures stent companies have focused more on the safety of drug levels then the efficacy of different drug levels. Therefore, there are a multitude of variables that need to be studied to determine what drug, release profile, and mode of delivery should be selected. Given the release matrix will be elastin the things to focus on are the drug choice, existing release profile, alterations to release profile, and mode of release.

The choice of drug is important as researchers have shown differences in drug distribution between hydrophobic and hydrophilic drugs. In the vasculature, hydrophobic drugs get deposited more heavily in the intima and adventia [66]. Drug uptake is also influenced by the organizational and variable avidity of drug uptake in different arterial components [67]. Drugs such as rapamycin and paclitaxel are both hydrophobic but have different uptakes and interact differently within arterial structures. Therefore one must look at both the physical and chemical attributes of a drug to determine which to use in a given application [68]. Stent based drug delivery can be misleading as the local concentration is linked to biological effect, but the proximity of the stent does not ensure needed local concentrations because physiological transport forces cause local

concentrations to deviate significantly from mean concentrations [69]. This is reinforced by the fact that drug deposition in the vessel is dominated by flow mediated deposition of blood solubilized drug instead of abluminal coating contact with the vessel [70]. The two most common choices for DESs are rapamycin(sirolimus) and paclitaxel. Research has suggested that LST occurred more frequently with paclitaxel stents compared to sirolimus[1]. These two drugs differ significantly in terms of their effects on cells and ability to prevent restenosis [68, 71-75]. The needed dose and duration of the drug are also drug dependent. In order to prevent smooth muscle cell over proliferation the drug should be kept around the minimum effective concentration for one month.

The release rate is primarily controlled by the drug and the matrix the drug is encapsulated within and as such by changing the matrix material and drug combination the duration of delivery can be altered. An ideal release rate will allow for a drug concentration in the local tissue with a concentration necessary to overcome restenosis. The ability of drugs to diffuse through a polymer coating is also polymer and drug specific as different drugs can diffuse through a common matrix material at different rates. Using paclitaxel as a model, drug in vitro release was shown to be dependent on the initial weight percent of the drug [76] and using HPLC in vitro drug release exhibited a first-order release profile in which 36% and 55% of the drug was released after day 1 and day 7 respectively [77]. The sirolimus slow release Cypher stent was found to have no significant difference compared to BMS at time points of 90 and 180 days while there was a 50% reduction in neointimal area at 30 days [78].

The bridge between release profile and mode of release resides in the ability of stents to deliver drugs for the necessary duration without having the concentration too

high in the initial stages. Extended release profiles have been demonstrated from DESs; however, the architecture of DESs provide only a thin coating from which to deliver drugs, therefore sustained drug delivery is possible but it tends to be at concentrations that are not relevant. The total amount of drug a stent can hold is usually dependent on the coating thickness. However, since bioabsorbable stents are made from a potential drug carrier the only limit will be to maintain the structural integrity of the stents [79].

Several modes of delivery exist for DESs that are a results of drug choice, matrix construction, encapsulation technique, and matrix. The most common method of release in commercially available stents is diffusion. Besides diffusion, degradation can also allow for drug release or in some cases release can come from both diffusion and degradation [80]. Diffusion has been favored as the by products of coating degradation have led to negative inflammatory responses. The bioabsorbable stents that have been researched have shown the potential to have both diffusion controlled release and degradation controlled release as long as the degradation is slow enough to preserve the mechanical integrity of the stent for extended time periods. Models have been developed to predict PLA degradation and drug release [81]. Coating stents with different types of matrices has also been studied. One example is elution of rapamycin from the Cypher stent through a permanent polymer, a bioabsorbable polymer and polymer free coating. In this case the drug in the polymer free stent was completely gone after two weeks and it had inferior efficacy while the bioabsorbable platform was as effective as the permanent polymer [82]. Layers of drug and polymers and drug reservoirs also allow for flexible and controlled pharmacokinetics profiles [83].

Enhancement of Endothelialization

The end goal of any stent lumen is to passivate the luminal surface of a stent with a quiescent endothelium. This need has been exacerbated by the current DES platforms which have lead to an increase in LST as discussed above. DESs have delayed endothelialization because the therapeutics they release cause endothelial cell death along the entire length of the stent compared to standard BMSs that limited cell death to the area of strut placement. In the BMSs cells only had to migrate short distances to cover the struts in comparison to the DESs which require cells to migrate the entire length of the stent. Therefore, the speed and reliability of endothelialization must be increased. Enhancing the rate of endothelialization can be achieved through the capture of circulating endothelial cells or enhancement of endothelial cell migration. This mirrors healing in the native vessel which occurs through the proliferation of resident cells and circulating endothelial progenitor cells. The two major methods to accomplish this are to increase the speed of migration and proliferation of cells once they are on the surface of the stent and to recruit cells to stent surface which can be achieved through several modalities such as the incorporation of growth factors, biopharmaceuticals, advanced surface topography, and binding motifs. Paradoxically it should be noted that enhancing endothelialization can lead to side effects such as unwanted angiogenesis and intimal hyperplasia as well as plaque expansion.

CHAPTER 2

Stent Design and Development

2.1 Introduction

In the field of stent development, there are tradeoffs between material selection, stent design, and fabrication. The goal of this work was to develop a stent platform that utilized a novel recombinant elastin mimetic protein polymer as the stent material. To successfully develop a novel stent platform from protein based materials, several benchmarks had to be achieved. In this Chapter we will explore different designs and validate or invalidate the designs based on their ability to perform the necessary stenting functions.

The wide array of stent designs currently being researched has been driven by patent and marketing issues rather than actual scientific considerations in most instances[84]. Variations of the standard stent design have been used in academia because of the interplay of novel materials and a lack of fabrication modalities available to researchers in the academic setting coupled with the limited fabrication modalities that can be used on novel materials. This interplay of material selection and stent design has already been discussed in detail in Chapter 1.

To create a viable stent platform that can compete with current standards, there are a several benchmarks that must be achieved (Table 2.1). The benchmarks are necessary for a stent to be successfully delivered to the target vessel, perform its physical function, and not cause unfavorable biological responses. Stents must possess certain physical properties that allow them to perform their function. The first property is

a reliable expandability which minimizes size mismatches and prevents the stent from migrating down the vessel. A stent must also possess a threshold radial strength to maintain vessel patency. Stent coverage consists of two parts: firstly it is necessary to act as a scaffolding and prevent plaque prolapse, and secondly it must not block or prevent blood flow to collaterals. Finally, since the stent is placed in the lumen of the vessel, the thickness must be minimized to maintain an open lumen.

Table 2.1 Design Considerations

Design Parameters For Stents		
Biological	**Physical**	**Deliverable**
Biocompatible	High Radial Strength	Minimal Profile
Thromboresitant	Reliable Expandability	Trackable
Drug Delivery Potential	Circumferential Coverage	Radiopaque
Endothelialiazable	Minimal Thickness	Prevent Migration

Endovascular delivery requires the stent to be flexible enough to allow surgeons to track the stent through tortuous vessels, to possess a low radial profile allowing them to travel through plaque laden arteries, and cross the narrowed lesion site. The stent must also remain cinched on the balloon so it does not migrate off of the balloon. Finally, stents must possess radiopaque agents to allow for the proper visualization during plcament.

Elastin mimetic protein polymers are known for their favorable biological properties. The design and development of a stent platform based on this material required exploring the biocompatibility, thromboresitivity, drug delivery kinetics, and endothelialization potential. Previous reports have spoken to the biocompatibility[85, 86] and thromboresitivity[46, 47] of this material, and these advantageous properties were

the reason that the material was developed into a novel stent platform. The next set of biological properties that an ideal stent possesses is the ability to release drug to overcome restenosis and the promote endothelialization. These are crucial for overcoming the limitations of current stent platforms. The ability to create stents from a polymeric based material allows researchers to tailor the material to allow for not only drug delivery but also enhanced endothelialization. Enhanced endothelialization can be achieved through the incorporation of chemical or physical binding motifs.

2.2 Materials and Methods

Elastin Mimetic Materials

The design, development, expression, purification, and preliminary characterizations of the elastin mimetic materials used to develop these protein based stents have been described elsewhere[87]. Briefly, the elastin mimetic material is composed of a 58 kDa hydrophilic central midblock composed of 28 repeats of the elastic sequence $[(VPGAG)_2VPGEG(VPGAG)_2]$ flanked by 75kDa hydrophobic endblocks composed of 33 repeats of the pentapeptide sequence$[IPAVG]_5$. To allow for enhanced crosslinking the residues [KAAK] were located at the C terminus and between the midblock and endblock.

Design Development and Fabrication

Stent patterns were fabricated by a casting and laser ablation process detailed in Chapter 3. In brief, 100mg/ml lyophilized elastin mimetic material in 2,2,2-Trifluoroethanol was cast into PDMS molds, and webbing was removed via a excimer laser ablation process. The planar sheets were then wrapped around a teflon mandrel, and the overlapping edges were solvent welded. In the initial studies on radial

expansion and mechanical properties, all stents were crosslinked via vapor phase glutaraldehyde crosslinking. In the second round of mechanical studies, the stents were crosslinked with solution phase genipin.

Expansion Ratio

The reliability of the expansion process was determined by measuring the stent after fabrication, crimping, hydration, and balloon expansion. After 1 week, stent recoil was measured. Once the stent was fabricated, it was removed from the forming mandrel, and the diameter was measured at 0º, 45º, 90º, and 135º. The stent was then crimped down, and the diameter was measured as noted previously. The stent was then hydrated in 37ºC PBS and imaged at 1, 10, 30, and 60 minutes. The stent was then balloon inflated using a 1.5mm, 3.0mm or 6.00mm balloon. The balloon was then deflated and withdrawn from the lumen of the stent and the diameter was imaged. The stents were then left in PBS azide for 1 week, and the diameters were imaged again to determine recoil. All images were then analyzed using image J software to determine expansion ratio and percent of expansion related to hydration.

Collapse Pressure Testing

The collapse pressure system was based on a design detailed elsewhere[88]. In brief, a chamber was fabricated that allowed for the stent to be deployed in thin wall tubing that served as a mock vessel. Once deployed, the pressure surrounding the vessel was increased until the stented tubing collapses. The pressure is then released through a release valve, and the stent is tested two subsequent times.

Crimping the Stent

Several crimping methods were explored and were dependent on design of the stent that was crimped. The crimping strategies were examined to determine the reliability of their crimp, the creation of failure points, and the achievable crimping ratio.

The coiled stents were crimped down by placing them on a mandrel with the desired crimped diameter. The stents were crimped down in the hydrated state, secured in that position and dried. The dried stents were removed from the mandrel and placed on the balloon catheter. The interlocking stents were assembled with an outer diameter similar to those of the crimped stents.

In the crown and connector design, the stents were crimped down in a variety of ways to minimize the radial profile and stress on the stent. The techniques used included manual crimping, belt crimping, and folding. Manual crimping of the stent was achieved by placing the stent on the balloon catheter and wrapping the stent in a pieced of aluminum foil. The foil wrapped stent was then crimped down by hand. The belt crimping setup consisted of a mylar sheet that was placed through a thin slit in a round piece of acrylic(Figure 2.6B). The stent and balloon catheter were placed in the lumen of the mylar sheet and diameter of the sheet was decreased. The final method og crimping was to pleat and fold the stent. To place pleats in the stent, a variety of techniques were used including vacuum pleating, funnel pleating, and manual pleating. Vacuum pleating was achieved by placing the stent on a die as shown in Figure 2.6. The stent was placed over the die, and a thin sheath was applied over the stent and connected to a vacuum source. The stent was then vacuumed on the die. The second way was to push the stent through a funnel with fins that pleated the stent as it was

pushed through. The final method was to use surgical tweezers to pleat and crimp the stent. The repeatability of the system was determined by the uniformity of the process and the repeatability of the final crimped structure. The radial profile was then examined by a ccd image acquisition system. The pictures were then brought into ImageJ and the diameter was measured at 0°, 45°, 90°, and 135°.

2.3 Results and Discussion

The protein polymers have the potential to be tailored to possess all of the traits necessary for a successful stent(Table 2.1). The physical characteristics were vetted first by exploring the potential to design a stent with reliable expandability and sufficient mechanical properties. Once these parameters were achieved, potential crimping methods were investigated to achieve the necessary delivery parameters. Finally, the ability to enhance the stent's performance by the selective incorporation of different factors was explored.

Stent Design: There are several standard designs that are employed by commercial stent manufacturers and researchers alike. Several of which were reviewed in Chapter 1. All designs have advantages and disadvantages and must be evaluated based on the design criteria outlined in Table 2.1. The three major designs explored were the coil stent design, the interlocking design, and the standard crown and connector design. The coil stent design has relative ease of fabrication and proven utility in the academic space [89, 90]. The interlocking design works without the need for plastic deformation and has been successfully utilized by the REVA group and Advanced Vascular. The connector and crown design is the most common stent design and is used, in some configuration, for most commercial stent platforms.

Coil: The helical coil design has been used by several research groups to show proof of principle when using a new biomaterial for a stent platform. The helical coil consists of a strip of the material of interest wrapped around a mandrel and then set in place via some type of physical or chemical modification. This design offers the potential for easy modification as it is created from a planar sheet and therefore modifications can be carried out to improve both its biological and physical characteristics.

Interlocking: The slide and lock design was also studied because of its potential to be fabricated from planar sheets. As will be discussed further in Chapter 3, the ability to fabricate a stent from a planar sheet and crimp it down in a facile manner allows it to overcome many of the development hurdles. From a design standpoint, this stent offers the advantage of locking onto itself to prevent recoil. This slide and lock design has been seen in the REVA medical stent[91] as well as a ratcheting modification of this stent in the nitinol form.

Generic Design: The vast majority of commercial stents consist of a crown and connector design. We used a MicroCT to obtain the exact dimensions of a commercially available nitinol and SS stent platform. This technique allowed us to reverse engineer designs based on current nitinol and SS commercial stent platforms. This starting point allowed for the comparison of a stent fabricated from elastin mimetic material with the materials currently used in the industry. The two commercial stents examined were the Boston Scientific Express Stent, which is made of 316L SS and has a length of 27mm, and a diameter of 6mm, and the IntraTherapeutics Protégé Carotid Stent, which is made of Nitinol and has a length of 40mm and a diameter of 6 mm. Current metallic

stent platforms have been revised over the years to obtain these designs. Since, these designs have been conceptualized for well known benchmarked materials, it would be a flawed approach to simply base the elastic mimetic design on these designs and expect them to perform competitively. The material properties of the elastin mimetic materials are so different that radically different designs needed to be considered. To increase the strength of stents fabricated from our material, we explored changes to the industrial stent platforms. The design we used maintained several crowns connected together and also incorporated several changes such as strut width and overall geometry.

Modification of Generic Design: In commercial stents, the width of the struts is usually a 1 to 1 ratio with the thickness of the stent. However, we did not want to increase the thickness of the stents so the only parameter changed was the strut width. The number of rows was decreased to keep the length of the stent standard as the circumferential strut width was increased. As mentioned earlier, the longitudinal strut widths were kept the same to maintain the pattern of the stent. This change created a stent design that was able to perform at an acceptable level as shown in the mechanical testing section.

Early in the mechanical testing process, solid thin walled samples performed very well in the collapse pressure tests. Therefore, it was hypothesized that if we would incorporate solid rings into the stents, we could overcome the limitations of solid stents and still achieve better mechanical properties. We attempted to leverage the strength of the thin walled tubes by incorporating ring segments into the stent. Since our material is fairly compliant, a design that incorporates rings should still allow for crimping and

expansion of the stent. To attain the necessary trackability, the width of the rings was kept small and connected by a stent matrix of connectors and struts.

The other modification that was explored was decreasing the cell size and increasing the cell number of the stent. Table 2.2 shows the critical design dimensions of these stent systems. A decrease in cell size was thought to allow for stiffer stents because the fenestrations in the stent are smaller. In order to do that, the stent cell had to be scaled down according to diameter to get proper stent coverage. Due to the geometry of the stent a 200μm width would not work so the top of the top of cell was blunted as shown in Figure 2.3 to allow for a connector width in line with the earlier models. This shortens the top and the bottom of the cell by 165μm and decreases the total height of the cell by 330μm. This change allowed for a connector width of 533μm and an increase in connector length from 342.5μm to 1.178mm.

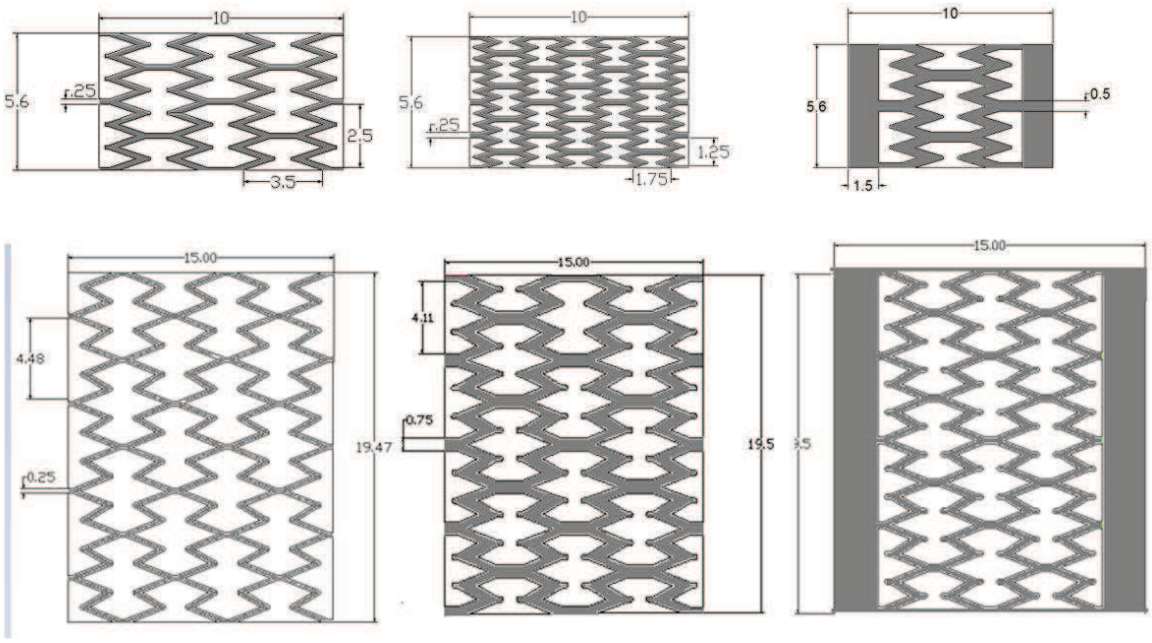

Figure 2.1. 1.5 mm and 6 mm stent designs (all dimensions are in mm)

Diameters: Stents are currently deployed in vessels with a wide range of diameters and, as such, a range of stent diameters exist in the market. Different stent designs and materials are best utilized at different diameters, and therefore, we sought to ensure that our methods could be used to fabricate a wide range of stent diameters. The initial diameter developed was the 6mm stent for two reasons. Firstly, these are common sizes for elastic stents placed in peripheral vessels that can be subjected to crushing blows, thereby allowing them to recover their shape and not be deformed requiring corrective surgery. Secondly, the 6mm stents were easier to fabricate, manipulate, and test in all of the outlined endpoints. The fabrication methods that were used had the potential to create stents with different diameters. In order to change the diameter on the crown and connector design, the cell had to be scaled down according to the final desired diameter to get proper stent coverage as is commonly done with commercial stents. Alterations to the cell size also caused changes to the connector width so they were modified as shown in Figure 2.3.

Thickness is not a variable that was greatly altered as the ideal stents should always minimize the thickness of stents and the final design will use the thinnest stent that still yields acceptable collapse pressure values. That is why the stent with solid rings appeared to be the best option because it allows for a minimal thickness and still has mechanical properties in excess of what is needed. In the original testing with the 6mm stents, a thickness of 200µm was utilized and in the later studies that focused on the 1.5mm stent a thickness of 100µm was utilized.

Table 2.2 Stent parameters

Stent Design	Surface Area (mm^2)	Cell Area (mm^2)	Crown Width (mm)	Connector Width (μm)	Connector Length (mm)	Cell Number	Ring Area (mm^2)	Stent Diameter
A	67.972	10.33	1.00	250.00	0.25	16	NA	6.00
B	102.9324	10.87	2.00	500.00	0.88	12	NA	6.00
C	126.612	10.98	3.00	750.00	1.52	12	NA	6.00
D	175.676	10.87	2.00	500.00	0.88	8	21.14	6.00
E	25.73	5.65	2.00	250.00	1.16	8	NA	1.50
F	38.09	5.26	2.50	500.00	1.92	6	NA	1.50
G	54.40	3.90	3.50	1000.00	3.48	4	NA	1.50
H	38.11	1.32	1.33	250.00	0.96	28	NA	1.50
I	37.33	5.26	2.50	500.00	1.92	6	9.04	1.50

Reliable Stent Deployment

Reliable stent deployment consists of consistent expansion with minimum recoil to ensure the stent will keep the lumen of the vessel patent. The ability to expand with a known diameter is important, allowing the clinician to select the proper stent for a given vessel. The rate of expansion must be sufficient to allow the stent to be deployed without migrating in the vessel or blocking the vessel blocked for too long during the procedure. Finally the stent must remain in the final deployed state and not recoil significantly which has been a limitation of bioabsorbable stent platforms[92].

Rapid and reliable expansion is usually achieved through the use of a balloon catheter or the utilization of a stent's shape memory properties. Balloon-expandable stents are made from materials that can be plastically deformed through the inflation of a balloon. After the balloon is deflated, the stent remains in its expanded conformation, except for a slight recoil caused by the elastic portion of the deformation. The ideal material for these stents therefore has a low yield stress, making it deformable at manageable balloon pressures, and a high elastic modulus for minimal recoil. Stainless

steel is the most common form of balloon expandable stent. The other major expansion type is shape memory, or self expandable, stents. These stents are made from material that can exist in two phases: the pre-expanded and post-expanded. Self-expanding stents are manufactured in the expanded form, crimped down on a delivery system, and constrained by a sheath. Upon removal of the sheath, the stent expands to its original diameter. Shape memory is usually considered a material property of the chemical structure and is mostly known to be temperature dependent.

Initial studies on stents fabricated from the elastin mimetic material showed that the stent could elastically recover most of its shape after it was crimped down, as long as it remained hydrated. In brief, a stent crimped and constrained in the hydrated state will regain its pre-crimped diameter when unconstrained. If the stent is crimped, constrained, and dried, then the stent does not regain its shape when unconstrained. However, upon rehydration, the stent reverts back to its pre-crimped diameter. It should be noted this is not simply an effect of the material hydrating and swelling, as stents that were fabricated at a smaller diameter and not crimped but subjected to the same crimping drying process did not expand upon hydration. In this system, the stent can be crimped down to a minimal diameter, confined and dried down, and upon hydration, the stent expands to 70% of its fabricated diameter.

A literature review discovered that other research groups have explored the potential of shape memory effect based on the hydration of a material. Chen et al. showed the potential to create a stent from a modified chitosan-based material that, upon exposure to water, the stent expanded in minutes[93]. Also in the area of

hydration strain recovery, Jung et al. demonstrated water-induced shape recovery in polyurethanes containing a strongly hydrophobic moiety in the hard segment[94].

There are some stents that use both expansion mechanisms. These are usually materials that can self-expand but the rate of that self expansion is not fast enough to deploy the stent on the minute time scale. In these cases, a balloon is used to expand the stent which allows for the fast deployment of balloon expandable stents with the added feature of outward expansion, coming from the self expansion of the stent, in the vessel that prevents recoil that has plagued polymeric stents. Since, the elastin mimetic stent possessed some shape memory, but the recovery rate and time are not sufficient for stenting, we employed a combination of balloon deployment and self expansion.

The first critical design variable that was explored was whether to fabricate the stent in the expanded diameter and crimp down or fabricate the stent with a nominal diameter and expand to the necessary dimensions. In previous reports, recoil of polymeric stents was a limitation in elastic stent design. Based on the elastic properties of the elastin mimetics compared to metallic stents, we hypothesized that the stent would have to be fabricated in the expanded diameter as the material has mostly elastic properties and trying to expand it would lead to severe recoil. Table 2.3 shows the results of our expansion test.

Table 2.3 Stent Expansion Studies

Stent Type	Design Number	Fabricated Diameter	Crimped Diameter	Hydrated Diameter	Expanded Diameter	After 48 Hours
Coil	C2	5.75 ± 0.32	2.09 ± 0.03	3.97 ± 0.52	6.12 ± 0.21	6.09 ± 0.26
Coil	C2	2.08 ± 0.27	2.10 ± 0.07	2.09 ± 0.45	6.08 ± 0.17	3.3 ± 0.45
Coil	C4	5.69 ± 0.34	2.13 ± 0.04	3.89 ± 0.45	6.09 ± 0.25	6.07 ± 0.22
Ratchet	R	2.17 ± 0.17	2.21 ± 0.27	2.31 ± 0.29	6.13 ± 0.19	4.14 ± 0.89
Ratchet	R	5.77 ± 0.25	2.17 ± 0.21	3.61 ± 0.39	6.08 ± 0.21	5.55 ± 0.45
Slide Like	SL	2.08 ± 0.12	2.17 ± 0.21	2.22 ± 0.37	6.08 ± 0.17	4.75 ± 0.45
Generic	A	5.82 ± 0.18	2.25 ± 0.45	3.49 ± 0.51	6.11 ± 0.18	6.03 ± 0.29
Generic	B	5.71 ± 0.15	2.36 ± 0.06	3.54 ± 0.59	6.17 ± 0.21	6.05 ± 0.31
Generic	C	5.69 ± 0.21	2.47 ± 0.06	3.62 ± 0.48	6.27 ± 0.17	5.97 ± 0.22
Generic	D	5.75 ± 0.19	2.51 ± 0.08	3.64 ± 0.49	6.09 ± 0.18	5.98 ± 0.39
Generic	A	2.79 ± 0.17	1.32 ± 0.17	1.98 ± 0.32	3.18 ± 0.12	3.02 ± 0.16
Generic	D	2.82 ± 0.14	1.39 ± 0.09	2.09 ± 0.36	3.09 ± 0.15	3.05 ± 0.19
Generic	A	2.87 ± 0.13	1.38 ± 0.16	1.98 ± 0.39	Stent Failed	Stent Failed
Generic	D	2.86 ± 0.15	1.31 ± 0.14	2.07 ± 0.42	Stent Failed	Stent Failed
Generic	Final	1.50 ± 0.11	0.89 ± 0.09	1.14 ± 0.36	1.61 ± 0.10	1.59 ± 0.11
Generic	Final	0.75 ± 0.09	0.75 ± 0.09	0.75 ± 0.14	Stent Failed	Stent Failed

To explore the potential of expanding the stent from a nominal diameter, a coil, ratchet, slide and lock, and three generic stent design were fabricated with a nominal diameter and expanded. The C2B helical stent was fabricated at a diameter of 2mm and was expanded to a diameter of 6mm. It is clear that the hydration of the stent does not expand the diameter of stent fabricated with a nominal diameter. This design also has mostly elastic deformation, as the recoil is approximately 45%. The ratchet design did not appreciably increase in diameter after hydration and, after balloon expansion, showed significant recoil at 30%. The slide and lock design allows the stent to be expanded, in theory without plastic deformation and revolves around the ability to expand the stent with ratcheting teeth lock each progressive position. The problem with this approach was that we could not get reliable expandability. The major limiting factor

seemed to be the failure of the ratcheting mechanism causing the gears to get stuck, which resulted in the stent tearing or stretching as the balloon was inflated, which in turn caused large amounts of recoil when the balloon was deflated. Generic designs A, D, and Final were fabricated at the nominal diameter and expanded. Table 2.3 shows that, like most polymeric stents, the stents were not able to expand from the minimal profiles. Balloon expansion of nominal diameter generic stents resulted in tearing and failure of the stent. These results demonstrate that this approach was not feasible, and stents should be fabricated in the larger diameter.

Stents fabricated in the expanded form and crimped down showed reliable expansion and minimal recoil. The coil stent was easily crimped down to a diameter of 2.09mm. Upon hydration, the stent's diameter increased by 86%, and upon balloon expansion, the stent was expanded to a final diameter of 6mm with minimal recoil after 48 hours. The ratchet stent design had similar hydration and balloon expansion as the coil stent. However, the failure of the stent to properly lock on itself caused it to have a recall of 8.3%. In the four generic designs fabricated at the 6mm diameter, all experienced no statistical difference at the different parameters of stent expansion. The stents were crimped from an average diameter of 5.75mm to a diameter of 2.45mm. Upon hydration, these stents averaged an increase of 50% over the crimped diameter. All stents were then balloon expanded to a diameter of 6.16mm and had an average recoil of 2.5%. The final stent design was fabricated with a diameter of 1.5mm and crimped down to a nominal diameter of 0.89mm. Upon hydration, the stent increased to a diameter of 1.14mm and then was balloon expanded to a diameter of 1.61mm. The recoil was also minimal at 1.3%.

The final measure of reliable expansion is the openness of the lumen. As mentioned above, the ability to minimize the thickness of the stent is paramount in ensuring lumen has the proper inner diameter. In the case of the helical coil, the material properties did not allow these stents to maintain their rigidity upon expansion, which caused some of the rings to overlap and not fully expand. This problem affected the thickness as the stent rings were overlapped increasing the stent thickness by a factor of 2 or more, leading to a narrowing of the vessel. The slide and lock design had a thicker profile based on its design, as it had some portions that overlapped. This is a problem as the blood could flow between the stents and ultimately cause part of the stent to prolapse into the vessel.

Radial Strength/Mechanical Properties

Once a stent is expanded in a vessel, it is subjected to an external pressure from the arterial wall. In order to keep the vessel expanded, the stent must be capable of withstanding these pressures. To determine this pressure, a collapse pressure setup has been postulated as the most representative way to quantify this pressure. Some groups have simply put the stent between two flat platens in a compression testing setup; however, in our opinion and several other researchers [59, 62-64, 95-100], this method is inferior to a collapse pressure setup. The required value of collapse pressure depends greatly on the vessel type and condition in which it is placed. Any stent design and material composition needs to attain a sufficient collapse pressure to prevent the collapse of the stent immediately after implantation and assure long term stability. Numerous researchers in the field of novel stent development have referenced the report by Agrawal et al., postulating the minimum collapse value that still provided a

safety factor was 300mmHg (39.98kPa)[59]. It should be noted that it is imperative that a stent has sufficient radial stiffness to allow for an open lumen; however, it is preferable for it to be adequate rather than have a high radial stiffness which induces unnecessary chronic trauma to the artery wall leading to an enhanced unfavorable biological response[101]. Therefore, we sought to achieve an acceptable collapse pressure with regard to the Agrawal et al. values but not a collapse pressure far in excess of that value.

To determine if the protein based stent possessed the needed mechanical properties, a collapse pressure setup was constructed based on the design of Stack et al.[88]. The collapse pressure system, detailed elsewhere[88], consists of a chamber with four ports. A tube, consisting of two rigid tubes connected in the middle by thin flexible tubing, is placed through the two ports on either side. The lid of the chamber contains two ports which allows for injection of water into the closed system and monitoring the pressure inside the system. The stent is then delivered into the tubing, allowed to hydrate for 5 minutes in 37℃ PBS, and t hen expanded to its full diameter. The system then has 37℃ PBS circulated through for 5 minutes. The flow is then turned off, and the tubing is left open to the atmosphere so that the tubing is not pressurized.

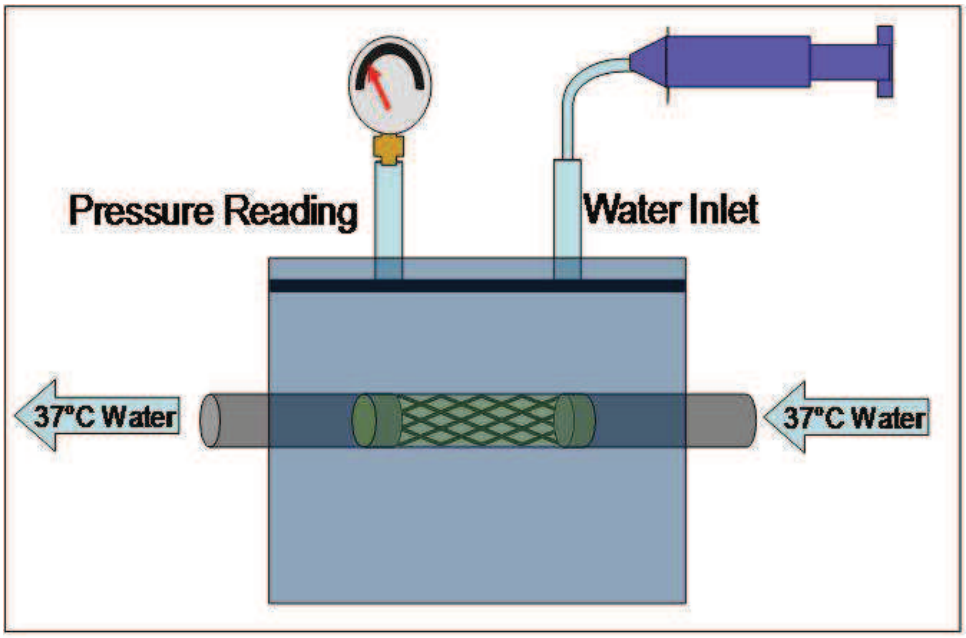

Figure 2.2 Collapse Pressure Setup

The pressure in the chamber is then increased by pushing water into the closed system at 1mL/sec. Once the first sign of stent collapse is evident, the syringe pump is stopped and the pressure is allowed to go to zero by opening the relief valve. This allows the stent to recover its initial shape before it is collapsed again. This is performed three times is to get an average collapse pressure for the stent and to ensure the stent can be collapsed and not fail. In all of the collapse pressure experiments on the elastin mimetic stent designs a minimal value of n=3 has been used. Therefore for each stent design, we have at minimum nine values of collapse pressure.

In the early stages of testing, solid thin walled tubes were used that were fabricated from dip coating. The thin walled tubes of elastin mimetic showed collapse pressures that were several times the needed collapse pressure proving the elastin mimetic materials, in their simplest form, had the necessary mechanical integrity(Figure 2.4A). In these initial studies, two varieties of elastin mimetic materials were studied and

demonstrated that LysB10 has more favorable collapse strength than B9. These results were in agreement with the previous mechanical properties that were ascertained for this material([87, 102]). In addition to the noncrosslinked varieties, we also explored the effect that vapor phase and solution phase glutaraldehyde crosslinking had on the collapse pressure of the LysB10 constructs. The vapor phase crosslinking was capable of increasing the collapse pressure almost six fold, while the solution phase increased the collapse pressure three fold. This illustrates the pronounced effect of crosslinking and the differences between different crosslinking strategies.

It should be reiterated that these initial studies looked at thin walled tubes and not fenestrated stents. In the literature there is mechanical data from other fields that highlights the differences in collapse pressure of thin walled tubes and slotted thin walled tubes. When the fenestrations are placed in the stent, the collapse pressure decreased substantially. With these studies as a building block, vapor phase glutaraldehyde crosslinked Lysb10 was chosen as the material for the next set of experiments.

Initially we were going to explore variations of the designs discussed in earlier sections; however, failures in deployment and a lack of reliable expansion prevented the stents from being tested properly in the collapse pressure setup. Therefore, the stent design that will be focused on for the collapse pressure tests is the generic crown and connector design. Table 2.2 outlines the design paramteres that were used in the first round of testing. The first variable that we examined was strut width. In all of these experiments the thickness was maintained at 200μm, the length was maintained at 15mm, and all materials were LysB10 crosslinked with vapor phase glutaraldehyde.

We hypothesized correctly that an increase in strut width would increase the collapse pressure of the stent(Figure 2.4B). The struts widths ranged from 250μm to 750μm. The stent with 250μm struts had a collapse pressure of 6.93±0.46 kPA. This is obviously well below the 39.98kPa that is required. When the strut's width was increased to 500μm, the collapse pressure increased to 19.43±0.90 which is a 2.8 fold increase in collapse pressure but still below the targeted collapse pressure. When the strut width was increase to 750μm the collapse pressure increased to 24.57±1.13, which was a increase of 3.5 fold over the 250μm strut.

The high collapse pressure of the solid ring structures gave the design cue of incorporating solid rings into these structures. The generic stent design with 500μm struts had rings placed on the proximal and distal ends. These solid segments increased the collapse pressure for the stents to 110.59±4.91 kPa and impart a 16 fold increase over a stent of the same design without rings(Figure 2.4C). This design was the only design that allowed us to get over the 39.98 kPa threshold that was determined to be the minimum collapse pressure of a stent. In fact, the stent with rings has a collapse pressure 2.7 fold above the threshold value.

The finally design cue examined in the first round of testing was the ability fabricate stents with different diameters and the effect this change has in collapse pressure(Figure 2.4D). A decrease from 6mm to 3mm in diameter, when all other things were kept the same, resulted in an increase in the collapse pressure value of the 3mm stent to 20.75±1.41kPA a 3 fold increase. This could prove advantageous as we could create thinner stents in the smaller diameter stents.

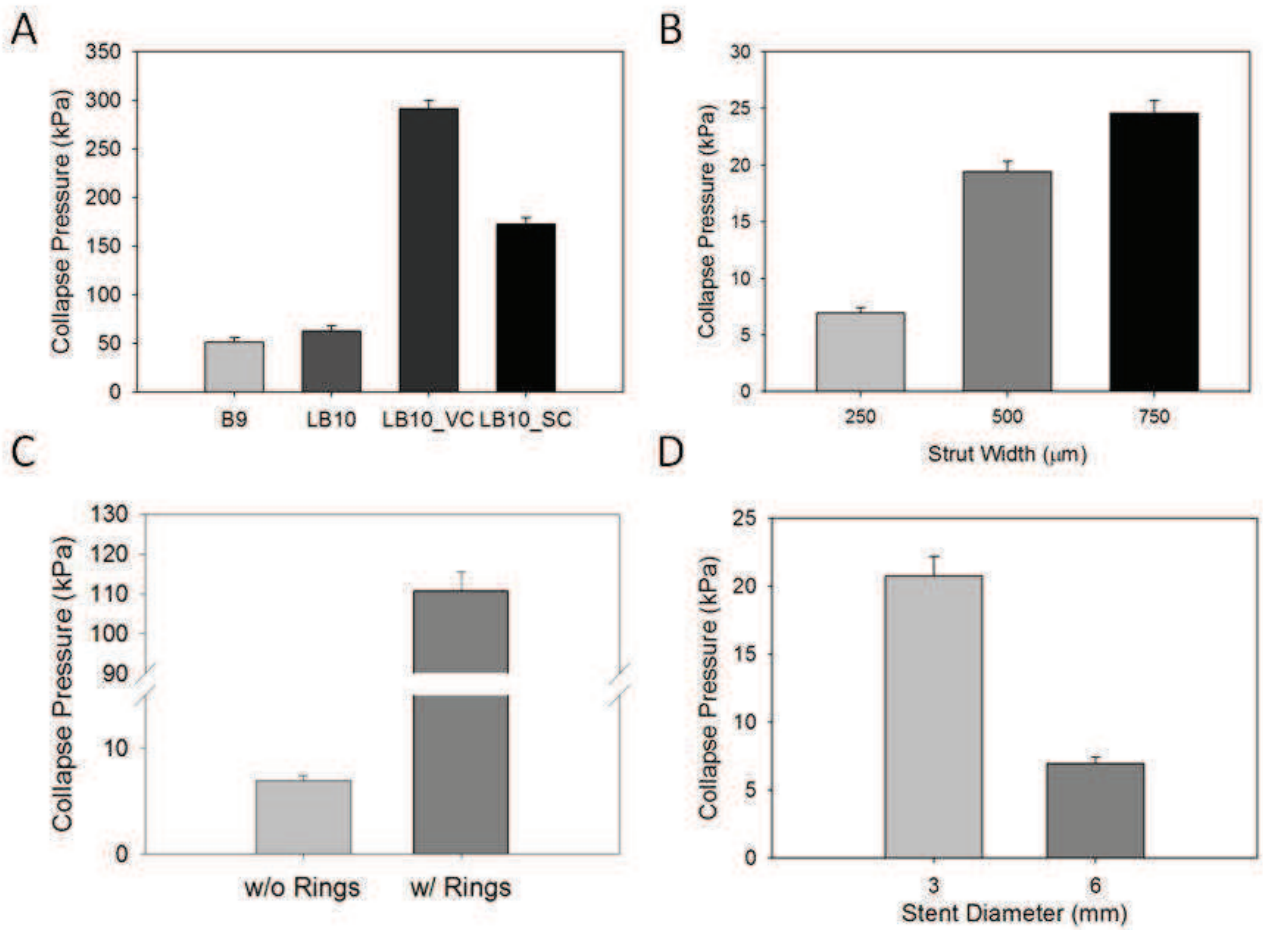

Figure 2.3 6mm Stent Designs with a 200μm thickness (A) Different elastin mimetic materials and crosslinking strategies (B) Changing the strut widths (C) Stents with and without rings (D) Altering the diameter but keeping the same design and thickness 200μm

The next round of mechanical testing highlighted in Figure 2.4 was performed on a 1.5mm stents crosslinked with genipin. As discussed in the in vivo portion of this thesis, the rat aorta was a model of interest and ultimately the animal model that we chose. Since, their vessels are small, we wanted to prove that we could fabricate a 1.5mm stent capable of having an acceptable collapse pressure. As with the previous results on the 6mm stent platform, the stent designs had a significant effect on the collapse pressures (Figure 2.4). In these tests we explored four main changes to the

1.5mm stent design; increasing the strut width from 250μm to 1000μm, decreasing cell area, incorporating rings, and changing the diameter.

The collapse pressure increased with increasing stent widths. The 500μm strut width had 2.84 times the collapse pressure of the 250μm wide strut design and 0.48 times the collapse pressure of the 1000μm wide strut design.

The second variable that was explored was a change was a reduction in cell size. The modification of cell size also significantly affected the collapse pressure. A cell size reduction of 50% increases the collapse pressure by 3.19 times.

As with the larger stent rings were incorporated into the design, however, as noted in Table 2.3, it is evident that the number of rings used was different, as well as the width of the rings. To achieve significantly higher collapse pressure while minimizing surface area of the stent, rings were incorporated into the stent structure. The rings imparted 3.05-fold increase in collapse pressure. The structure with rings had significantly higher collapse pressure than any other design. The other variable that was explored was the affect of the diameter on stent development. Figure 3 panel D shows that maintaining all design aspects and increasing the diameter of the stent causes a decrease in collapse pressure. Compared to the 1.5mm stent, increasing the stent diameter to 3mm decreases the collapse pressure by 1.70 times, and increasing the stent to 6mm decreases it 3.48 times. This shows the need to alter design specifications to get a necessary collapse pressure.

The purpose of this research was to explore and validate the 1.5 mm stent design. However, in the previous experiments, we demonstrated that a decrease in diameter would yield a stent with higher collapse pressure. In this instance we

increased the size of the stent to look at the effect of collapse and noted a similar trend. For, the purposes of this report we did not optimize a design for the larger diameter stents.

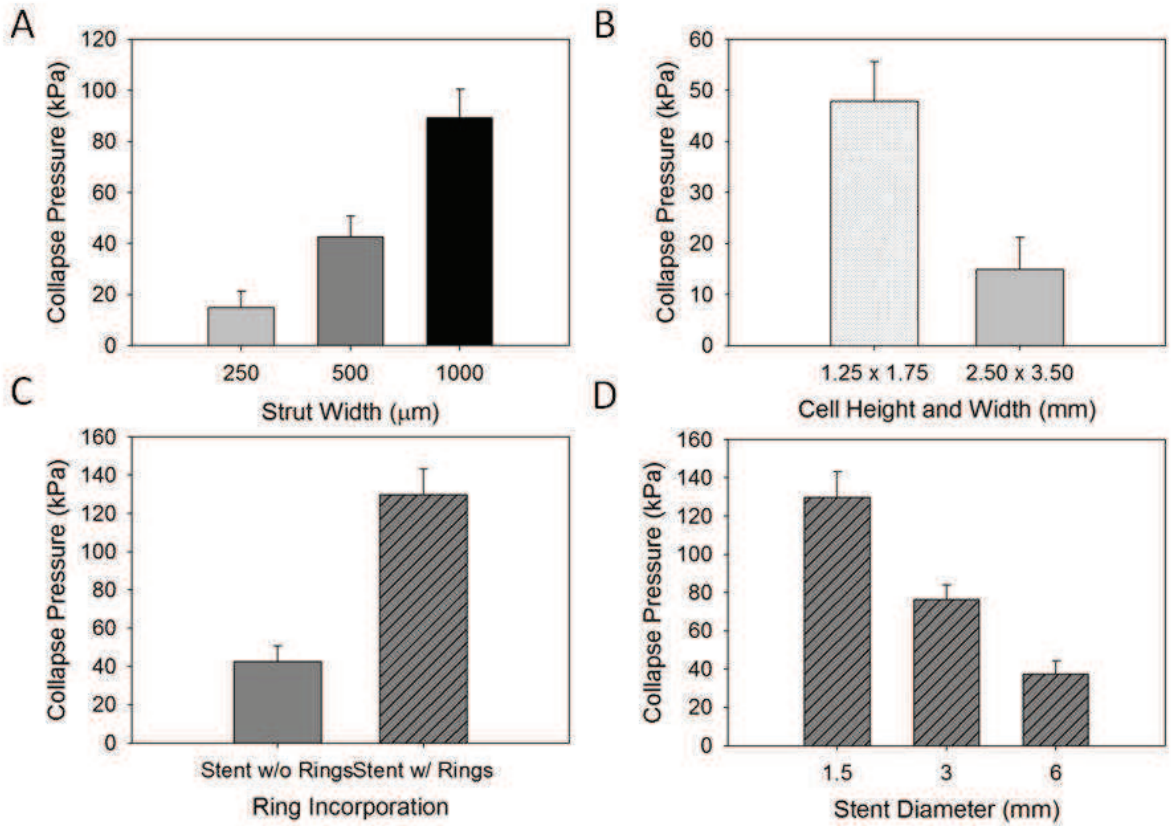

Figure 2.4. (A) Collapse pressure for stent with different widths, (B) collapse pressure for stent designs that have different cell sizes, (C) collapse pressure for stent designs without and with rings, and collapse pressure of stent design with ring fabricated into stents with different diameters.

Deliverability-Crimping

In order for a stent to perform its needed functions, it must be capable of being delivered and deployed at the site of vessel narrowing. Radial profile is one of the most important parameters of stent delivery because stents must travel through tortuous vessels that are often partially occluded. To achieve a minimal radial profile, a process was developed to crimp down the stent. Several crimping strategies were explored to allow for stents fabricated in the expanded form to be crimped down to an acceptable radial profile. To determine the efficacy of each method, the endpoints that were examined were repeatability, creation of failure points, and radial profile. The repeatability was determined by examining the crimped profile and determining whether the stent is being crimped in a repeatable pattern or if the stent undergoes random crimping. The next endpoint that was examined qualitatively was the amount of stress that the stent is subjected to during the crimping procedure. The goal was to minimize the stress with controlled crimping and eliminating areas of high stress, such as, tight corners and out of plane bending. As suspected, this qualitative value correlated to the creation of failure points very well. Finally, the radial profile was determined by measuring the stent at 0º, 45º, 90º, 135º, and 180º. The widest point of the stent was taken to be the minimum profile.

Crimping Setups

Several crimping strategies were explored ranging from those used in the stenting industry to those that have been explored by other researchers. Most of the current stent crimping methods exploit the stent's repeating cell pattern and minimize the size of the stent's open cells, as shown in Figure 2.6.A, to achieve their ultimate

goal of a decreased radial profile. In most cases, the crimping system applies a force to the stent equally in the circumferential direction which allows the stent's cells to close, decreasing the outer diameter of the stent. The current gold standard in commercial stenting shown in Figure 2.6 A is not applicable to crimp current elastin mimetic stent designs because the geometries of the new stent designs prevent hinging at the joints. Most commercially available stents have a width to thickness ratio of one, whereas our new designs have a much higher ratio and therefore, successful crimping strategies must crimp the stent without making the cells smaller.

The first technique used was manual crimping. This technique has it roots in the early adoption of stenting as a way for physicians to secure a stent to a balloon and allow for a small radial profile. The elastic component of the stent material provided a challenge to manually crimp the stent. To prevent the stents from returning to their original diameter, they were wrapped with aluminum foil. This allows for the system to be a malleable process, similar to the way stainless steel stents can be crimped down. However, the process resulted in subpar radial profiles, lacked repeatability, and created failure points in the stent. Also the stent was not secure on the balloon, and therefore the stent would migrate off the balloon as they traveled to the site of expansion.

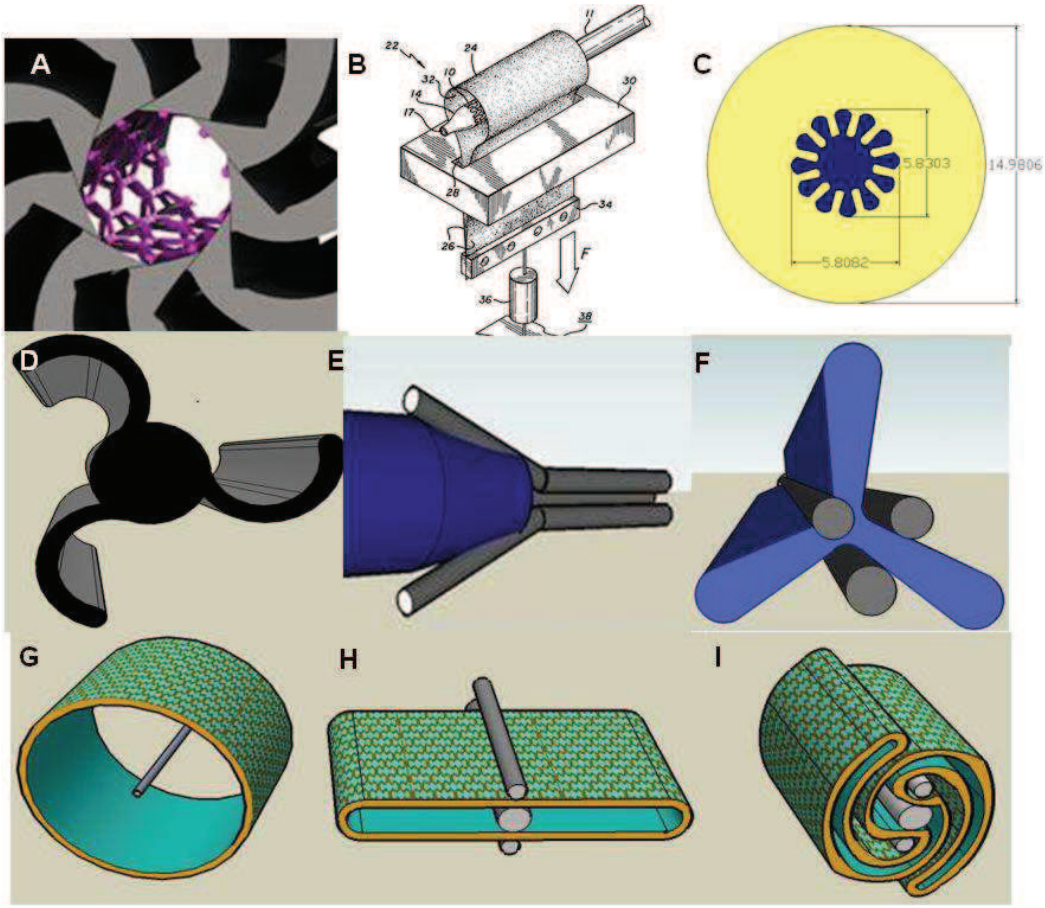

Figure 2.5 (A) Commercial Crimping Strategies, (B) Mylar sheet crimping strategy, (C) advantage of pleating the balloon with regard to radial profile (D) die for pleating balloon and stent, (E) Funnel pleating device to pleat the balloon, (F) Pleated Balloon, (G) stent on balloon before pleating (H) folded Stent (I) wrapped stent

The second method consisted of a sliding Mylar belt that went around an uncrimped stent and balloon catheter assembly and through a thin slot in a rigid acrylic block. A downward force was placed on the Mylar sheet which decreased the diameter of the Mylar belt, thus crimping the stent onto the balloon. There was a limit of about 2.3mm for the final diameter. This method also did not cinch the stent on the balloon very well and therefore traveling the vessel would be difficult.

When the prior two crimping procedures were examined it, became obvious that the process occurring was akin to pleating the stent. Since this was occurring, we sought to control this pleating so the stents would be crimped in a reliable manner and stress on the stent could be minimized. The process consists of placing pleats in the stent and then folding these pleats around the center of the catheter to create a minimal profile. It is obvious that the creation of multiple pleats can dramatically affect the diameter of the stent without further adjustment (Figure 2.6C). However, in the case of stents, the rigidity and thickness limit the number of pleats that could be formed. Instead we focused on creating two, three, or four pleats depending on the outer diameter of the stent.

The pleating was achieved by three processes: the first was to pleat the stent by passing the stent through a funnel type pleating device, the second was to place a die inside the stent and apply vacuum, and the third was to form the pleats by hand. The first pleating technique used a funnel like device to form pleats on the stent(Figure 2.6DandE). This technique allowed for the creation of pleats on the balloon and stent. The main advantage of this technique is the ability to pleat the stent and balloon simultaneously which allows the stent to be intertwined with the balloon and prevent the stent from slipping on the balloon during delivery. The second pleating strategy consisted of placing a die on the inside of the stent and using an applied vacuum to form the stent. The biggest limitation of this process is that the pleating does not take place on the balloon. The final pleating technique formed pleats by hand using surgical tweezers. This option has been used on the smaller stent profiles to ensure the stents are not damaged and to create tightly wrapped structures. Table 2.4 summarizes the

endpoints of the crimping process and shows that overall the pleating and folding techniques have been very success in producing repeatable crimping and minimal radial profiles. Crimping by hand seems to be the best method as it allows for the stent and the balloon to be intertwined, keeps the stent from slipping off the balloon, and prevents major stresses from being imparted on the stents. It should also be noted that the crimping ratio decreases as the stent diameter decreases because the smaller stents are more difficult to crimp and the intrinsic size of the catheter does not change among the different diameter groups.

Table 2.4. Crimping strategies

Crimping Technique	Repeatable Crimp	Prevents Failure Points	Starting Diameter (mm)	Minimimum Profile (mm)	Crimping Ratio
Manual Crimping	✗	✗	6	3.47	0.58
Belt Crimping	✗	✗	6	2.41	0.40
Folding Wrapping	✓	✓	6	2.25	0.38
Folding Wrapping	✓	✓	3	1.31	0.44
Folding Wrapping	✓	✓	1.5	0.9	0.60

2.4 Conclusion

Using a novel material, we were able to create a stent design that leverages the strength of the elastin mimetic material and minimizes the material's limitations. This required the design and development of a novel stent platform. This stent also required novel crimping methods to allow for the production of a deliverable stent. These stents have proven to have reliable expansion and minimal recoil. These stents have also shown that they possess the required mechanical properties for stent deployment.

Final Stent Design: The ultimate stent design that we have moved forward with consists of solid rings that have a width of 1.5mm with stent mesh pattern and a total length of 7mm(Figure 2.6)

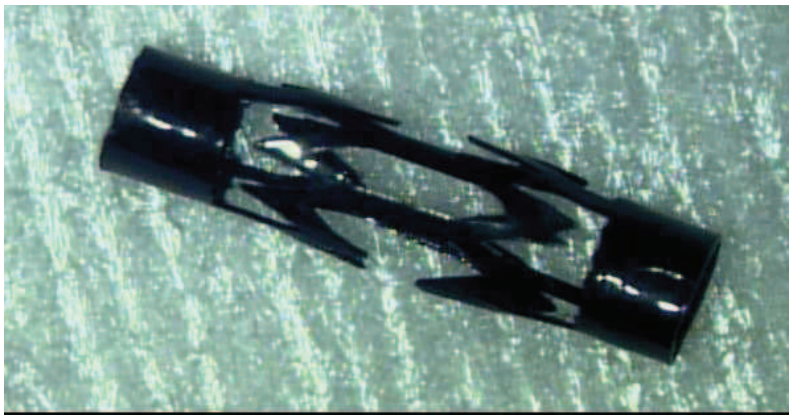

Figure 2.6 Final fabricated and crosslinked stent

CHAPTER 3:

Fabrication of Protein Based Materials

3.1 Introduction

The utilization of biological materials provides a promising approach for attenuating deleterious responses to current implantable medical devices. However, despite considerable research advances over the past decade, these materials are still mainly limited to injectables versus fabricated devices. Compared to bioabsorbable polymers, biological materials pose challenges that are not easy to overcome, and their attributes can lead to a hindrance in fabricating devices. As far as we know to date, there has been a lack of fabrication of patterned robust films made from native materials. We describe herein the development of mechanical robust constructs from biomimetic materials for use in cardiovascular stenting.

Stent Fabrication

Laser machining of stents from thin walled tubing is the most common form of stent fabrication. Stents can be machined through a direct write method, where the laser is focused directly on the substrate, or a masked projection method in which the laser passes through a mask before hitting the substrate. Laser micromachining creates stents by removing material to create open cells via sublimation, melting, or oxygen reaction. Sublimation is not commonly used because the cutting speed is slow. However, this technique does minimize the adherence of solid impurities, or dross, and the extent of the heat affected zone in which adjacent microstructure and mechanical properties are altered by heat. Melting and oxygen reaction remain industry standards because of their high processing speeds, but often lead to the deposition of the removed material on the surface, oxidation at the cuts, and burr formation. Dross and

spatter that stick to the backside of the cut can be removed with additional finishing steps, such as microblasting with aluminum oxide powder, pickling, or soft etching. Schemes to manipulate laser type, pulse length, power level, and different mediums that contain the laser, have been sought to address these drawbacks.

The neodymium:yttrium-aluminum-garnet (Nd:YAG) solid-state laser is the most frequently used laser for stent fabrication because of its short fundamental wavelength of 1064 nm. Nd:YAG lasers have been shown to make slits on the order of 50 - 100 μm with short pulses and high repetitions [103]. The main drawback of the Nd:YAG laser is the size of the heat affected zone and dross adherence. Metallic materials exhibit exceptional absorption of infrared (IR) light, which allows for efficient and rapid machining with IR lasers. However, bioabsorbable polymers are optically transparent, therefore different lasers are required. Femtosecond and excimer lasers are capable of machining optically transparent materials, such as bioabsorbable polymers with high fidelity[104]. Femtosecond lasers are usually based on the titanium:sapphire solid state laser and can machine objects on the nanometer scale with a cut width of 30 μm on nitinol [105, 106]. The femtosecond laser has also been used to fabricate biodegradable magnesium alloy stents [107]. Their major shortcoming is cost. Excimer lasers do not cause ablation by heat but through disruption of molecular bonds through absorption of laser light in the ultraviolet range. While adverse heat effects do not exist, lateral resolution is about 10 μm with beam quality not as good as other laser systems [108]. Polymeric stents have also been machined using CO_2 lasers [109, 110]. However, CO_2 lasers may induce chemical changes in the treated material [111].

Laser parameters that can be varied are the pulse length and energy level. Pulses longer than 10 ns are associated with heat diffusion and conduction, which can impact the properties of material in the vicinity of the pulse beam (Fig 3.) [112]. Shorter pulses, in the femtosecond range, and higher pulse repetition reduce the heat affected zone, which is especially critical for polymeric materials [113].

Photoetching, Electroforming, and Microelectrodischarge Machining for Fabrication of Metallic Stents

Alternative stent manufacturing techniques include photoetching, electroforming, and micro-electrodischarge machining (μEDM), which are capable of producing burr/dross free cuts with minimal roughness. The μEDM process has been used to fabricate stents from planar 50 μm thick stainless steel foil [114] and demonstrate the capacity to incorporate sensor systems to monitor intravascular pressure and flow [115]. Photochemical etching uses a photoresist and etchants to chemically remove unmasked material from metallic sheets or tubes in order to produce complex designs with high resolution[116]. The stainless steel NIR (Boston Scientific, Inc), the stainless steel LP (Interventional Technologies, Inc) [117], and the nitinol aSpire (Vascular Architects, Inc.) stents were produced via this process. Photochemical etching has also been used in the fabrication of an origami stent fabricated from nitinol foil [118] and in conjunction with 3D lithography to produce patterns on nitinol films formed via magnetron sputtering [119, 120].

Fabrication of Polymeric Stents

Laser machining has been used to produce polymeric stents, such as the REVA™ stent [121]; however, concerns related to thermal or chemically induced alterations in polymer properties have motivated the evaluation of injection and compression molding processes. These techniques are particularly suitable for polymeric materials because of their thermoplastic behavior with recent efforts directed at optimizing micro- and nanomolding processes [122-126]. Solvent cast films have been fabricated into stents by cutting the films into strips and wrapping them around a mandrel into a coil like structure [127]. As a related process, fused deposition molding (FDM), which consists of repeated deposition of thin layers of polymer, has been evaluated for the production of 3D microstructures that display micron level resolution with short processing times [128]. Likewise, melt spinning has also been used to form bioabsorbable polymer fibers on the range of 150 μm to 200 μm which can then be woven or knitted into stent-like structures [97, 129]. The technique of controlled expansion of saturated polymers allows for drug loading during the fabrication process [130] and can form bioabsorbable stents that posses proper mechanical integrity [131]. To date, photolithography has been used to produce biodegradable scaffolds for tissue engineering applications, but has not been utilized in the fabrication of stents.

Table 3.1 Literature Fabrication Table of Stent and Scaffolds

Reserch Group	Material	Fabrication Method
Uurto et al	PLA	Melt Spinning
Venkatraman et al	PLLA	Solvent Cast
Chen et al.	Chitosan/Epoxy	Solvent Cast
Poppas et al.	Chitosan	Solvent Cast
Tami et al.	PLLA	Monofilament
Su et al.	PLLA	Melt extruded
Liu et al.	PCL	Injection Molded
Bioabsorbable Therapeutics Inc	Salicylate	Laser Fabrication
Reva Medical	Tyrosine Based PC	Laser Fabrication
Abbott Vascular	PLLA	Laser Fabrication

Our Fabrication Process

In these studies we explored the use of excimer laser fabrication and PDMS molding. Excimer laser has proven to be a valuable tool in the biomedical field because of its ability to ablate the material it contacts without heating the surrounding material making it a cool laser. Excimer lasers are able to ablate biological materials by projecting a tightly focused UV beam onto a substrate which breaks down the molecular bonds of organic materials. The heat that is created is usually dissipated as the material is ablated the potential to ablate biological has been expertly reviewed[132]. The applicability of patterned biological materials is evident when one explores the medical device industry. From stents to bladder meshes there exists product that require the interplay of fenestrated materials. The advantage of these materials is the potential to add another knob to allow for the modulation of their mechanical properties. It has been shown that placing holes in polymers allowed for an increase in compliance[133] of blood vessels.

This Chapter focuses on the fabrication techniques used to create a protein based stent. This is a platform technology that has already been used in several diverse applications relating to other thesis and grant work. This section will explore the potential to create protein sheets with fenestrations and then form these sheets into stents.

3.2 Materials and Methods

Production of Elastin Mimetic Materials

The design, development, expression, purification, and preliminary characterizations of the elastin mimetics used in these experiments has been described elsewhere[87]. For all of the analysis, films were solvent cast from 100mg/ml lyophilized protein, LysB10, in 2,2,2-Trifluoroethanol (TFE) at room temperature, unless otherwise noted.

Excimer Laser Approach

The excimer laser setup consists of an excimer laser (Resonetics Inc., Nashua, NH) operating at a wavelength of 248 nm with a pulse duration of 20ns and a frequency of 60Hz. Parameters such as power, demagnification, spot size, pulse number and speed were selected based on the fabrication design and whether the laser was used in the direct write method or masked method. A LysB10 film was attached to a quartz substrate that was (10cm x 10cm) and placed onto sliding stage below the laser.

The ideal laser parameters used to ablate the elastin were determined using a characterization protocol described earlier [134]. In brief the quartz and elastin film was placed on the stage in the excimer laser and a 10 × 10 matrix of laser shots were fired

onto the protein film using a 20 μm laser spot size. A sample of this characterization protocol can be seen in Figure 3.1 panel B. As noted on the picture with each shot the power was increased in the *Y* direction and number of pulses in the *X* direction. The ablation depth of each hole was measured using an optical microscopy setup with depth evaluation software.

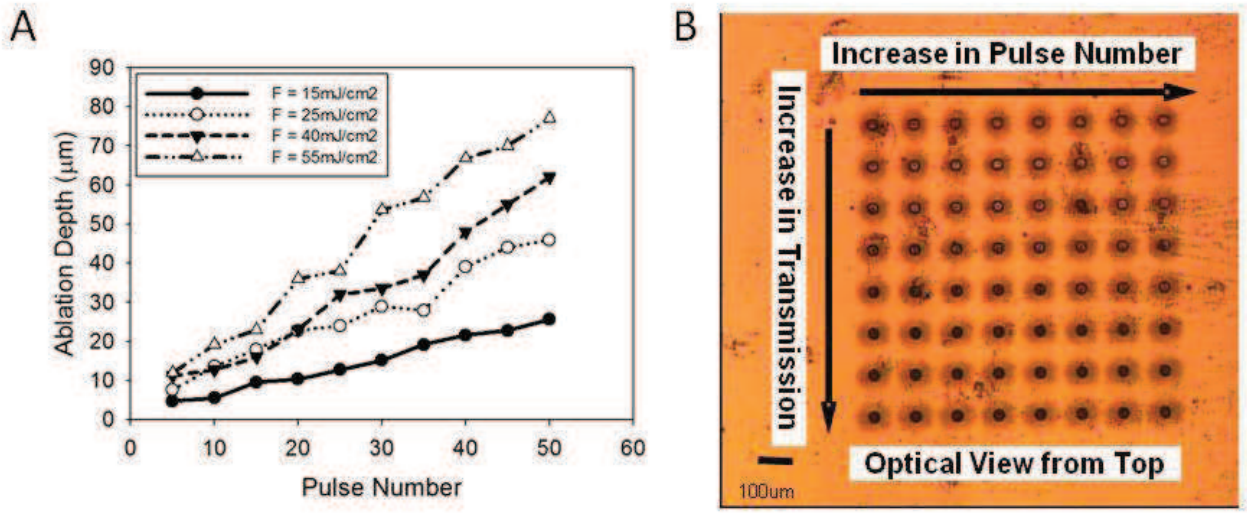

Figure 3.1. (A) Ablation depth vs. pulse number curve for 10 energy levels, (B) SEM micrographs of EM ablated holes with an increase in pulses in the x direction and energy in the y-direction

The laser energy was determined by multiplying the energy(mJ) by the transmission. The energy used was 200mJ and the power transmission was 75% resulting in a laser spot energy was 150mJ. The focal area for the 3mm square mask was 0.0056cm^2, and the focal area for the 200µm mask was 0.0000196cm^2. The fluence of the laser was calculated by dividing the laser spot energy by the focal area for a value of 26.79 J/cm^2. The laser raster speed was 5mm/sec and the pulse rate was 100Hz.

Direct write method conditions

In the direct write setup the CAD file of patterned design was uploaded into the laser operating system. Using the laser program the CAD file was turned into a coordinate system that allowed the laser to trace all edges of design creating fenestrations. A spot size of 25μm was used.

Masked Method Conditions

Creation of a pattern mask was made by designing the pattern in CAD and then transferring it to the IR laser. The mask was fabricated from stainless steel so it could be sterilized since it contacts the protein material. An additional step in this process is that the mask is placed over the protein film and attached to glass substrate to keep the mask aligned.

The masked ablation setup consists of a laser mask with a 3mm x 3mm spot size, a demagnification of 4x, a mask of the patterned design, a protein sheet, and a glass substrate. A rastering sweep of the laser was used to ablate the portions of the protein film not covered by the mask. The program makes the laser raster the entire length of the mask, then the laser moves down by 0.75mm and rasters another line the entire length. This command is continued until the laser has rastered the entire width of the construct. The laser then returns to the origin and moves up 0.375mm and rasters the entire surface to eliminate potential problems of overlap and correct for beam nonuniformity.

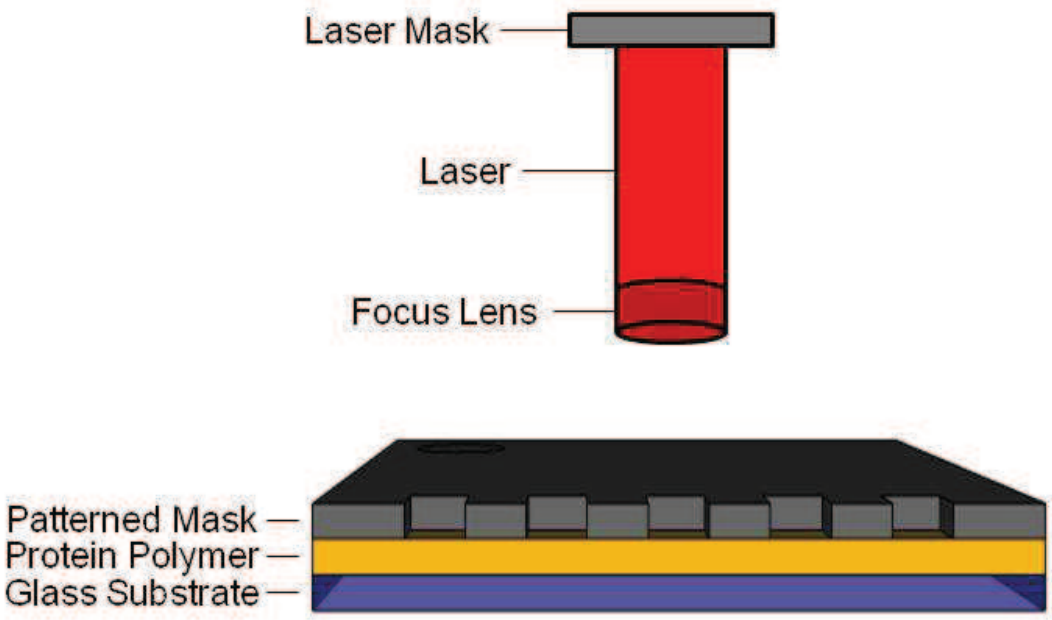

Figure 3.2. Schematic of Excimer Ablation

Fabrication and Utilization of PDMS Molds

All patterns were designed in AutoCAD and imported into the LSL550 program that runs the CO_2 laser (LS500 Laser Engraving System, New Hermes-Gravograph Inc., Duluth, GA). The laser was then run in the raster mode to create the acrylic molds as shown in Figure 3.3. A power setting of 20% was used, and the number of passes varied from 3 to 12 and the corresponding depths ranged from 100um to 1mm. The acrylic was then cleaned with compressed air and isopropyl alcohol. Optical characterization was used to ensure the molds had the proper geometry. The mold was then placed in an aluminum reservoir and premixed PDMS (Sylgard 184, Dow Corning) was poured onto the acrylic molds and placed under vacuum for 45 minutes to ensure the PDMS was pulled down into the mold and all trapped air was removed. The molds

were then placed in the oven at 80℃ for 2 hours. T he PDMS was then allowed to cool for 1 hr at room temperature and demolded from the acrylic.

Casting Elastin Mimetics in PDMS Molds

The PDMS molds were sterilized with ethanol, and dried in a vacuum for 24hrs. Molds used for subsequent castings were also washed in TFE to remove any residual protein from previous castings. The casting material was LysB10 dissolved in TFE at a concentration of 100mg/mL. The PDMS molds were attached to a rigid substrate to prevent mold deformation. To cast the films solutions were aspirated into a 1ml BD syringe with an 18 gauge needle, degassed, and dispensed through a 25 gauge needle. The solution was syringed into the recesses of the mold until they were slightly overfilled with the protein solution. Care was taken not to overflow the mold to minimize webbing. The mold was filled either under 5X or no magnification depending on the shape of the 3D structure.

The molds were placed in Petri dishes that were subsequently closed and sealed with parafilm to decrease the rate of solvent evaporation. The solution was allowed to equilibrate for twelve hours in the closed Petri dish. The Petri dish was opened every four hours to release the vaporized TFE four times to provide for a gradual evaporation of the TFE. In processes that required multiple coats the casting conditions were followed again. These steps were repeated to get the desired thickness. The raised portions of the PDMS mold were then wiped with a sterile TFE coated cotton swab. The Pertri dishes were sealed for 24 hours to let any residual TFE from the washing step evaporate.

To examine the effect of different casting conditions, several variables were examined independently to achieve optimal casting conditions. The variables that were explored were mold depth, evaporation time, casting solution concentration, and cast number.

Combinatorial PDMS casting and excimer laser approach

In the combinatorial approach the PDMS molds were overfilled with protein solution. The material was then rastered using the same material ablation profiles as the masked approach.

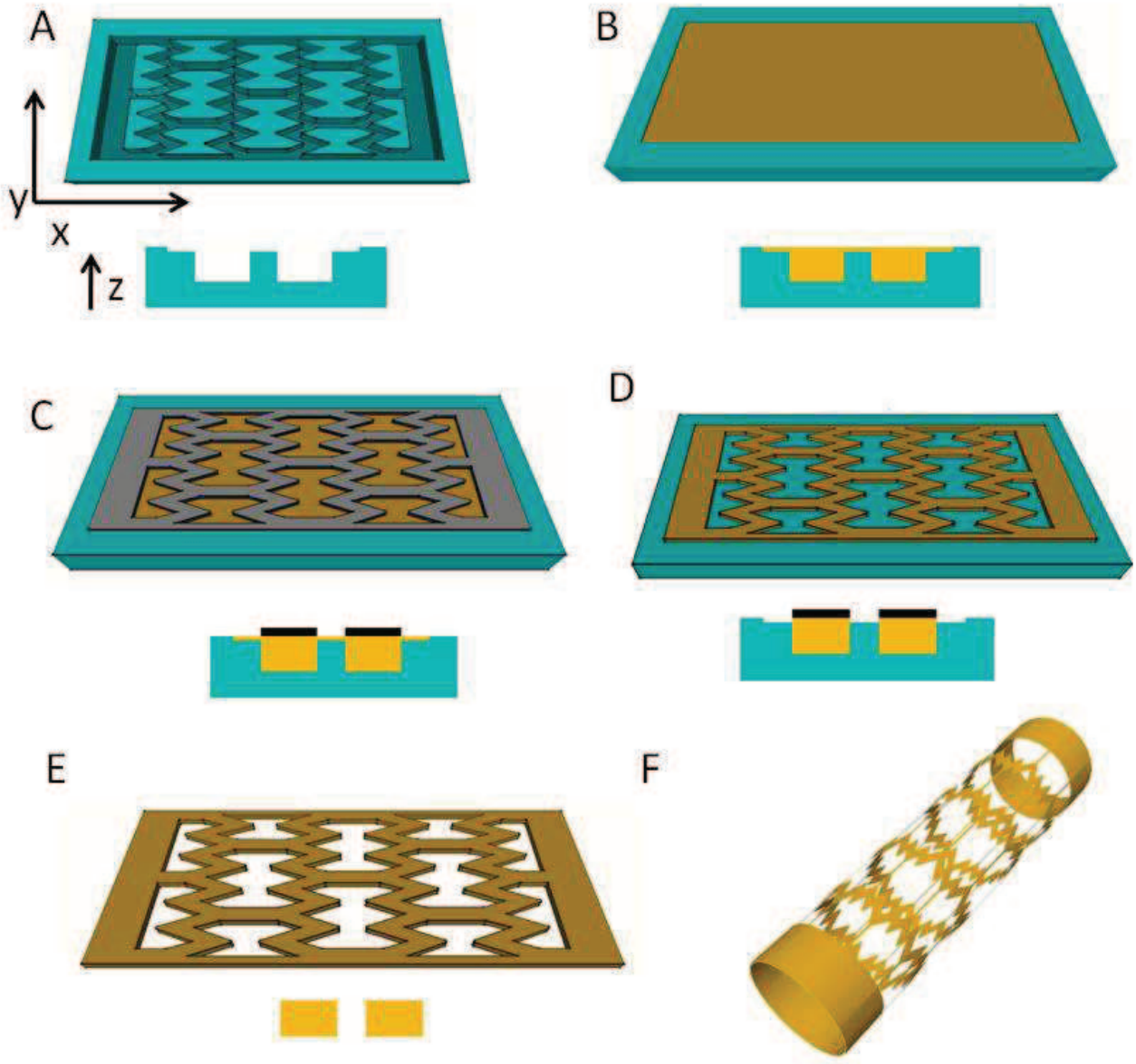

Figure 3.3 A combinational approach was used to generate stents from protein polymer solutions. (A) PDMS mold patterned with the stent design. (B) PDMS mold overfilled with elastin mimetic material. (C) Mask placed on top of the webbing from the solvent casting (D) Elastin mimetic in mold after the webbing is ablated with an excimer laser. (E) A stent that has been unmolded. (F) A rolled and attached stent.

Optical Characterization of Micofabricated Protein Polymer Sheets

To validate the fabrication processes, the patterned protein sheets' surface morphology and thickness were examined using a scanning electron microscope (SEM) (Topcon DS-130F Schottky Field Emission SEM/STEM) and optical microscopy.

Determination of Design Parameters

Fabrication fidelity, and therefore dimensional stability, arises from the accuracy of the fabricated patterns. To determine the fabrication fidelity, the widths and thickness of the constructs were measured after different fabrication approaches.

Determination of Cost Parameters

The time required to fabricate a patterned sheet was calculated for each process. All times were the summation of time required to fabricate the device, including relevant times needed to evaporate solvents. Material waste was calculated by subtracting the weight of the final construct from the weight of the materials used in the process. Equipment costs were determined as both initial sunk costs and costs of the consumables used in the process.

Determination of Physical Parameters

The extent of protein crosslinking and/or degradation was determined through the processing of proteins with excimer ablation. To provide a more rigorous test bed unmasked protein sheets were ablated with increasing number of passes from one to three. The films were then resolubilized in TFE and subsequently extracted in molecular grade water(MGW). The solution was centrifuged at 3000 rcf to pellet the protein which was then was resuspended in another 25mL of MGW and centrifuged again. This step was repeated one more time. The final pellet was resuspended in 10mL of MGW, frozen

at -80℃ for 24 hours, and lyophilized for 72 hours . The samples were then run on SDS PAGE gels. In brief, Sodium dodecyl sulfate-polyacrylamide gel electrophoresis (SDS-PAGE) analysis revealed protein bands at 250 kDa. A total of 40 µg of elastin-mimetic proteins was run along with molecular weight markers (Precision Plus Protein Kaleidoscope, Bio-Rad) on a 7.5% gel and stained with Coomassie stain (Bio-Rad).

To determine the sterility of material pre and post fabrication, lyophilized protein was resuspended in sterile MGW at 1 mg/mL, and endotoxin levels were assessed according to manufacturer instructions using the Limulus Amoebocyte Lysate (LAL) assay (Cambrex, East Rutherford, NJ).

Tubular Construct Formation

To fabricate the planar sheets into tubular constructs, the stents were hydrated and placed on a sheet of sterile aluminum foil. The aluminum foil was then wrapped around a mandrel 10% smaller than the final desired diameter. The stent was then allowed to dry for 24 hours under vacuum. The foil was removed, and the stent was taken off the rolling mandrel and placed on the attachment mandrel. The two abutting ends were either solvent welded or overlapped and solvent welded.

Thin Walled Tube Formation

The fabrication of thin walled tubes of elastin mimetic material was achieved through a dip coating procedure. Stainless steel mandrels were dipped into 100mg/ml LysB10 in TFE solutions. The mandrels were then inserted into a rotating chuck and rotated at 60 rpm. This allowed for a uniform distribution of the elastin mimetic material.

3.3 Results and Discussion

The development of a fabrication process revolved around the ability to fabricate stents from an elastin mimetic material without damaging the material. The fabrication of stents from elastin mimetics required different fabrication processes than commercial stent manufacturing and experimental stent manufacturing as noted in Table 3.1. Processing conditions can severely alter the material properties of the elastin mimetic; therefore the first step in fabricating the stents was perfecting the ability to process the elastin mimetic materials which are concentration and solvent dependent. The solubility limit of elastin mimetic polymer in TFE was 200mg of protein in 1ml of solvent. TFE was chosen as a solvent because of its potential to provide an organic solvent that maintains the structure of the protein[135, 136] and this allows for the formation of mechanically robust constructs[102]. Previous reports in our lab have shown that casting elastin mimetic materials from TFE can create stiffer films than those cast from water[102]. All of the fabrication techniques that were explored looked at the evaporation of solvent from the protein solution to create sheets or thin walled tubes. Thin walled tube fabrication was achieved through a simple dip coating process. The development of thin walled tubes allowed us to determine the initial mechanical properties of the elastin mimetic constructs and proved that solvent cast thin walled tubes have sufficient strength to perform stenting applications. To allow the thin walled tubes to perform other stent functions fenestrations had to be added to them. Unfortunately none of our fabrication, techniques were able to create fenestrations in the thin walled tubing. Therefore, we explored the second major fabrication process which was planar sheet fabrication. This method allowed us to create two main stent designs, as noted in

Chapter 2. The first was the helical coil stent design that has been used by other research groups to explore novel stent materials[80, 89, 90]. This stent was easily fabricated by wrapping a thin film 4mm X 40mm to fabricate a stent with a 6mm inner diameter and a length of 10mm. The second design and the focus of the majority of this thesis was a generic design that is similar to the majority of commercial stents platforms. These stents were created from planar sheets with fenestrations formed into tubes.

In order to create planar sheets with fenestrations, laser ablation and micromolding approaches were explored. These are two techniques that are used extensively in the MEMs field to create biomedical devices from biologically relevant polymers. The initial approach that was adopted for the fabrication of stents was a laser based technique that is similar to the procedures used to develop stents in the industrial settings. The initial limitations that made us pursue dual strategies were the process time, material waste, and potential contamination of the material. The second path that we pursued consisted of casting the elastin mimetic into PDMS molds to generate the desired stent design. This molding technique allowed for a high throughput process that minimized material waste.

Excimer Laser

The excimer laser was chosen because of its history of ablating biological materials with minimal thermal damage. Most traditional lasers often ablate materials with high temperatures which could denature or burn the elastin mimetics. The method of excimer ablation inputs highly focused UV energy into the material, thereby disrupting the molecular bonds which leads to material ablation. Therefore, the elastin mimetics

should be able to be cut without changing the mechanical properties of the material that is left behind.

To explore the potential of using the excimer laser to fabricate fenestrations in the protein sheets, a characterization protocol was used to determine the proper parameters that were needed. Figure 3.1 shows the ablation profiles when the number of pulses and the transmission are increased. The goal was to use the lowest fluency possible to ensure that the protein was not damaged. To determine the ablation depth for a given number of pulses and a given fluency, the protein sheets were examined under optical microscopy. The edges were also examined to ensure there was no edge damage or heat affected zone. Ultimately these tests proved that excimer laser ablation was feasible.

First, we used a direct write method to fabricate a stent using the setup depicted in Figure 3.2 without a patterned mask. This process was capable of making fenestrations in the protein sheets, however, the time required to make a stent with this direct write method is not feasible (Table 3.2). Other limitations with this approach were material waste, laser consumable waste, and a lack of throughput.

Table 3.2 The fabrication times for the different modalities are defined in terms of initial sunk time and time per stent.

	Fabrication Techniques			
	Solvent Cast Molding	Excimer Direct Write	Excimer Masked	Combinational Approach
Sunk Time Per Design	8 hours	1 hour	3 hours	11 hours
Time Per Stent	1.5 hour	7.5 hours	0.75 hours	0.25 hours

The excimer laser schematic depicted in Figure 3.2 shows that two masks can be placed in the path of the laser. The first is an inline mask that allows the user to project that shape on the substrate to get ablated. Based on the output of the laser the largest opening in the mask can be 5mm x 5mm. Once the beam goes through the focus lens, the largest the beam can be in the direct write method is 1.25mm x 1.25mm. However, the size of the laser was not big enough to allow us to pattern a single stent cell. If this was the case the stents could be ablated one cell at a time which would drastically decrease the fabrication time. Therefore, we chose another way to decrease the cutting time is to use an in line pattern mask on the protein construct as shown in Figure 3.2.

Excimer Laser with a Mask

To overcome the time limitations of the direct write method, a masked laser ablation process was explored. Once the patterned mask was fabricated it was placed on top of solvent cast elastin mimetic sheets which allowed for the implementation of a high throughput way of making fenestrations. The masked approach allowed for the entire surface to be rastered, allowing us to employ a larger spot size and thereby reducing the time to5 minutes. To ensure complete ablation, six raster passes were used, and each alternating pass was offset by half the laser spot size to ensure even ablation. This method also allowed us to use a faster cutting time because of the simplicity of the laser movements. As shown in Table 3.2, the mask method allowed us to decrease the cutting time by 90%. This technique also performs well at these length scales. As the pattern becomes finer, more care must be taken to address potential shadowing and mask fidelity issues.

While the masked laser approach offers the high throughput process, it still did not ameliorate the material waste and sterility concerns. Therefore, we sought a cheap high throughput fabrication process that would conserve our protein material and allow us to fabricate sterile constructs.

PDMS Molding Technique

The second fabrication technique that we explored was a PDMS molding technique commonly used in the MEMs field to fabricate 3D structures. The basic schematic can be seen in Figure 3.3. The fabrication of PDMS molds has more sunk time than the previous methods because of the time required to fabricate the reverse acrylic molds and PDMS molds. However, the PDMS molding strategy allowed for new stent designs to be tested in a day by providing a high throughput method, since several PDMS molds can be made simultaneously. The PDMS molding technique also minimized the amount of wasted protein polymer; therefore this process proved to be the most efficient method to fabricate, test, and analyze multiple designs. However, the biggest limitation of this modality is the design fidelity as noted in Table 3.2. This is caused by the biggest limitation of the molding process which was the formation of webbing.

Casting Elastin Mimetics in PDMS Molds

The casting solvent, TFE, has a low vapor pressure which caused the solution to evaporate quickly in the fume hood. When the solution evaporated too quickly stresses were formed in the polymer leading to nonhomogenous film thicknesses, wavy films, webbing on the intricate molds, and prevented casting a construct with multiple

layers[137]. To minimize and eliminate these limitations, the rate of vaporization was decreased by placing the molds in Petri dishes which were subsequently closed and sealed with parafilm. This setup created a TFE saturated environment which decreased the rate of solvent evaporation and increased the drying time of the constructs. The Petri dish was opened every twelve hours to release the vaporized TFE, a total of four times. In processes that require multiple coats, the casting conditions are followed again, and these steps can be repeated to get the desired thickness. The raised portions of the PDMS mold were then wiped with a sterile cotton swab that had been dipped in TFE.

Since this technique worked other variables were altered independently to evaluate their effect on casting. These alternatives consisted of: mold depth evaporation time solvent weight percent and cast number. It had been hypothesized that molds with deeper wells could be rinsed with solvent to eliminate webbing in the z direction as shown in Figure 3.4. However, this was not the case, and the films were ultimately unusable. In the end, the cleanest films were obtained by limiting the mold depth to the desired thickness of the constructs. Extended evaporation times did help the process by allowing for the formation of flat films which allowed for serial casting and minimized webbing. In our studies, the ability to change the weight percent was not beneficial. It was believed that increasing the concentration of the casting solution would allow us to cast the material without as much webbing. However, the 15% solution was overly viscous and did not pull into the molds properly, and therefore led to worse webbing the 10% solution that was currently being employed. Finally, the serial casting strategy worked very well, and the subsequent cast layers solvated the previous layer well

enough to prevent any problems of creating a layered structure that ultimately could delaminate. With these changes in place we sought to explore the dimensional fidelity of the molding process.

Examining the Design Parameters

To explore the quality and versatility of the fabrication process, the design fidelity was determined for stents with strut widths of 250μm, 500μm, and 750μm(Table 3.3). The cell areas, crown widths, and connector widths were measured at six points for each parameter to determine the design fidelity of the different processes. In order to determine the dimensional fidelity of our fabrication process, stent sheets were examined under optical microscopy, and the parameters of interest were determined and compared to our design number as shown in Table 3.3 When compared to the designed dimension, it was clear that the molding approach produced the constructs with the lowest design fidelity. The molding fidelity increased as the scale of the widths increased and these trends held for the other parameters as well(Table 3.3). Table 3.3 also shows that the direct write fabrication method and masked projection methods are extremely accurate and created constructs that had close to the same width as the targeted design. The scale of the dimensions did not seem to affect the design fidelity of these processes. However, it should be noted that all three of the designs highlighted had feature sizes on the same order of magnitude. These results dictated that an optimized casting process had to be obtained to move forward with this fabrication modality. Since, the molding process offered many advantages, we explored the potential of optimizing the process to overcome its design fidelity limitations.

Table 3.3 Design Fidelity of Fabrication Processes

	Fabrication Modality	Cell Area mm²			Strut Width µm			Connector Width µm		
Design 1	Designed	10.58	±	0.00	750.00	±	0.00	750.00	±	0.00
	PDMS Molding	9.88	±	0.22	785.82	±	15.23	774.19	±	17.72
	Excimer Masked	10.47	±	0.05	756.43	±	8.54	754.34	±	6.89
	Combinational	10.37	±	0.07	758.42	±	9.65	752.34	±	8.34
Design 2	Designed	10.88	±	0.00	500.00	±	0.00	500.00	±	0.00
	PDMS Molding	9.67	±	0.26	555.84	±	27.83	561.53	±	27.64
	Excimer Masked	10.72	±	0.08	512.12	±	0.92	501.14	±	8.67
	Combinational	10.68	±	0.10	507.82	±	8.34	505.00	±	7.56
Design 3	Designed	10.99	±	0.00	250.00	±	0.00	250.00	±	0.00
	PDMS Molding	9.35	±	0.31	323.63	±	41.54	318.25	±	38.25
	Excimer Masked	10.76	±	0.10	255.93	±	11.53	253.23	±	10.37
	Combinational	10.69	±	0.11	265.32	±	9.96	254.52	±	8.75

Overcoming Molding Issues

The results from exploring design fidelity demonstrated that the widths of the struts and connectors were wider than anticipated. To ensure this was not caused by distortions or swelling of the mold, the mold was filled with TFE, allowed to incubate for 48 hrs to represent the casting process, then the mold was measured. It was determined that the solvent does not swell the mold and dimensional instability was arising from webbing. The examination of the planar stent patterns illustrated two forms of webbing as shown in Figure 3.4 A. The first type of webbing occurs in the z plane and accumulates on the walls of the mold. The second type of webbing type happens in the xy plane and can cover the fenestrations in the mold.

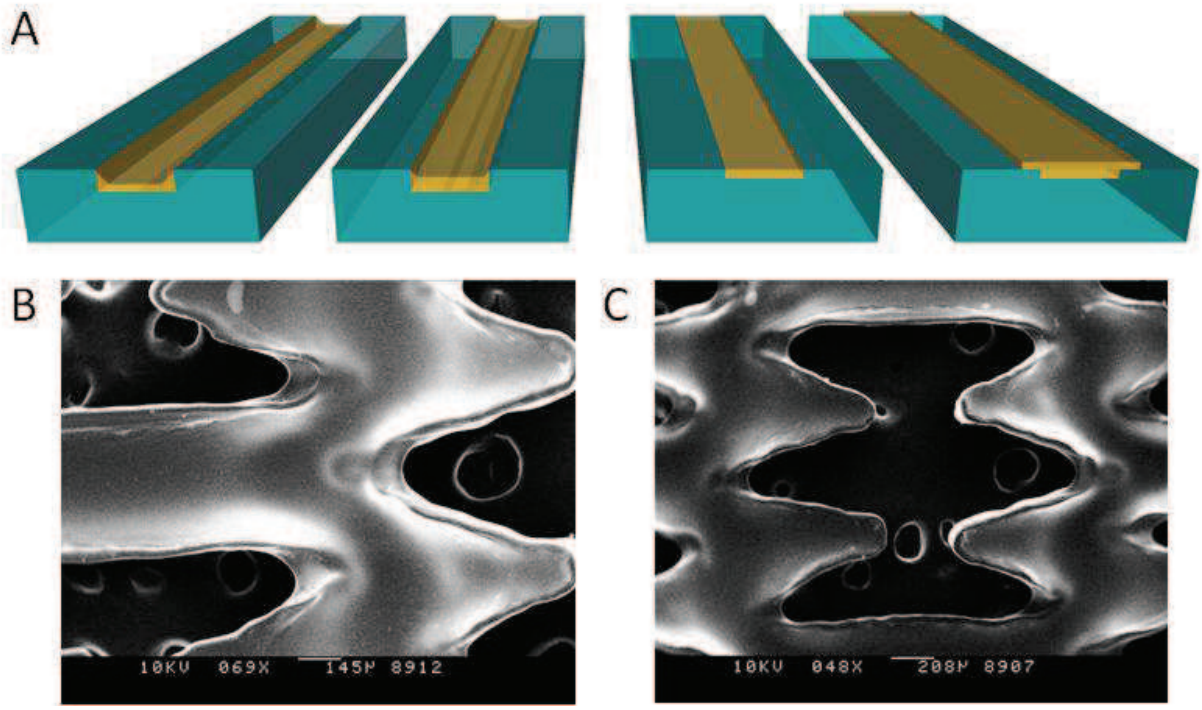

Figure 3.4 PDMS molding was used to generate 3D structures from protein polymers. (A) The filling of a PDMS mold with protein polymers illustrated in webbing perpendicular to surface after one pour, webbing perpendicular to surface after three pours, an ideal case with no webbing and a filled well, and an overfilled mold with webbing parallel to the surface.

The webbing in the z direction affected the thickness of the stents. As seen in Figure 3.4, the webbing can create thin portions of material that increase the overall thickness of the stent. Since one of the major design considerations was to minimize the overall stent thickness, this webbing must be eradicated. Any webbing in this direction will generate a weaker stent with regard to total thickness. A side profile showed that there is a base level of material, as well as webbing that was formed as the protein solution was evaporated in the mold. The initial experiments focused on making molds with deeper wells of 750µm. Once the film was cast, the thinner side wall webbing would be removed by adding excess TFE into the mold. When imaging the stents, it

was clear that the stents with the deeper wells had significantly more webbing even after the thorough washing steps. The interesting thing is that these peaks were higher with increasing well depth. However, the peaks were not as deep as the well. This observation showed that the side wall webbing was able to be reduced with washing but not eliminated. The next approach to minimize webbing in the z direction was the use of serial castings and shallower molds. This technique limited the webbing more than any other technique but it still left webbing that was not acceptable for the final stent design.

The webbing in the xy plane affects the width of the struts and the area of the fenestration. While webbing in this direction can hurt the design fidelity, overall this webbing is easier to remove. The consensus from a fabrication point of view was to eliminate webbing in the z direction at the cost of having xy webbing. Therefore, we moved forward with overfilling the mold and creating webbing in the xy plane. Care was to taken to make the webbing in the xy plane as thin as possible so it would be easier to remove.

Since webbing could not be completely eliminated by optimizing the molding conditions, a combinational approach was sought that would allow for forming the stent in the mold and a finishing step would be employed to eradicate the webbing in the xy plane. The strategies that were employed consisted of washing, cutting, reactive ion etching, and laser ablation. The thinner the top film, the easier it was to remove that film with either of the processes listed above. The initial approach was to wash the surface of the mold after casting to eliminate the xy plane webbing. This works to a large extent but upon inspection there was still some residual webbing. Also the cast sheet can be removed from the mold if the washing is too aggressive. A cookie cutter

type device was fabricated that acted as a die and cut the stent; however, this had limitations regarding alignment and tearing the stent. Reactive ion etching was successfully used to selectively ablate the thinner protein based material; however this led to concerns that the chemically reactive plasma denatured the remaining material. The final approach was to use the excimer laser to ablate the webbing. We showed that the laser was able to ablate the webbing with and without a mask (Figure 3.5). We used a mask to prevent the laser from ablating the surface of the stent material. The reason that this method was effective was the thickness of the film was much less than the previous excimer attempts.

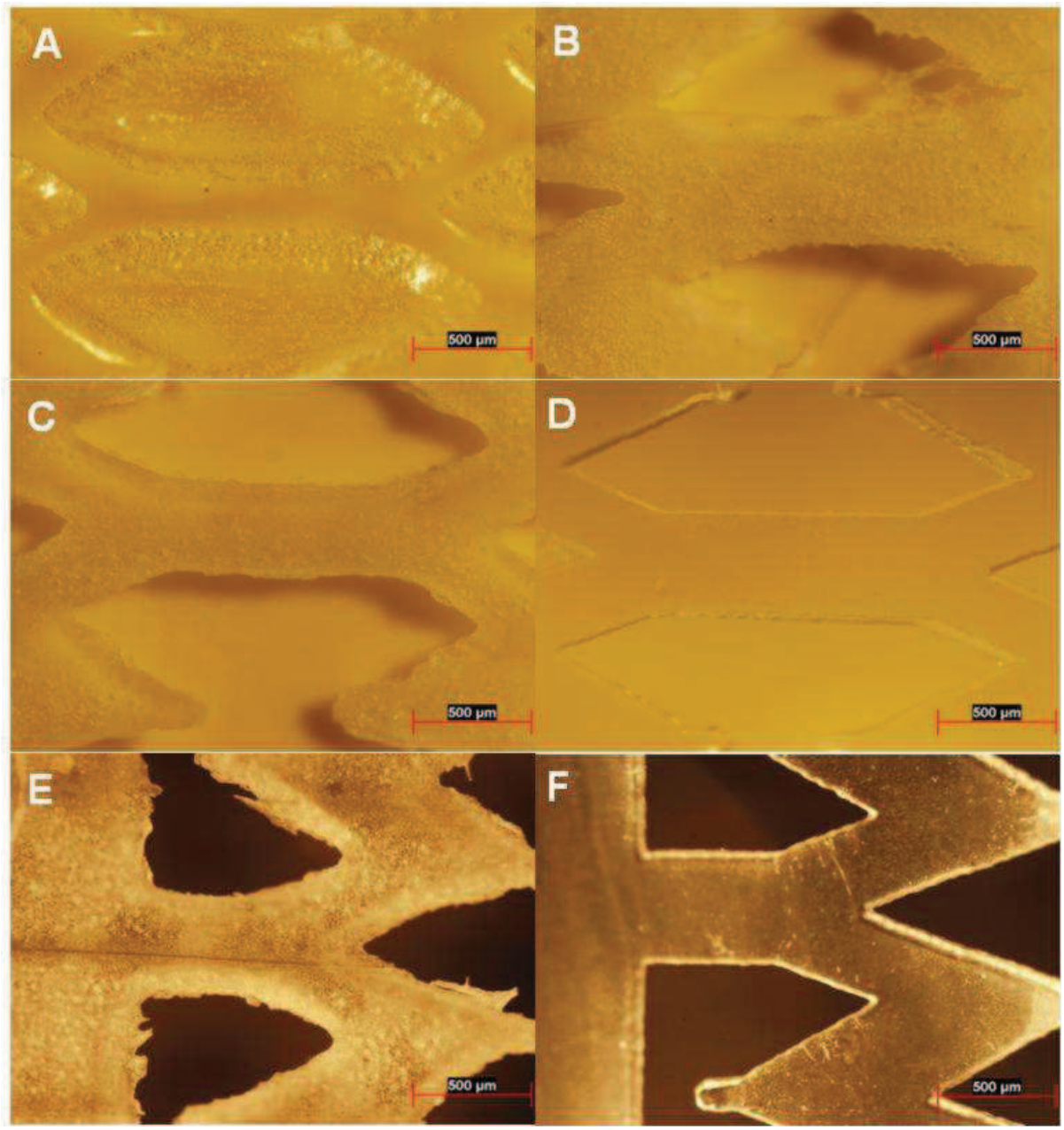

Figure 3.5 Samples A-F are 10X optical images (A) after over filled molding (B) and (C) after one and three rasterings respectively unprotected (D) after three rasterings with mask, (E) unmasked rastering three passes and (F) masked rastering after three passes.

In conclusion, the molding process was optimized to allow for casting from low weight percent solution and generating minimal webbing. This webbing was

subsequently able to be removed with a finishing step. This method allowed for molding to successfully fabricate different stent designs in a high throughput process with minimal material waste.

Determination of Protein Degradation and/or Crosslinking

The biggest concerns about using laser-based fabrication processes for biological materials are the incorporation of contaminants and the alteration of the biological material. In the molding studies, all components can be sterilized, and the casting can take place in a sterile hood with standard sterile technique. However, in the laser approach, contamination can come from the lack of sterility of the laser setup and the incorporation of radical particles during the fabrication process. There has been much thought into selecting processes that minimize the chance of contamination and denaturation. The utilization of the excimer laser to fabricate the final stent platforms required examination of the damage caused by thermal and UV exposure and potential crosslinking. To explore the effect on protein degradation, the proteins post fabrication were run on an SDS PAGE gel, and their percent extractables were calculated. In all of the stent designs that were fabricated we determined that there was no crosslinking as 100% of the material was able to be extracted. Also, there appeared to be no generation of shorter protein sequences from the ablation, as the SDS PAGE gels had no unexplained protein bands. To further explore this we subjected the protein to unmasked rastering as noted in the methods sections.

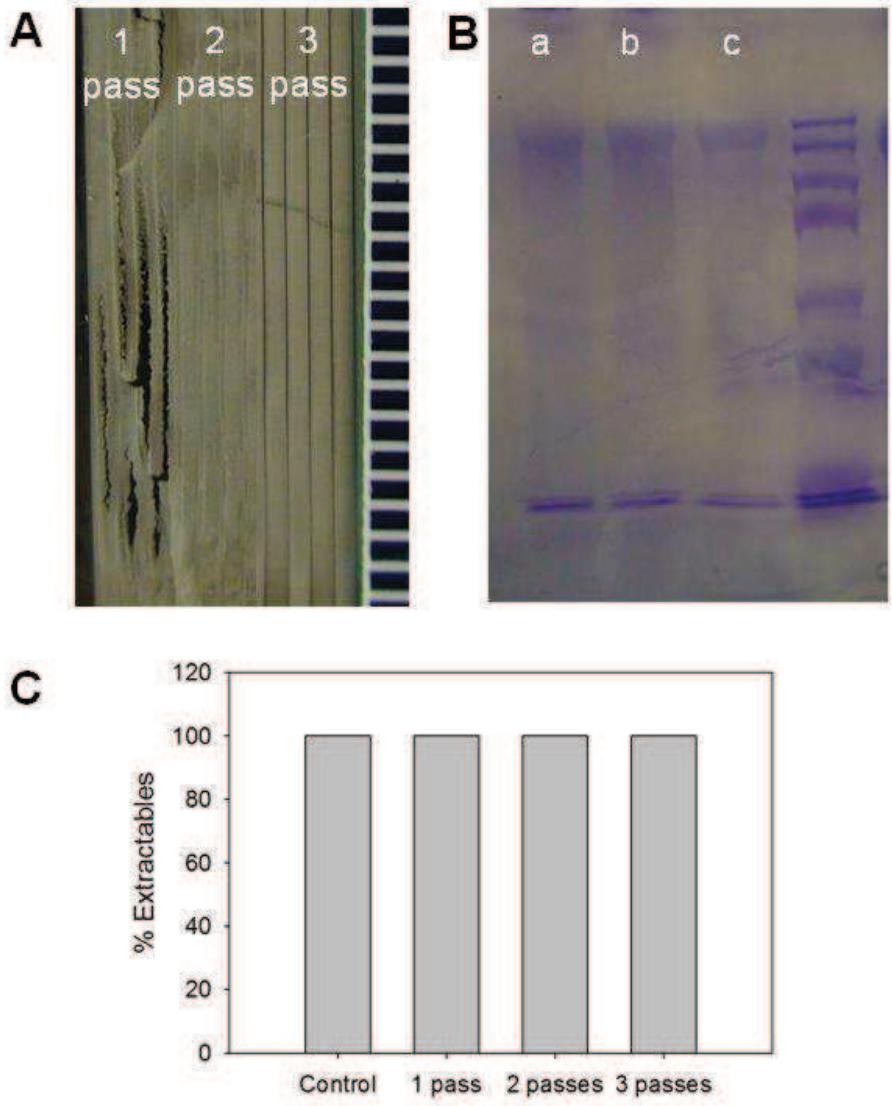

Figure 3.6 (A) LysB10 film raster with excimer laser for 3passes 2 passes and 1 pass. (B) SDS Page gel of three samples a) LysB10 in water, b) lys B10 cast from TFE, c) laser ablated LysB10 (C) % extractables from laser ablated samples and control LysB10.

Preventing Contamination

A potential side effect of fabrication is the incorporation of endogenous and exogenous materials in the stent platform. In the laser process, the material that was ablated was redeposited on the surface. Based on the SEM evaluation, it appeared the

material redeposited on the surface could be removed by washing the sheet after ablation. The other point of emphasis was the ability to keep the material sterile throughout the process. However, the incorporation of the excimer laser prevented the process from being sterile throughout. Therefore, we needed to determine the sterility level of the protein sheets before and after fabrication to determine if the fabrication process was promoting the incorporation of endotoxins into the material. In order to explore the sterility of the different processes, the LAL assay was utilized. Levels of 0.1 EU/mg were obtained (1 EU¼100 pg of endotoxin), which corresponds to endotoxin levels for clinically used alginate (Pronova sodium alginate, endotoxin_ 100 EU/g) It was determined that there was no statistical difference between the three different methods.

Denaturation

In a standard ablation process only the edge of the protein exposed to the UV and heat damage, and the edges tend to make up a small fraction of the entire material. Therefore, we believed that an effect of the UV laser on the protein sheet could be lost if we solubilized our patterns. Therefore, the denaturation and crosslinking experiment sought to make these effects more prominent by ablating the entire surface with multiple passes. In the current studies, it takes five passes with the laser to ablate the material completely and ensure there is no protein webbing left behind. We looked at protein sheets that were not covered with a mask and, instead, exposed them to direct ablation from the excimer laser. The fact that the stents completely went into solution shows that the crosslinking in not a problem(Figure 3.6).

Table 3.4 - Comparing the advantages and limitations of each approach

		Fabrication Techniques			
		Solvent Cast Molding	Excimer Direct Write	Excimer Masked Method	Combinational Approach
Design Criteria	Design Flexibility	++	++	±	±
	Fabrication Fidelity	--	+++	++	++
Cost Parameters	Throughput (Time)	++	--	+++	+++
	Material Waste	+++	--	--	++
Material Properties	Denaturation	+++	--	±	++
	Sterility	++	±	±	±

Ideal +++ Good ++ Neutral ± Poor --

Creating Stents from Planar Sheets

The chief drawback of the planar approach is the process required to form the stent from a planar sheet into a thin walled cylinder. The current procedure for attaching these stents begins by hydrating the patterned sheets for 1 hour in 37℃ PBS which makes the material more pliable and allows for the material to be fixed in a shape when dried. Once hydrated, the stent was then placed onto sections of aluminum foil which allowed for easier handling of the stent and prevented the stent from tearing. The foil and patterned sheet were wrapped around a Teflon mandrel that is 10% smaller than the desired final inner diameter. The stent was then allowed to dry at room temperature for 24 hours. Once the stent dried, the aluminum foil was removed and the stent

conformed to the Teflon tubing. The next step was the attachment of the opposing sides of the sheet to make uniform cylinders, as shown in Figure 3.7. Several variables in the attachment process were explored, ranging from the type of solution used to attach the two sides and whether the ends should be attached by abutment or overlapped.

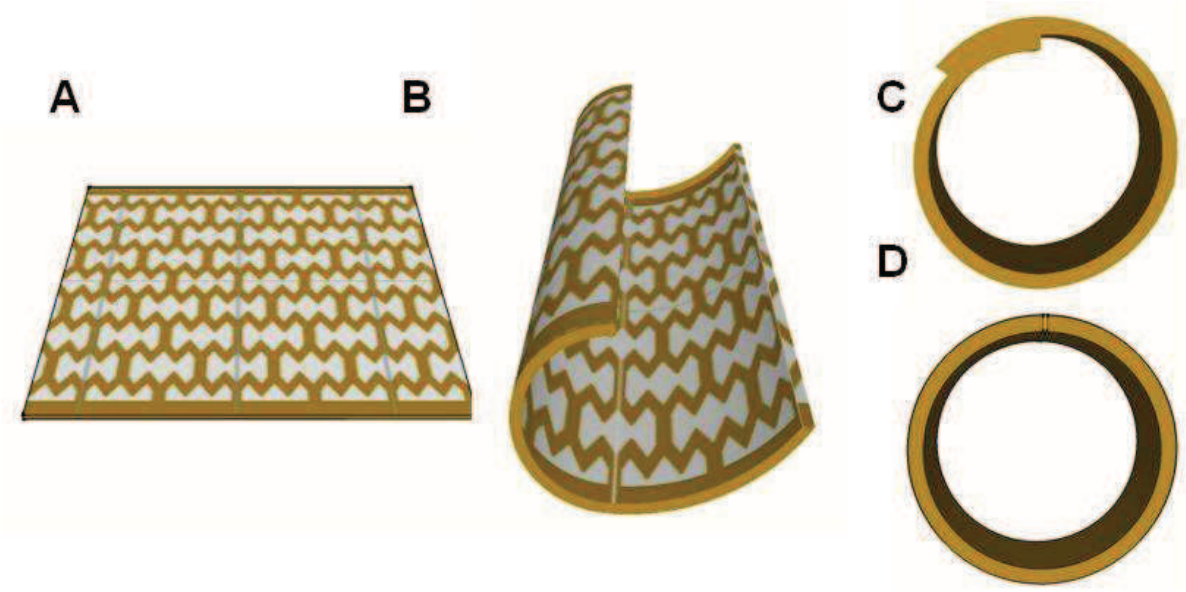

Figure 3.7 (A) Planar Stent Sheet (B) Picture of planar and rolled stent (C) End profile of stent overlapping (D) End profile of stent abutment attachment

The attachment solutions that were explored were TFE, 100mg/ml LysB10 in TFE and 200mg/ml LysB10 solution in TFE. The LysB10 solutions were syringed onto the abutting sides with 30 and 25½ gauge needles, respectively. The 20% solution was used because the 10% solution has such a low viscosity that it spread along the length of the attachment site. The TFE solution was syringed onto the attachment site with a 30 gauge needle. The stent material was then brought in contact, and the adjoining

sides were solvent welded together. This solution worked best for solvent welding because the elastin mimetic solutions created webbing and exogenous material on the mandrel.

The attachment of the stents was the largest hurdle that had to be cleared to employ planar sheets in the fabrication of the stents. Two methods for attaching the stent were explored: the first was abutting the two sides of the stent, and the second was overlapping the film as depicted in Figure 3.7.

The ability to successfully fabricate stents form planar sheets was based on three endpoints; can the stent be successfully attached, removed from the forming mandrel, and created with no webbing. The favored attachment method from a design standpoint was to create stents by joining the two abutting sides. However, this method failed on all three of the criteria noted above. Firstly, it is difficult to bring the two abutting sides into contact and solvent weld them together. These connections were successfully formed in some cases, but there was a problem removing the stents from the mandrel as the attachment process allowed the stent to stick to the mandrel. This problem was exacerbated by the fact that the patterned sheets do not have much rigidity in the longitudinal direction and therefore if even one strut stick the stent will tear at that point yielding the stent useless. Therefore, the success rate for fabricating a stent with adjoining sides resulted in a success rate of less than 15%. The overlapping stents were able to be fabricated with a higher success rate. In the case of the overlapping stents attachment was facilitated by the fact that the wrapping allows the stent to have a fixed overlap so all that must be done is to tighten that overlap and add the attachment solution. Also since the attachment is mainly between the two ends the stent did not

stick to the mandrel with the same intensity as the previous attachment method. Therefore, the majority of the stents they were able to be removed from the mandrel.

Once the stents were fabricated they were tested to ensure the quality of the attachment at the weld joint. The preliminary test of the attachment zone was to expand the stent. Initially the stents were imaged at the attachment zone to ensure the attachment was complete. The stents were than expanded to 1.1 times the fabricated diameter. Upon inflation the stents were examined to ensure that the welds at the attachment zone held. In many cases it was noted that the abutment attachment failed completely or in several points. This was attributed both to the contact area of the welds as well as reliability of the welds. In the overlapping case the amount of overlap was altered to increase the success of the stent. It was determined that in the 1.5mm stent design an overlap of 20% of the circumference or 942μm was sufficient.

The attachment of these stents is not ideal. However, the ability to overlap the stents provided a method to move forward and test the stents further. The ultimate goal is that a fabrication setup will allow us to fabricate these stents from thin walled tubes and ultimately eliminate the need to attach these stents.

3.4 Conclusion

Laser fabrication has proven a powerful tool for creating complex 3 dimensional structures out of biological material. The ability to use this fabrication method in tandem with PDMS molding allowed for a decrease in laser time while simultaneously minimizing the waste of these highly valuable materials. The ability to fabricate fenestrations in biological materials expands their applicability as smart mechanical design allows researchers another tool to recapitulate the native environment while

designing for a mechanical need. Fabricated films showed excellent fidelity and minimum laser issues. It has been shown with collaborators that this method builds the foundation of excimer ablation and allows for a process to fabricate constructs. In this regard, these methods have impact in a range of fields that are now turning to mimetic materials to improve efficacy and applicability. While specific applications for this technology are stated herein the potential to expand to other biomaterial applications offer the potential for this to become a platform technology for biomaterial engineering.

Chapter 4:

Advancing the Biological and Physical Properties of the Elastin Mimetic Materials via Crosslinking, Drug Incorporation, and Enhancing Cell Binding

4.1 Introduction

The elastin mimetic stent platforms allow for the incorporation of additional factors that provide ways to augment their performance. In standard stent platforms, this is very challenging as seen by the laborious efforts to achieve stent coatings that have beneficial results without detrimental side effects[138]. The modifications of these elastin mimetics were explored on three fronts to combat the most common causes of stent failure. The first was the crosslinking of the elastin mimetic stents to examine the effect it had on the biological, physical, and mechanical properties of the stent. We compared different crosslinkers and their effect on mechanical properties and drug retention time. We then examined the potential of incorporating pharmaceuticals and biopharmaceuticals into the stent platform.

The crosslinker selection was explored in such depth as the crosslinking agents were able affect all aspects of stent design, including the physical, mechanical, biological, and drug release properties. Preliminary studies have shown that vapor phase crosslinking of protein sheets provides robust mechanical properties and a reduction in the thickness of the crosslinked films compared to the uncrosslinked films. Genipin was the second crosslinker that was explored because of its known biocompatibility. Finally we will explore the potential of modifying the glutamic acid

residues in the elastin mimetic sequence with a cystamine residue that can be reduced and then oxidized to form disulfide crosslinks.

The physical properties of the elastin mimetic materials were observed to determine the effect of crosslinking on these materials. Effects of particular interest for this research included the thickness, swelling ratio and water content of the constructs upon hydration. The potential to modulate the mechanical properties of these materials was explored to tailor the stent designs and to use different designs based on the achievable strength. The ability to incorporate drugs and tailor the drug elution properties was investigated for their potential to successfully combat the smooth muscle cell overproliferation event. As a corollary, the potential to enhance the endothelialization of the stent constructs was examined as endothelialization is of paramount importance to combat late stage thrombosis. This can be achieved by enhancing the healing ability of the stent through pharmacologically promoting, as well as physically trapping circulating endothelial progenitor cells. Finally, the biocompatibility of the different crosslinkers was explored. Crosslinking and modulating these biomaterials must not come at the expense of the biocompatibility of the material. While glutaraldehyde is a well documented effective crosslinker, its lack of biocompatibility has decreased its utility. Therefore, other biocompatible agents such as genipin have become more common.

4.2 Materials and Methods

Production and Fabrication of TFE Films

The recombinant elastin mimetic polymer, LysB10, studied in this report has been described elsewhere[87]. Briefly, the elastin mimetic material is composed of a 58 kDa hydrophilic central midblock composed of 28 repeats of the elastic sequence $[(VPGAG)_2VPGEG(VPGAG)_2]$ flanked by 75kDa hydrophobic endblocks composed of 33 repeats of the pentapeptide sequence$[IPAVG]_5$. To allow for enhanced crosslinking the residues [KAAK] were located at the C terminus and between the midblock and endblock.

These proteins were further modified to allow for sulfide crosslinking. The LysB10 was dissolved in phosphate buffered saline(PBS) with a 20-fold molar excess of cystamine and 5-fold molar excess of N-(3-dimethylaminopropyl)-N‘-ethylcarbodiimide (EDC). These were allowed to react for 72 hours at 4ºC. The elastin mimetic was then purified with dialysis. When necessary, the cystamine group was reduced with (tris(2-carboxyethyl)phosphine(TCEP) to form thiols.

For all of the analysis, films were solvent cast from 100mg/mL lyophilized protein dissolved in 1mL 2,2,2-Trifluoroethanol(TFE). The solution was solvent cast in Teflon molds, yielding films with a thickness of approximately 100µm ± 12µm. The films were then placed on a sterile glass grid and diced into the desired dimensions. The samples were then weighed to ensure that any change in size was accounted for; the average weight of the films was 8mg ± 1.7mg

Crosslinking Conditions

Cast films were crosslinked via one of the following crosslinking methods. Glutaraldehyde vapor phase crosslinking was achieved by placing the films on a glass plate suspended above a reservoir of 25% (w/v) solution of glutaraldehyde (GTA) (Sigma Aldrich, St. Louis, MO) in water in a closed chamber and then vapor crosslinked for 48 hours. The thiol air oxidation setup consisted of leaving the film in a Petri dish for a period of 5 days. The films were then removed, vacuum dried for 48 hours, and then rinsed.

Solution phase glutaraldehyde crosslinking was completed using 0.5% glutaraldehyde. The solution was made from 25% glutaraldehyde and molecular grade water. The films were immersed in the solution phase GTA for 24 hours. Genipin crosslinking was completed by solubilizing 6mg/ml Genipin into phosphate buffered saline (PBS). The solution was allowed to crosslink for 24 hours. The solution phase thiol crosslinking was accomplished by reducing the cystamine groups with TCEP for six hours. The films were then placed in 0.1% H_2O_2 solution made from 30% sodium hydroxide(Sigma Aldrich) and PBS. The pH of the solution was raised to 7.3 using sodium hydroxide.

Confined crosslinking was achieved through the device shown in Figure 4.1. The device consists of two glass slides(2.5mmx7.5mmx1mm) and filter paper(Millipore) placed on the top and the bottom of the protein film. Two U shaped plastic connectors were compression fit over the setup to minimize swelling. The confined system was placed in a Petri dish filled with the applicable solution phase crosslinkers.

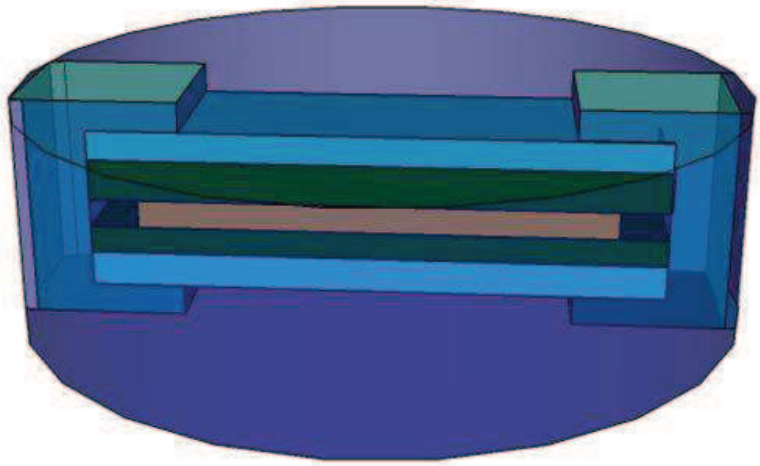

Figure 4.1 Confined crosslinking setup

To remove unbound crosslinker, a rinsing procedure was utilized after all crosslinking procedures to remove any residual crosslinker. It consisted of 5 exchanges of PBS over a 48 hour period.

Evaluation of Physical Properties

The surface area, thickness, and weight of the films were measured in the dried and hydrated state after crosslinking. The films were imaged under 4x and 10x magnification to determine their surface area and thickness. The weight of the films was obtained on a mechanical balance (Mettler-Toledo, Columbus, OH). The thickness ratio, equilibrium water content, and equilibrium swelling ratio were determined according to Equations 1, 2, and 3, respectively, and were expressed as mean ± standard deviation. Six protein strips were tested for each experimental group.

Equation 1.

$$Thickness\ Ratio = \frac{T_{HAC}}{T_{BC}}$$

T_{HAC} → Hydrated thickness after crosslinking

T_{BC} → Dried thickness before crosslinking

Equations 2 and 3.

$$Equilibrium\ Water\ Content = \frac{W_H - W_D}{W_H} \qquad Swelling\ \ Ratio = \frac{W_H}{W_D}$$

W_H → Hydrated Weight

W_D → Dry Weight

2.4 Evaluation of Degree of Crosslinking

The amount of extractable protein was obtained by placing the cast protein films into 1mL of the casting solvent for seven days at 37℃. The films were removed from the TFE solution, placed in a vacuum chamber for 72 hours to remove any residual TFE, and then weighed. Six protein strips were tested for each experimental group. The percent of extractable protein was determined using Equation 4 and expressed as a mean ± standard deviation.

Equation 4.

$$\%\ Extractables = \frac{W_D - W_E}{W_D} * 100$$

W_D → Dry Weight

W_E → Weight After Extraction

The extent of crosslinking site utilization was determined using the ninhydrin assay for lysine residues and Ellman's reagent for thiol groups. The extent of crosslinking was calculated using Equation 5 and expressed as a mean ± standard deviation. Six protein strips were tested for each experimental group.

Equation 5.

$$\%\ Crosslinked = \frac{X_U - X_C}{X_U} * 100$$

X_u → Free sites in uncrosslinked samples

X_C → Free sites in crosslinked samples

To determine the quantity of amino groups that were not crosslinked the ninhydrin assay was used[139]. The elastin mimetic samples were weighed and heated with a ninhydrin solution for 20 minutes. Then the solution was allowed to cool to room temperature and diluted in 95% ethanol. The optical absorbance of the solution was quantified with UV–visible spectrophotometer (Cary 50; Varian Inc., Palo Alto, CA) at 570 nm using glycine at various known concentrations as a standard curve. Six protein strips were tested for each experimental group.

Ellman's reagent was utilized to quantify the extent of thiol modification of the elastin mimetic. A cysteine standard curve was generated with 0 to 1.5 mM cysteine dilutions in a reaction buffer of 0.1 M sodium phosphate with 1 mM EDTA, pH 8.0. Ellman's reagent solution was prepared by dissolving 4 mg Ellman's reagent in 1 mL of

reaction buffer. Reduced 10 mg/mL elastin mimetic-cystamine solutions and the surfaces of a 10wt% hydrogel were reacted with Ellman‘s Reagent solution diluted in reaction buffer and incubated at room temperature for 15 minutes. Absorbance at 412 nm was quantified with UV–visible spectrophotometer (Cary 50; Varian Inc., Palo Alto, CA). Values were compared to a standard curve to obtain the experimental sample concentrations.

Mechanical Analysis of Hydrated Films

Uniaxial stress strain tests were performed on the different crosslinked films. The test consisted of a preconditioning protocol that consisted of 10 cycles of 10% strain with offloading periods of 5 minutes between each cycle; preconditioned samples were then tested until failure. The instrument used was a dynamic thermal analyzer(DMTA V, Rheometric Scientific, Inc. Newcastle, DE) with a 15-N load cell in the inverted orientation to allow samples to be immersed in a jacketed beaker with 37℃ PBS. The tensile tests were used to calculate the elastic modulus, strain at failure, and ultimate tensile strength. The elastic moduli for the confined and unconfined films were taken at two linear regions, 5%-15% strain and 50%-175%, occurring before and after the yield point. Since the maximum travel distance of the DMTA is 23mm some of the more extensible materials had to be moved to be tested to failure on the miniature materials tester (Minimat 2000, Rheometric Scientific) in tensile deformation mode at a rate of 5 mm/min conducted in air at room temperature. All samples were coated with a thin layer of mineral oil to prevent dehydration. For both DMTA and Minimat testing, samples were cut into a dumbbell shape using a stainless steel die with gauge dimensions of 13 mm x 4.75 mm.

Drug Studies

The model system used to explore the drug elution of these materials was based on a ring from the current stent design. The surface area of the current three ring stent prototype has a surface area of 157.78mm^2 and contains a drug volume of 220µg. This yields a surface area drug concentration of 1.39µg/mm^2. The model system has an area of 28.27mm^2 and requires 39µg of drug. The samples were cast in a 30x24mm mold and resulted in a film thickness of approximately 100µm ± 12µm. The films were then cut with a razor blade into the six equal strips that approximate the drug eluting ring. This is accomplished by placing the sample on a sterile glass sheet that is placed onto a grid structure that facilitates accurate cutting of the samples. The samples are then weighed to ensure that any change in size was accounted for; the average weight of the films is 8mg ± 1.7mg. The constructs were placed in centrifuge tubes containing 2mL of release medium and placed on a shaker rotating at 500rpm at 37℃. The release mediums used were 90:10 PBS and Ethanol at 37ºC[80]. To ensure that the release mediums were not significantly altering the constructs their thicknesses and weights were recorded. Samples of the release medium were removed at 2 hours, and 24hours and every subsequent day until the drug release was no longer quantifiable. All of the elution profiles were determined with UV spec and a standard curve ranging from 0.5µg/ml to 150µg/ml.

There were three drug incorporation strategies that were utilized. The first consisted of two depositions of 333µl of 100mg/ml LysB10 protein TFE solution and a top coat of 333ul of 100mg/ml LysB10 in TFE with 1mg of drug. The second strategy consisted of three casts of 333µl of 100mg/ml LysB10 in TFE with 333µg of the drug.

The third strategy consisted of one layer cast from 333µl of 100mg/ml LysB10 in TFE, a second layer of 333µl of 100mg/ml LysB10 with 1mg of drug, and a third layer of 333µl of 100mg/ml LysB10 in TFE. The effect of crosslinking was determined on the stent with drug throughout the stent. The films were crosslinked as previously described. The samples were removed and placed in sterile PBS, and this process is repeated for a total of 8 washes. Because some of the drug could elute during the process, a drug retention quantity will be calculated as seen in Equation 6.

Equation 6. Drug Retention

$$DR(\%) = \frac{weight\ of\ drug\ in\ stent\ after\ crosslinking}{weight\ of\ drug\ in\ stent\ before\ crosslinking} x100\%$$

Cell Studies

In all of the cell experiments, 75µl of 10% elastin mimetic were cast into wells of a 96 well plate and allowed to evaporate over 48 hours with the lid on and subsequently placed in a vacuum for 120 hours. The films were then subjected to their respective solution phase crosslinking procedures. All samples, including the control films, were washed 10 times over the course of 48 hours at room temperature. The samples then had 50 µl of 250ug/mL solution of Fn adsorbed to the surface for 24 hours. The samples were then washed once with PBS and cells were seeded. Since the assay used was a terminal assay, the 2 hour and 48 hour plates were discrete but were prepared at the same time from the same solutions.

All of these studies used human umbilical vein endothelial cells (HUVECs) (Clonetics). Prior to use, HUVECs were cultured in a t75 flask with endothelial growth medium-2 (EGM-2, 2% serum, Clonetics) and were kept in a humidified, 5% CO_2

environment at 37℃. The cells were passaged, upon confluence, using standard culture techniques. All cells used in the study were between passages 4 and 9.

For the adhesion assay, HUVEC suspensions were prepared at a density of 200,000 cells/mL, and for the proliferation assay the density was decreased to 50,000 cells/mL. The samples were seeded with 100µL of the cell suspension. The plates were then incubated for 2 hours at 37℃. To determine ad hesion, after 2 hours the wells were washed three times with PBS. The plates were then placed in the -80℃ freezer for 24 hours. To explore cell proliferation on these materials, the cells were seeded as discussed above. At two hours the surfaces were rinsed with 100µl of media three times to remove unbound or loosely adhered cells. The bound cells were cultured for a total of 48 hours in 100µl of media

Cell adhesion and proliferation was determined with the CyQuant Cell Proliferation Assay Kit (Molecular Probes). Briefly, after thawing frozen cells to enhance lysis, the CyQuant cell lysis buffer was added to each sample, along with CyQuant fluorescence reagent. Samples were then measured in a microplate spectrofluorometer. A standard curve ranging from 50,000 to 100 cells was created for each sample set.

Statistical Analysis

Comparison between groups was analyzed via ANOVA and a paired, two-tailed student‘s t-test, with $p<0.05$ considered to be significant. Results are presented as mean ± standard deviation. The minimum sample size had an n=6 value

4.3 Results

Results Physical Properties

The physical properties of the elastin mimetic materials were modulated by the crosslinker used. The thickness ratio, swelling ratio, and water content were the physical properties that were explored. Changes in the area of the film were also measured in the x and y direction but there was no significant difference in any of the films. The following results demonstrate an ability to modulate the physical properties of the stent by careful selection of both crosslinking agent and crosslinking setup.

Thickness: There were two major trends in the crosslinking thickness data(Figure 4.1A). First the vapor phase crosslinkers produced the films with the lowest swelling ratios. Second the ability to confine the films when using solution phase crosslinkers allowed for a reduction in the thickness ratio. The thickness of the noncrosslinked elastin mimetic films had a swelling ratio of 44%. The genipin was slightly less at 36%. The confined crosslinking setup was able to significantly reduce the thickness ratio to 14%. In the glutaraldehyde system, the unconfined samples had the highest swelling ratio although it was not significantly higher than the controls. The confined crosslinking reduced the swelling ratio to 25% and that was further reduced to 6% by the vapor phase crosslinking method. In the thiol based systems, the thickness ratios of the unconfined samples were slightly lower than the controls at 38%. The confined crosslinking thickness ratio was significantly lower at 21%, and the vapor phase crosslinking method yielded an ever lower ratio of 7%.

Water Content: In the water content studies, both the solution phase crosslinkers and the confined crosslinkers were not significantly different from the controls. However, the confined samples had a significantly lower water content

compared to the unconfined crosslinking samples. The water content of the two vapor phase crosslinkers was significantly less than all other groups, but they were not significantly different from each other. On average the confined crosslinked films had 19.3% less water than the solution phase crosslinkers and the vapor phase crosslinked constructs had 30.4% less water than the solution phase unconfined samples.

Swelling Ratio: The swelling ratios for the solution phase crosslinkers were higher than the controls; however, the difference was not significant. The swelling ratios between the solution phase unconfined crosslinked constructs and the solution phase confined crosslinkers were significantly different in all crosslinking groups. The crosslinking modality with the largest difference was the glutaraldehyde samples. The vapor phase crosslinked constructs were significantly different from the unconfined crosslinked samples but were not significantly different than the confined crosslinking setup. Compared to the unconfined crosslinking, the confined crosslinking and vapor phase crosslinking setups were able to reduce the average swelling ratio by 8.3% and 11.8% respectively.

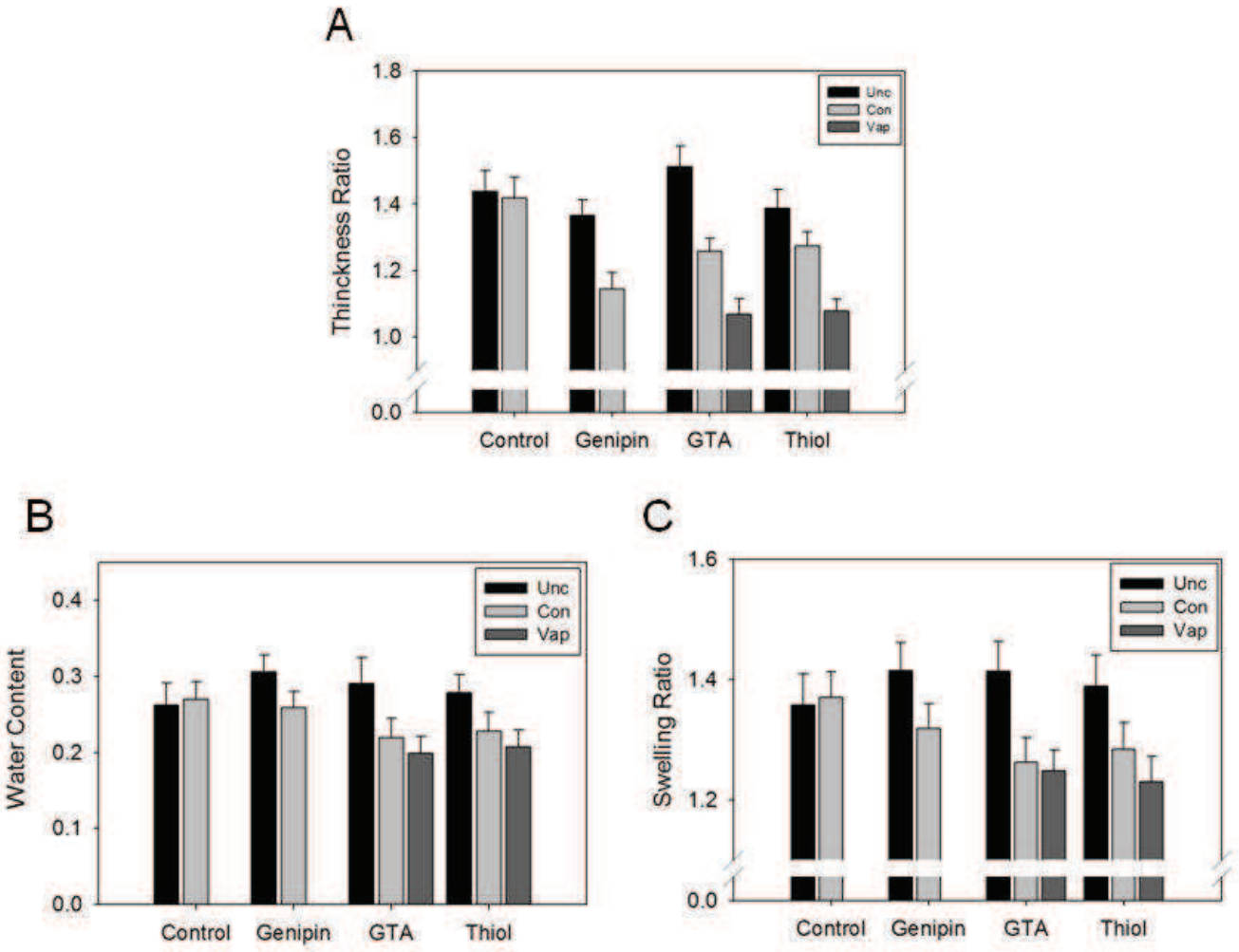

Figure 4.2. (A) Thickness ratio of the different crosslinked samples, (B) Water content of the various crosslinked films, and (C) The swelling ratio of the different crosslinked samples. The unconfined samples are shown in black the confined are light gray and the vapor are dark gray.

Results Mechanical Analysis

Samples were preconditioned and then strained until failure. All of the hydrated films possessed plastic-like deformation, consisting of a linear stress strain relationship, until a yield point and then another linear stress strain relationship until failure. The four parts analyzed were the elastic modulus from 5-15% strain and 40-175% strain, ultimate tensile strength, and the strain at failure(Figure 4.3).

The stress strain plots of the control and crosslinked samples all have two linear stress strain curves from 5 -15% and 40-175%(Figure 4.3). On the stress strain plots, there is a region from 0-3% that shows some minor plastic deformation occurring during the preconditioning step. The plastic deformation region is larger on the crosslinked samples then the control samples.

The moduli for 5-15% strain in the control samples were not significantly different. However, they were significantly different than all crosslinked samples. The materials with the highest modulus in this range were the GTA samples, and the vapor and confined crosslinking thiol samples which were significantly different than the other crosslinking methods. In the higher 40-175% strain zone, the uncrosslinked samples were significantly different from all other materials tested. The stiffest sample in this range was the vapor phase crosslinked sample. The genipin samples wee also the least stiff of the crosslinked samples.

The confined crosslinking setup produces stiffer materials than the solution phase crosslinking setup. In the case of genipin, confined crosslinking increased the modulus by 46% in the 5-15% range and was not statistically different in the 40-175% range. The glutaraldehyde samples had a higher modulus than all respective groups. The other trend worth noting is that the values from the confined samples were higher than those of the unconfined samples. These values are 1.5 to 3.5-fold greater than those calculated for the uncrosslinked control.

The 5-15% modulus of the control confined and unconfined samples were almost identical at 0.20MPA. The glutaraldehyde confined and vapor phase crosslinking setups had the highest average moduli at 0.73MPa and 0.69MPa, respectively. The genipin

crosslinked samples had the lowest modulus values but were still more than 50% higher than the control uncrosslinked samples. The thiol crosslinking also showed a high modulus especially for the vapor phase and confined samples.

The second modulus is two orders of magnitude smaller than the first for both control samples and genipin crosslinked samples. The vapor phase glutaraldehyde and thiol crosslinking strategies have significantly higher moduli from 40%-175% strain. In both the genipin and thiol samples, the solution phase unconfined was significantly lower than the solution phase confined crosslinking setup.

The slope of the second modulus is much less steep than the modulus in the 5-15% range. In the control samples, modulus 1 is 52 times greater than modulus two. The solution phase glutaraldehyde samples and the genipin unconfined solution phase crosslinker samples all have a second modulus that is approximately 60 times smaller than the modulus between 5-15%. The thiol vapor had the smallest ratio of modulus 1 to modulus two with modulus 1 being 34 times greater than modulus 2.

The strain at failure of the control samples was significantly higher than any of the crosslinked samples. Also the strain to failure of the solution phase unconfined glutaraldehyde and thiol samples were significantly higher than the vapor phase crosslinking samples. The glutaraldehyde confined crosslink samples were significantly different than the solution phase crosslinker.

Overall the ultimate tensile strength of the material can be increased by 42% for solution phase genipin up to 107% for vapor phase glutaraldehyde over the control samples. In both the thiol and vapor crosslinking samples, the vapor phase and unconfined solution phase crosslinking setups were significantly different. In all three

setups the confined crosslinking tended to produce a higher UTS although it was not significant.

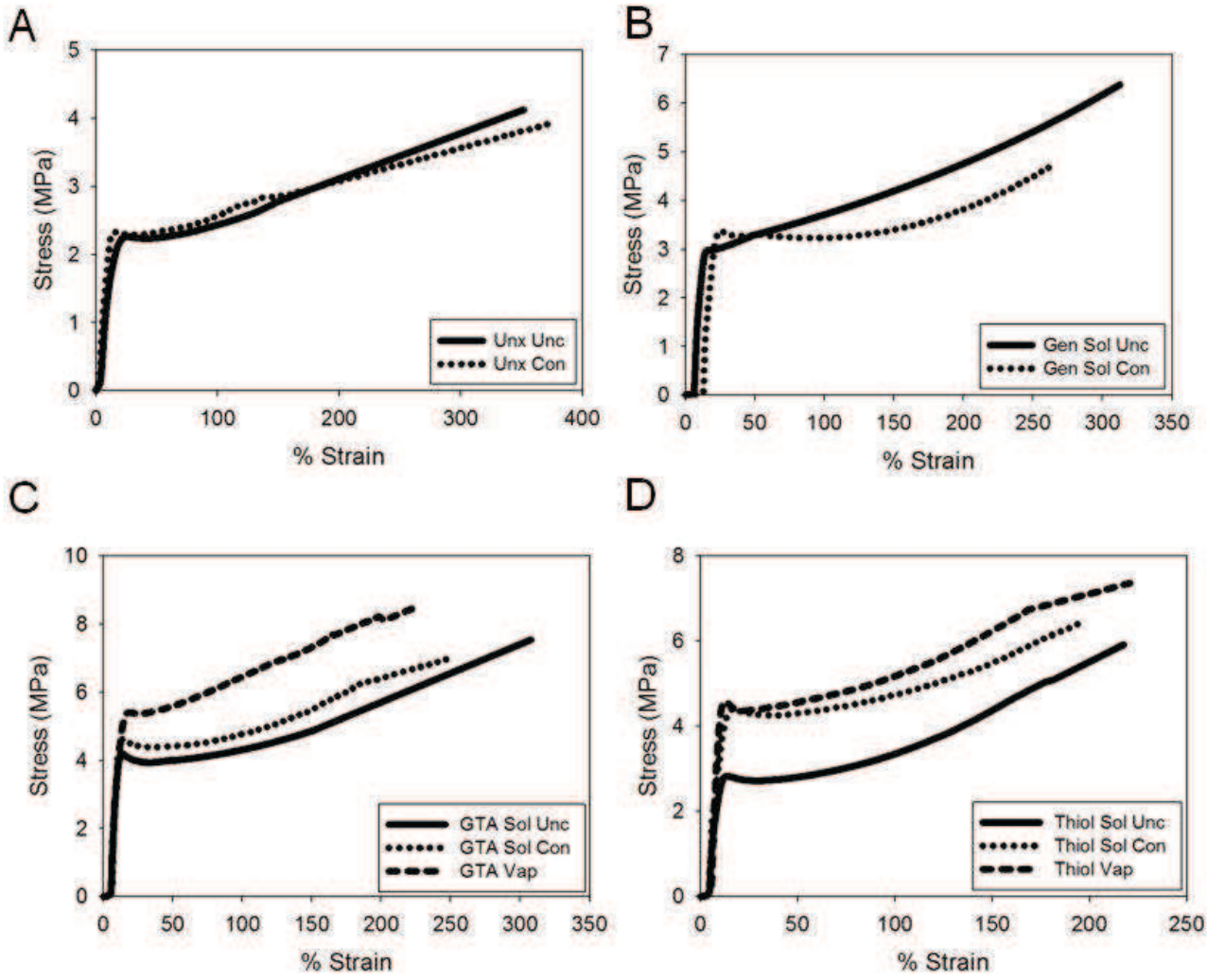

Figure 4.3. Stress strain plots for (A) control constructs, (B) genipin crosslinked constructs, (C) glutaraldehyde crosslinked constructs, and (D) thiol crosslinked crosslinks**.**

Table 4.1 Compiled mechanical parameters of noncrosslinked and crosslinked protein films

Sample	Modulus (MPA) (5-	Modulus (kPA)(50-	Strain at Failure (%)	Ultimate Tensile
Control Unc	0.20 ± 0.01	3.79 ± 0.36	389.24 ± 43.00	4.05 ± 0.33
Control Con	0.20 ± 0.03	3.86 ± 0.50	375.81 ± 31.00	3.89 ± 0.38
Glut Sol Unc	0.62 ± 0.02	10.00 ± 2.04	302.28 ± 31.00	6.77 ± 0.63
Glut Sol Con	0.73 ± 0.07	12.10 ± 1.76	254.81 ± 22.00	7.51 ± 0.48
Glut Vap	0.69 ± 0.08	17.20 ± 2.16	231.41 ± 25.00	8.39 ± 0.53
Genipin Sol Unc	0.32 ± 0.08	5.28 ± 1.44	273.72 ± 26.00	5.78 ± 0.45
Genipin Sol Con	0.36 ± 0.06	8.24 ± 1.03	319.92 ± 31.00	6.25 ± 0.46
Thiol Sol Unc	0.43 ± 0.05	9.54 ± 1.23	281.72 ± 28.00	6.61 ± 0.61
Thiol Sol Con	0.61 ± 0.08	12.27 ± 1.26	238.39 ± 21.00	7.43 ± 0.57
Thiol Vap	0.63 ± 0.07	18.23 ± 2.40	216.19 ± 19.00	7.60 ± 0.55

Results Determination of Degree of Crosslinking

The degree and type of crosslinking was calculated using percent extractables as a measure of crosslinking between chains and degree of crosslinking as a measure of interaction among crosslinking sites(Table 4.2). To explore the percent extractables, the samples were placed in their casting solution and the percent incapable of being resolubilized was determined. Noncrosslinked films placed in the casting solvent dissolved instantaneously, resulting in 100% extractables. The next highest was the thiol vapor phase crosslinker at 16.62 ± 1.96%. It should be noted that the thiol solution phase crosslinked sample had much lower percent extractables, 6.81±1.28%. The genipin confined had the third highest percent extractables at 11.74± 2.5% which was significantly higher than the solution phase genipin crosslinking. The glutaraldehyde

vapor phase samples had the highest percent extractable and the solution phase unconfined had lower percent extractable values; however the differences were not significantly different. The values for percent extractables are good agreement with previously published values[85].

Table 4.2 Shows the percent extractables of the different crosslinking methods and shows the degree of crosslinking group interaction.

Sample	Percent Extractables	Degree of Crosslinking
Control Un	100.00	3.27 ± 2.74
Control Con	100.00	2.56 ± 1.54
Glut Sol Unc	7.55 ± 2.19	90.64 ± 2.01
Glut Sol Con	8.98 ± 1.96	91.93 ± 1.58
Glut Vap	9.38 ± 1.66	95.68 ± 0.26
Genipin Sol Unc	6.93 ± 1.51	92.61 ± 0.50
Genipin Sol Con	11.74 ± 2.59	88.53 ± 1.65
Thiol Sol Unc	6.81 ± 1.28	94.89 ± 0.46
Thiol Sol Con	8.90 ± 2.18	87.91 ± 1.23
Thiol Vap	16.62 ± 1.96	66.29 ± 2.59

The degree of crosslinking in the elastin mimetic materials was determined quantitatively with ninhydrin and Elleman's reagent. The GTA and genipin crosslinking strategies rely on lysine residues to form their crosslinks, and the thiol based crosslinking system utilizes modified carboxyl groups. The elastin mimetic films contain 8 lysine residues per repeat and 28 glutamic acid residues per repeat. The thiol modification procedure was able to modify 64±3.5% of the glutamic residues resulting in 17 or 18 crosslinking sites per repeat. The confined crosslinking setups had a

significantly lower degree of crosslinking compared to the unconfined except for the glutaraldehyde. The vapor phase thiol crosslinking system had the lowest degree of crosslinking at 66.29±2.59 compared to the two solution phase crosslinking setups which had degrees of crosslinking that were more than 30% higher than the vapor phase. In the glutaraldehyde samples, the vapor phase has the highest degree of crosslinking followed by the confined solution.

Results Drug Elution

To determine the drug elution of the protein materials, a model system was used. To ensure that this release medium did not change the physical properties, the material thickness and swelling ratio were noted. There was no significant difference between the samples placed in PBS and release medium. The different drug layering and crosslinking techniques were used to see if the drug elution could be tailored.

The first scheme consisted of two layers of elastin mimetic with no drug and a top layer of elastin mimetic with 3.3% rapamycin. The second scheme had the drug mixed in the protein solution and was cast in triplicate. The third sample scheme consisted of a base coat of elastin mimetic with no drug followed by a layer of elastin mimetic with 3.3% drug followed by a top layer of drug free elastin mimetic. Figure 4.4A shows that scheme one has the highest initial burst and an overall faster drug release profile, and scheme three gives the lowest burst and overall slowest drug release. The burst release was 17.91±1.71µg for scheme one, 13.98±1.26 µg for scheme two and 9.55±1.24 µg for scheme three. Interestingly, the release rate for scheme two was the fastest. Also worth

noting was the release of 50% of the drug quantity was delayed from half a day to one day by placing the drug in the middle of the stent instead of throughout the matrix.

The second round of experiments looked at the effect crosslinking would have on the drug delivery kinetics. The drug was distributed throughout the material as described for scheme two. Glutaraldehyde was able to significantly reduce both the burst release and increase the delivery duration. The vapor phase crosslinking was able to retard the drug delivery the most followed by the confined crosslinking. The solution phase unconfined sample had a faster release then the other two (Figure 4.4B). Solution phase genipin crosslinking was able to slow the drug elution profile compared to the control. Also confined crosslinking further suppressed the drug delivery curve (Figure 4.4C). The thiol crosslinking strategy showed the same potential to slow drug delivery. The thiol vapor crosslinking was able to retard the drug elution the best followed by the confined and then the unconfined (Figure 4.4D). The crosslinking studies showed that vapor phase crosslinking materials allows for the slowest drug elution profiles with vapor phase glutaraldehyde and vapor phase thiol having the lowest initial burst (1.44±0.07μg and 2.08±0.78μg) respectively. The confined crosslinking also showed potential to decrease the burst profile and slow the drug release profiles. Finally, it should be noted that crosslinking alone was capable of reducing the initial burst from 13.98±1.26μg to 1.77±1.71μg for glutaraldehyde, 4.55±0.69 μg for genipin, and 9.43±0.93μg for thiol.

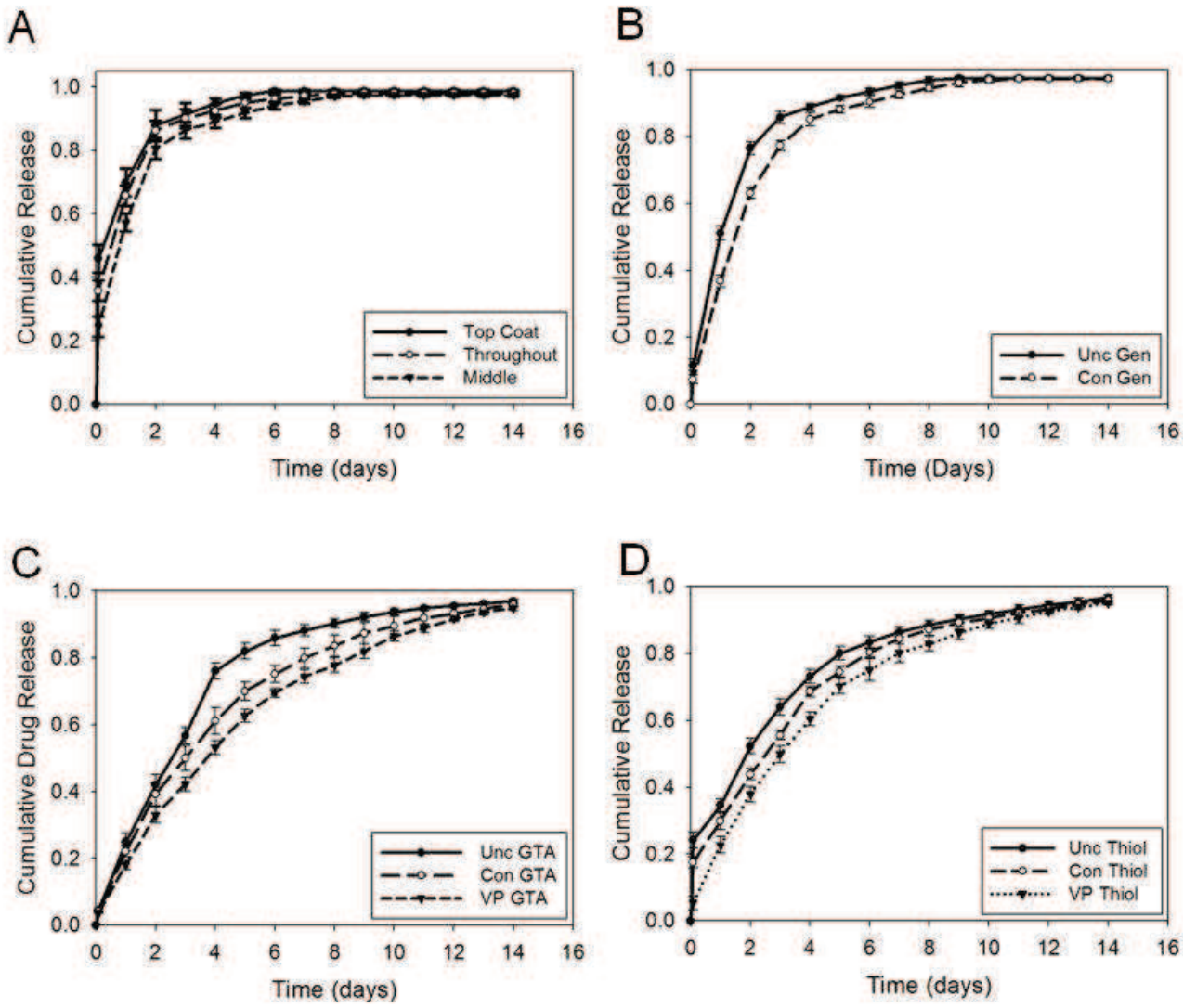

Figure 4.4 (A) Illustrates the elution profile of LysB10 and three types of drug distribution. (B) Depicts the difference between different genipin crosslinking conditions, (C) Shows affect of different GTA crosslinking methods, and (D) Shows the difference between thiol crosslinking methods

Table 4.3 Drug Elution Parameters

Sample Group	Burst Amount (µg)	Rate (% days^{-1})	50% Drug (Days)	DurationAll Drug
Top Coat	17.91 ± 1.71	22.13 ± 0.67	NA ± NA	5.60 ± 0.55
Throughout	13.98 ± 1.26	26.07 ± 1.15	0.49 ± 0.08	6.80 ± 0.84
Middle Layer	9.55 ± 1.24	21.17 ± 0.12	0.95 ± 0.18	8.00 ± 0.55
Glut Sol Unc	1.77 ± 0.09	16.00 ± 0.96	2.69 ± 0.10	11.80 ± 0.84
Glut Sol Con	1.58 ± 0.05	13.20 ± 0.79	3.22 ± 0.29	13.40 ± 0.55
Glut Vap	1.44 ± 0.07	11.83 ± 0.21	3.75 ± 0.09	13.80 ± 0.84
Genipin Sol Unc	4.55 ± 0.69	25.30 ± 0.35	1.26 ± 0.09	8.20 ± 0.84
Genipin Sol Con	2.90 ± 0.54	19.93 ± 0.58	1.80 ± 0.08	9.80 ± 0.55
Thiol Sol Unc	9.43 ± 0.93	10.27 ± 0.12	2.15 ± 0.21	10.56 ± 0.55
Thiol Sol Con	6.83 ± 0.63	8.97 ± 0.21	2.95 ± 0.17	11.98 ± 0.84
Thiol Vap	2.08 ± 0.78	8.60 ± 0.78	3.75 ± 0.14	12.65 ± 0.55

Results Endothelialization

The adhesion and proliferation of endothelial cells on the various crosslinked surfaces was explored. Images of the cellularized surfaces were taken at 2 and 48 hours to observe both cellular morphology and qualitative cellular properties of the material(Figure 4.5). The elastin mimetic film with no Fn adsorbed had notably fewer cells and the morphology of the cells was rounded and not spread out(Figure 4.5A and B). The elastin mimetic with Fn adsorbed showed that the Fn aided in cell adhesion and spreading on the elastin mimetic material. However, there are visibly less cells on this material than the crosslinked materials (Figure 4.5C and D). The genipin crosslinked films with adsorbed Fn showed good morphology, a high cell number, and a large increase in cell number(Figure 4.5E and F). The glutaraldehyde crosslinked films with

adsorbed Fn showed good morphology and cell number; however, the cell number on the 48 hour samples did not show good proliferation(Figure4.5G and H). The thiol crosslinked material seemed to perform best in both adhesion and proliferation(Figure 4.5I and J).The final set of pictures is of the control wells which had Fn adsorbed to non tissue culture polystyrene at 2 and 48 hours, respectively. In all of the crosslinked samples with adsorbed Fn, HUVECs were capable of adhering and spreading. These images give a qualitative value of cell adhesion and proliferation on the different surfaces. To achieve a quantitative value of cell adhesion and spreading, a CyQuant assay was used.

The first parameter that was explored was cell adhesion. The control elastin mimetic with no adsorbed Fn had the lowest cell adhesion and the Fn on non tissue culture treated polystyrene yielded the highest adhesion value. The elastin mimetic film without adsorbed Fn had a cell adhesion equivalent to 20% of the value for the Fn adsorbed control well. This value is half that of the elastin mimetic well that had adsorbed Fn. The fact that adsorbing Fn causes a 2 fold increase in cell binding is a significant finding. The crosslinked samples performed better than the non crosslinked samples. The genipin crosslinked samples performed best with an adhesion rate of over 89% that of the Fn control. The thiol was close at 70% and the glutaraldehyde was the least effective of the crosslinked samples.

To explore the proliferation rates of HUVECs seeded on different surfaces, the cell number was measured at 2 hours and 48 hours. As mentioned in the methods these studies had a lower cell seeding density to allow for proliferation without overcrowding. The uncrosslinked elastin mimetic without Fn does not promote cell

adhesion nor cell proliferation. In all of the other samples, the HUVECs were capable of adhering, spreading, and proliferating. It should be noted that at the 2 hour time point the trends are the same as those of the adhesion assay even with the decreased cell seeding number. As with the earlier adhesion studies, the poorest and best performers of the Fn treated samples are the uncrosslinked elastin mimetic and the polystyrene, respectively. A fold increase in proliferation was determined by dividing the 48 hour time point by the 2 hour time point. The genipin sample had a 5.37±.26 fold increase, the thiol surface had a 4.64±0.39, and the Fn on PS produced a 4.92±.47 fold increase. These were all significantly higher than the other samples, but not significantly different from each other. The elastin mimetic Fn control had a significantly higher fold increase then GTA at 3.93±.34 compared to 3.31±.21. The cells were not able to proliferate well on the elastin mimetic surface with no Fn adsorbed with a 1.44±.67 fold increase. Figure 4.6A and B are the average of four separate experiments consisting of 6 wells for each group.

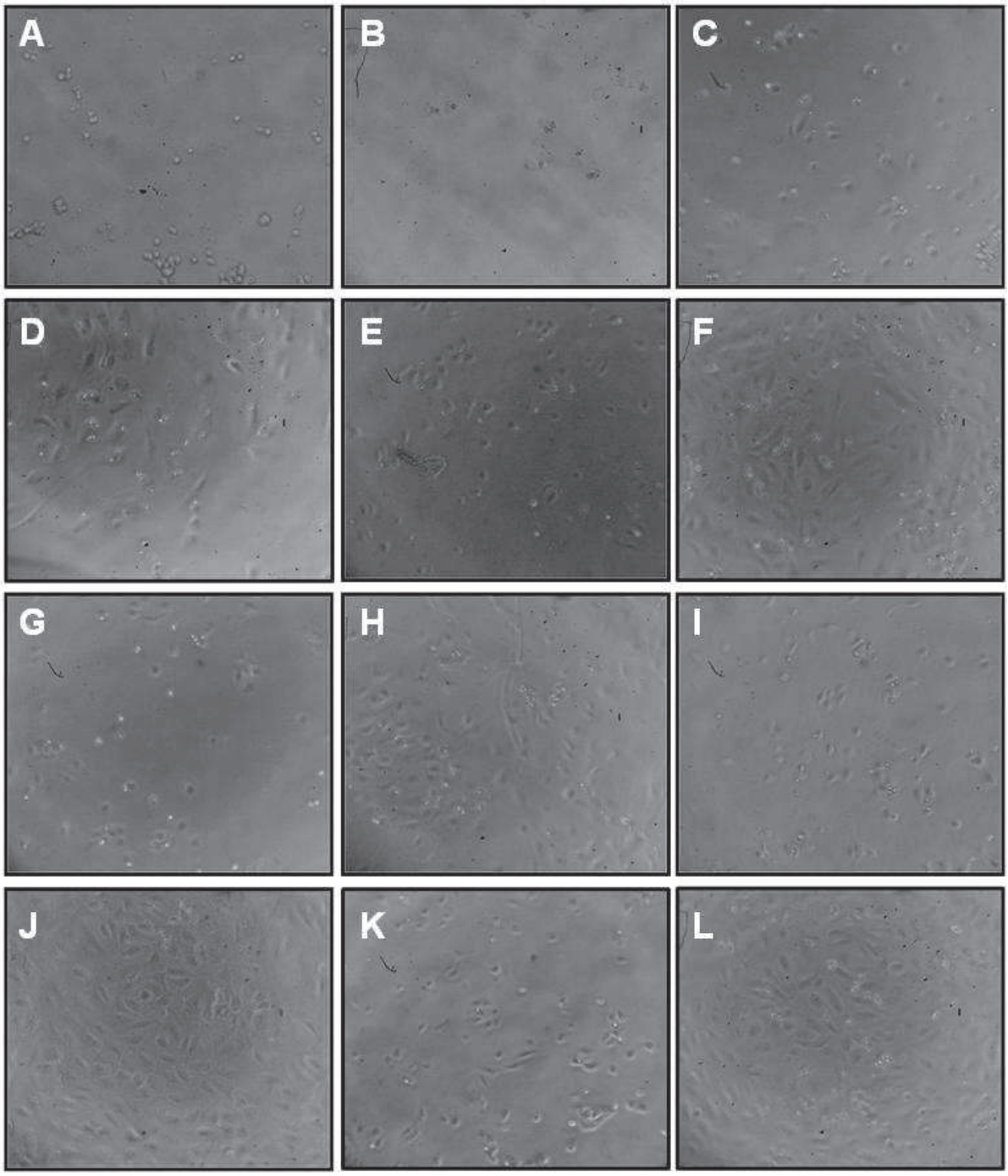

Figure 4.5. Optical images of LysB10 solvent cast films seeded with cells at 2 and 48 hours. Images A and B are for Lys B10 with no Fn adsorbed at 2 and 48 hours respectively. Images C and D are for Lys B10 with Fn adsorbed at 2 and 48 hours respectively. Images E and F are for Lys B10 with Fn adsorbed after a genipin crosslinking step. at 2 and 48 hours respectively. Images G and H are for Lys B10 with Fn adsorbed after a glutaraldehyde crosslinking step at 2 and 48 hours respectively.

Images I and J are for Fn adsorption onto thiol modified Lys B10 crosslinked via disulfides crosslinking step at 2 and 48 hours respectively. Images K and L are for Fn adsorbed non tissue culture PS at 2 and 48 hours respectively

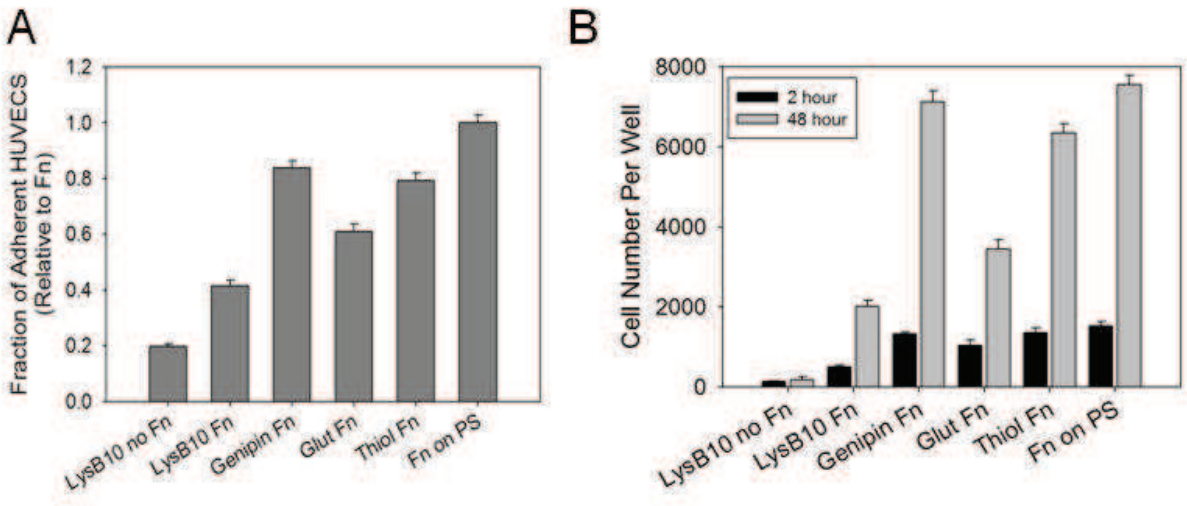

Figure 4.6 (A) Shows the cell adhesion on the different crosslinked surfaces with Fn adsorbed. In this panel all cell numbers have been normalized to the Fn surface. (B) Shows the adhesion and proliferation on the different crosslinked surfaces.

4.4 Discussion

Crosslinkers are a valuable tool to modulate the physical properties of elastin mimetic materials. The initial mechanical testing experiments discussed in Chapter 2 showed that the vapor phase glutaraldehyde crosslinking system provided the necessary mechanical and physical properties for stent development. However, glutaraldehyde does not provide the needed biological properties as it has been linked to inflammation and cytotoxicity. Glutaraldehyde is still used because of its widespread availability and its crosslinking properties are well characterized. However, as the biocompatibility data continues to support the need for implementation of other crosslinking setups, glutaraldehyde will continue to lose favor as an acceptable

crosslinking modality. To this end, we explored a biocompatible lysine crosslinking strategy and a glutamic acid residue modification followed by disulfide crosslinking. The first crosslinking strategy consisted of solution phase genipin crosslinking which is able to crosslink primary amine groups[140]. The second crosslinking method involved further modification of the protein backbone to allow for thiol based crosslinking. An advantage of this thiol crosslinking is that it can take place in the air or, for a higher crosslinking density, constructs can be placed in mild hydrogen peroxide solutions.

The majority of crosslinking agents are solution based and the few vapor based crosslinking strategies are limited to toxic chemical based crosslinkers. Therefore, we attempted to achieve physical properties similar to the vapor phase crosslinkers by confining the solution phase crosslinking process. This process was demonstrated and allowed us to obtain crosslinked films with properties closer to the vapor phase crosslinked constructs.

Physical Properties

There are a range of physical properties that could be examined with regard to crosslinking performance. The physical properties that we explored were selected based on the end goal of using these materials in stenting applications. The first was the thickness ratio, which is useful in ultimate translation into stent design. The ability to minimize the thickness of the material construct allows for the stents to have a higher material percent allowing for the fabrication of more robust stents. The other two physical properties that were explored were the swelling ratio and water content. These parameters were benchmarked, as they translate into the degree of crosslinking, and

allowed us to compare and contrast crosslinking strategies. These properties play a large role in the drug delivery potential of the material.

The goal of this work was to minimize the increase in thickness ratio by looking at a range of crosslinking modalities. Overall the solution phase crosslinkers were not able to decrease the thickness ratio compared to the controls and actually the solution phase glutaraldehyde samples had higher ratios; although they were not significant. The vapor phase and confined crosslinking setups were able to decrease the swelling ratio compared to the control constructs.

It was also noticed that the solution phase crosslinking of the constructs had a higher thickness ratio than the vapor phase. When these parameters were further explored, it was determined that the thickness ratio of the vapor phase constructs could be misleading. As shown in Figure 4.2A, the thickness ratio of the vapor phase crosslinked construct increased by 7.3%. However, this was determined by measuring the dried film pre-crosslinking and the hydrated film post-crosslinking. In the case of the vapor phase crosslinking, the thickness of the construct decreased once it was crosslinked by almost 10% which means that it has an actual ratio of 18.88% which was close to the confined solution phase crosslinker value of 25.83%. The same process occurs for the thiol vapor crosslinking setup. The confined control shows that the confinement itself does not alter the thickness ratio of the construct. The confinement in the other three cases was able to decrease the thickness.

The confined setup seems to produce a very real effect with regard to the thickness ratio, swelling ratio, and water content. The initial thought was that the swelling of the construct occured on a shorter time scale than the crosslinking[141]. It

was hypothesized that confinement limited the swelling of the film, but still allowed the solution phase crosslinker to diffuse in and out of the construct, thereby decreasing the physical parameters discussed above. Overall our unconfined results correlate with another study on genipin and glutaraldehyde crosslinking [142].

Mechanical Analysis

The mechanical behavior of the constructs was studied through stress strain curves obtained from stress strain tests. The samples were preconditioned to allow the microstructure of the constituent polymer chains to obtain a fixed structural relationship allowing for repeatable material properties[143, 144]. Previous characterization of LysB10 under different casting conditions used preconditioning loops of an initial 50% strain followed by 19 loops at 20% strain. That was not possible with these films due to the amount of plastic deformation that was not recoverable, therefore, the constructs were strained to 10% for 20 cycles. Also the calculated stress was based on the force obtained from the DMTA and divided by the cross sectional area of the sample. Since the samples had different physical properties, the cross sectional areas were calculated accordingly. The characteristic curve for these materials has a higher modulus at lower strains, 5%-15% strain, then a yield point, which is followed by a lower modulus until failure. This has been seen in native pig elastin by other researchers[145].

TFE is capable of solvating both the hydrophilic and hydrophobic blocks of this elastin mimetic material which yields a film with interpenetrated blocks upon solvent evaporation. When these constructs are rehydrated, there could be some phase separation and block aggregation. However, some of these portions will remain kinetically trapped. This interphase mixing of incompatible endblocks allow these

materials to have tensile properties that resemble those of polystyrene[102]. This effect can be more dramatic in the vapor phase crosslinking system, as this crosslinking is performed in the dried state preventing the blocks from separating and aggregating like they would when placed in water. This could be a reason the vapor phase glutaraldehyde and thiol crosslinking lead to constructs with stiffer properties.

The other parameter that could explain the difference in the mechanical properties is the hydration level, which can greatly affect the mechanical properties of elastin[146]. Researchers have shown that the hydration of the hydrophobic residues of these materials significantly contribute to the elasticicty of the material[147]. We have previously seen that protein based materials that have decreased water uptake have greater material rigidity and tensile strength. While our previous work focused on changing the hydrophobicity of the protein sequence to achieve this result, we were able to produce it based on crosslinker type and method thereof[87]. Interestingly, the solution phase glutaraldehyde appears to be a more rigid material than the control even when given equal water content.

In order for comparison between the different materials, a modulus was calculated for the linear portion of the plot before and after the yield point. The materials with the highest modulus on the first region of the plot also corresponded to have the highest modulus in the second part of the plot. The control shows that there is no significant difference between the control confined and unconfined samples ensuring that the film was not mechanically altered during the process. In the solution phase crosslinking subset, the glutaraldehyde produced a stiffer material. It has previously been reported that collagen cross-linked by disulfide bridges can attain mechanical

properties equivalent to GTA crosslinked collagen[148]. Our mechanical tests also showed a strong correlation between the vapor phase glutaraldehyde and the vapor phase thiol crosslinking.

The results of the mechanical tests demonstrated the potential to modulate the mechanical properties of the materials by crosslinking them with different crosslinking agents and setups. Most crosslinkers are solution based and, therefore, the ability to increase the mechanical rigidity of a film by confining it during the crosslinking setup was a significant finding. In the field of crosslinkers, most are soluble which in our case, lead to less rigid films due to the hydration of the film before the crosslinking could occur.

Degree of Crosslinking

The degree of crosslinking for glutaraldehyde and genipin have been documented in many reports[139, 149]. However, none of these groups have attempted to crosslink materials in a confined setup. Therefore, it was unknown to what degree of crosslinking was achievable with the crosslinking systems we were using. Our working hypothesis was that we could minimize the swelling of the film through confinement. The confinement would also let the solution phase crosslinker migrate into and out of the material through diffusion. However, initial attempts to confine the crosslinking failed to produce complete uniform crosslinked films. This was most evident in the genipin crosslinked systems, as genipin crosslinking is a colorimetic process in which the protein turns blue. It was evident that the initial crosslinking strategy of confining the protein based material between two glass slides would not allow for the diffusion of crosslinking solution into and out of the material. This resulted in a crosslinking gradient

where the first few hundred microns were deep blue transitioning to a gradient of light blue protein transitioning into uncrosslinked material. To overcome this limitation, the protein sheets were sandwiched between filter paper in the constrained setup. The schematic for this final design is depicted in Figure 4.1. The filter paper allowed for the crosslinking to be present at the top and bottom of the film and decrease the path necessary for diffusion. Once this setup was used, films turned a deep blue and, as noted in Table 4.2, the degree of crosslinking was close to that of the unconfined solution phase crosslinking system.

Thiol vapor phase crosslinked samples had the highest percent extractables of all crosslinked subsets. We believe this is related to the limited mobility of the polymer chains in the dried state. Glutaraldehyde, even in the vapor form where chain mobility can be considered to be the least mobile had the highest degree of crosslinking which seemed counterintuitive. We surmised it is related to glutaraldehyde's capacity of polymerizing crosslinks, thereby allowing it to bridge larger gaps then the other crosslinkers. Amongst the glutaraldehyde crosslinking strategies, the vapor phase crosslinker had the highest percent extractables, possibly related to the lack of movement of the chains in the dried state.

The percent extractables were also higher in the confined cases than the unconfined cases which agrees with the previous thought that less fluid equates to less chain movement. However, this is also counterintuitive because as the swelling increases it could potentially increase the distance between crosslinking sites. There seems to be a question of chain movement and distance caused by swelling.

To determine the crosslinking density, the number of crosslinked groups was determined by subtracting the chemically determined number of groups available before crosslinking and those determined to exist after, via the crosslinking assay. The most accurate way to perform these experiments was in polymer solutions, however, for our studies it was not feasible to solubilize the films. Therefore, we performed these assays on films and the results allowed for comparative analysis between crosslinker type and condition. It should also be noted that the controls showed very little crosslinking and therefore the crosslinking groups seemed to be fairly accessible.

Lysine residues were initially added to the elastin mimetic backbone to aid in crosslinking[87]. Therefore, the ability to crosslink our films by chemically modifying an existing residue rather than recreating an entire recombinant insert allowed us to manipulate the physical properties of the material. The addition of thiols to collagen has been demonstrated previously[150]. The thiol crosslinking strategy showed a degree of crosslinking on par with the solution phase chemical crosslinkers. This was an important finding as the lysine residues capable of crosslinking numbered eight and the number of thiol sites was measured to be between 17 and 18 for a given repeat. The 17 or 18 comes from the degree of modification; our modification scheme resulted in 64±3.5% modification of the film. Therefore, if we could increase the efficiency of the modification we could even have a more crosslinked system. As this crosslinking method does not use an exogenous compound that allows for bridging to occur between the two crosslinking sites a lower crosslinking density and higher percent extractables can be expected. Once the H_2O_2 was added, the chains had an added mobility and the oxidation reaction was more favorable from both a kinetics and chemical view point.

This was shown in both the low percent extractability number and the high degree of crosslinking. Also of interesting note was the ability to subsequently increase the degree of crosslinking with a very mild H_2O_2 solution.

Discussion in Vitro Drug Release

The ability to monitor and tailor the drug delivery kinetics was crucial to optimize drug choice, drug concentration, and incorporation strategy. In order to quantify the delivery kinetics from our test system, we utilized UV spectroscopy because it has high throughput and cost effectiveness compared to HPLC. The ability to monitor the drug release from part of the stent allowed for the testing of more samples while conserving valuable elastin mimetic material and drug. Researchers have shown that planar films of the same thickness as stent coatings provided the same release profile for drugs. They also showed the ability to extend the duration of delivery by changing the bioabsorbable material and drug combination[80]. The drug dose used was based on the BX Velocity from Cordis which is a sirolimus-eluting stent that contains 140 µg of sirolimus per square centimeter of stent-surface area within a copolymer matrix that was 5 to 10 µm thick and was designed to release approximately 80 percent of the total dose of sirolimus in 30 days [5]. A study of a bioabsorbable everolimus-eluting stent had a dose of 98µg for 12mm stent and 153µg for the 18mm stent[151]. In our system, we used a drug dose of 1.4 µg/mm^2 of construct.

The construct was placed in a release medium because of the low solubility of rapamycin in PBS. The solubility of rapamycin in water is 2.6µg/ml and 90mg/ml in ethanol[152]. The release medium ensured there were no boundary conditions that would lead to a slower release profile than expected. We also showed that the release

medium did not affect the physical properties of the construct. However, there was no doubt that the dissolution time of the drug and the ultimate diffusion could be greatly enhanced by the sink conditions that the release medium created. In the body, the diffusion of the drug to the lumen of the vessel could be limited by solubility of the drug in the tissue, as has been shown in studies that examined the process of accumulation, duration, and distribution of the drug in luminal wall[70, 153].

Determining the proper drug elution profile was complicated by the delicate balance between adequate drug dosage over time and minimal local toxicity. The biggest unknown in the drug eluting stent literature is the range for acceptable drug release profiles. Drug elution exists to combat the smooth muscle cell overproliferation that occurs after stent expansion. An argument can be made that the drug elution only needs to occur during this period of overproliferation. Edelman et al. proposed the most referenced model for vascular healing after stenting, and this model shows smooth muscle cell proliferation escalates until day 10 [154]. Since there was no consensus as to an ideal system, we referenced the literature on existing stent platforms. These references showed release systems that had two unfavorable conditions. First, the bulk of the antirestenotic agent remain entrapped in the drug eluting coating, and there was limited sustained release. In the case of the TAXUS stent, the slow and moderate release showed a burst but no sustained release. The fast release had a large burst and then a slowed sustained release at a very low drug concentration [155]. The goal of our research was to be able to incorporate the drug into the stent matrix and get an initial burst, sustained release, and total release of the drug from the matrix.

Since the constructs were made from serial castings of elastin mimetic several strategies to incorporate drugs exist. The first incorporation strategy employed utilized a top coat similar to the commercial stent platforms. Since serial castings do not solubilize the previous layer, we were able to perform serial castings of different layers. For the top coat strategy, we deposited two layers of elastin mimetic solution without drug and then a final third layer of elastin mimetic with drug incorporated. The drug elution profiles from these constructs were rapid and included a big burst as seen in Table 4.4. The second strategy looked at incorporating drug throughout the matrix, which is common in the bioabsorbable stent literature. The second strategy had the most dilute drug concentration and drug diffusion was able to occur at both surfaces at time zero. This system did not have as large a burst as the top coat strategy. However, the drug diffusion was still rapid, and the drug was exhausted between day six and seven. The third strategy explored the potential of placing the drug in the middle cast layer. We believed that concentrating the drug in the middle of the construct would allow us to increase the drug concentration leading to a longer dissolution time and ultimately a longer elution time from the construct. Incorporating the drug in the middle layer did allow for a decreased burst and a slower release profile. The goal of this strategy was to increase the path length that the drug must travel and increase the dissolution time.

It was hypothesized that the addition of a crosslinker could alter the drug elution profiles. The first issue examined was the potential for drug elution into the crosslinking solutions. The drug retention was calculated using Equation 6. As documented previously, the solubility of the rapamycin in PBS is very low. As such we believe this is why the drug did not elute into the crosslinking solution. The drug release into the

crosslinking solution was examined by testing the crosslinking solution for drug release. Also the sample constructs were solubilized in TFE and the drug concentration was noted. The drug retention rate of the stents was 98.21±1.34%.

The ability to modulate the drug release occured on several fronts. First, the films had decreased swelling ratios which were proportional to drug released because higher swelling ratios aid in solubility and diffusion of the drug. Secondly, the crosslinks provided a higher degree of tortuosity, thereby increasing the elution time of the drug from the material. Researchers have shown that the drug diffusion coefficient through hydrogels decreases as the cross-linking density increases and as the equilibrium degree of swelling decreases[156].

Crosslinking has been shown throughout the literature to increase the effective diffusivity of the constructs [157]. Glutaradehyde has been known to substantially change the microstructure of gelatin constructs which in turn altered the rate and extent of drug released from such implants[158]. The higher the crosslinking density, the larger effect it can have on the microsturcture, thereby modulating the drug release[159]. This was observed in our system as well. The crosslinks have the ability to decrease the porosity of the films[160]. As shown in the physical parameters section, some of the crosslinking strategies were able to increase the volume fraction of the protein as well as decrease the solution inside the construct. Both of these should increase the drug elution profiles from the construct as they decrease the space available between macromolecular chains[161].

Since our current system is diffusion controlled, the ability to extend the retention time of the drug further would be very challenging because of the hydrated structure of

the matrix. We have shown that placing the drug in discreet sections and crosslinking can influence both the initial burst and the release times. In the future work section of Chapter 6, we discuss ways to delay the dissolution time of the drug and slow the diffusion of the drug from the construct.

Discussion Cell Studies

It has been noted in previous studies carried out in our lab that the elastin mimetic material is not ideal for rapid endothelialization. Therefore previous investigations have lead to the incorporation of cell binding motifs into the protein backbone and the incorporation of Fn. The concentration of Fn allowed for adhesion to these constructs and enabled us to achieve the desired endpoint. However, it should be noted that increasing the Fn concentration should allow for increased adhesion rates in the two hour study.

There are several potential ways to incorporate Fn onto these biomaterials. Mixing the Fn in the material was not practical as the Fn would be throughout the stent, ultimately wasting Fn and providing Fn to the smooth muscle cells. The Fn concentration on the surface would be relatively low as well. Therefore, we adsorbed Fn onto the surface to avoid the detriments of mixing. The adsorption of FN on the surface can be performed either before or after the crosslinking step. Initially we thought incorporating the Fn onto the surface before crosslinking would enhance the long-term availability of Fn on the surface of the materials. However, we found that adsorbing the Fn onto the matrix before crosslinking did not yield beneficial results. It was hypothesized that the strenuous washing process used to ensure all crosslinker was

removed also washed out the Fn. For our application, the most feasible economical choice parameters to incorporate Fn onto the surface of the stent was explored.

The most unexpected result from the cell studies was the lower adhesion and proliferation characteristics of non crosslinked elastin mimetic films with Fn. Before performing the experiments, these films were expected to perform equal to or better then the crosslinked groups. However, throughout all of the tests these films had lower cell adhesion numbers than the other materials. A plausible explanation is the Fn adsorbs at a different concentration or conformation compared to the other three surfaces. In previous work completed by our group[162],a couple of trends were noted that seem to exist in these materials. The first is that cells preferred 10% elastin mimetic compared to 6%. Therefore, there is a possibility that denser gels allow for enhanced Fn adsorption. The other trend is that cells adhered at higher rates on crosslinked materials compared to noncrosslinked materials, and it was attributed to the crosslinked materials' ability to retain the Fn[162]. However, it has been shown in the literature that the stiffness of the materials the cells are grown on can greatly affect their behavior[163].

Amongst the crosslinked materials, genipin and thiol had very good adhesions rates while glutaraldehyde significantly trailed these two, which fits with the current literature in this area. Xi –xun et al. showed HUVEC cell number over a 1, 3, 5 , 7, and 9 day time course increased on the control and on genipin; however, the constructs crosslinked with glutaraldehyde showed a decrease in cell proliferation[164]. Sung et al. showed cell viability was decreased in porcine pericardium crosslinked with glutaraldehyde compared to genipin[165]. The ability of cells to adhere to collagen

crosslinked with a variety crosslinkers was markedly different and the cellular morphology was directly related to the crosslinker[166].

4.5 Conclusion

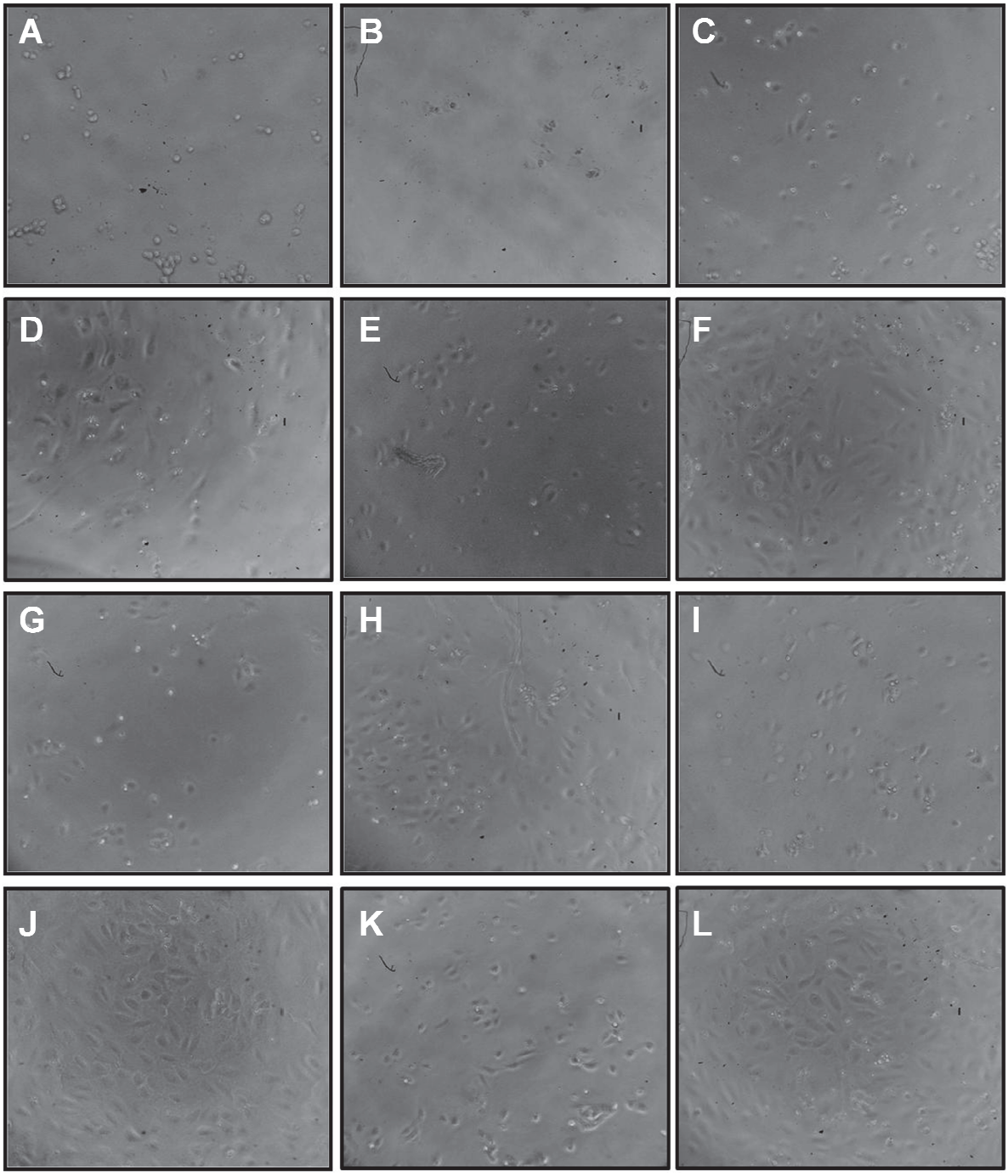

The ability to tailor the physical, mechanical, drug delivery, and endothelialization properties while achieving favorable biocompatibility was achieved. The ability to minimize the physical parameters of thickness ratio, swelling ratio, and water content allowed for the creation of thinner struts and also helped achieve favorable mechanical and drug delivery properties. The ability to modulate the mechanical properties allowed for the use of biocompatible crosslinkers capable of producing acceptable mechanical properties. The drug delivery release kinetics were able to be slowed by changing the crosslinking conditions and setup. The successful endothelialization of the crosslinked constructs was also demonstrated. Finally, this work also showed the ability of using thiol based crosslinking to act as another method to crosslink elastin mimetic materials. The ability to confine the crosslinking process showed that the properties can be shifted to be more comparable to those of vapor phase crosslinkers.

CHAPTER 5

In Vitro and In Vivo Stent Deployment

5.1. Introduction

The development of a protein based stent provides the framework for a method to overcome the limitations of existing stent platforms. In the previous three chapters, we have reported the ability to design, fabricate, test, and tailor protein based stents. To our knowledge, this is the first time that the development of a purely protein based stent has been explored, much less reduced to practice. However, the system still needed in vitro testing to ensure proper delivery. We also wanted to explore the feasibility of incorporating radiopaque markers, antirestenotic drugs, and cell binding motifs into the stent structure. Once this was accomplished, the work shifted to the in vivo model. The testing that was done in the preceding chapters validated the potential to crimp, tract, and expand the elastin based stent platform. However, these tests did not prove that the stent platform could be delivered and deployed in an animal vessel. Therefore, we needed to prove that this system was capable of being used as it was designed.

In vivo models for stenting often focus on the rabbit iliac and porcine coronary models[167]. Compared to these, the rat model has been shown to be simple, inexpensive, rapid, and accurate[168]. Researchers have also documented similar vascular responses in the rat aorta model with more benchmarked models, such as the porcine and rabbit models[169]. There are strengths and limitations with all of the animal models discussed above, and in view of the cost and surgical time required for

large animal models, the rat aorta model provided a cost effective and simplified model for a first round of stent testing.

In order to facilitate the deployment of the elastin mimetic stents in the animal model, a delivery system was developed. The delivery system consisted of two major components: a balloon catheter and a sheath. Novel balloon catheters have been developed in other novel stent platforms to allow for proper stent deployment[89]. In this specific case, we needed to develop our own catheter to minimize the radial profile of the crimped stent system. Sheaths have been commonly used in the development of shape memory stents to prevent premature expansion of the stent. In our case, a sheath is needed to prevent the stent from hydrating prematurely.

The aim of this study was to validate the potential to deliver and deploy a 1.5mm stent in vitro. Then the drug delivery and endothelialization potential of an entire stent was examined. Upon successful completion of these aims a stent deployment strategy for implantation in the rat aorta was performed out. It was hypothesized that the stent could be delivered and expanded in a section of the aorta distal to renal arteries and analyzed for its success over time and its ability to stimulate vascular wall healing. In this chapter, we outline the parameters necessary to create this approach and illustrate the progress that was made. This work was the first step in the validation of protein based stents.

5.2 Materials and Methods

Stent Fabrication

The development and fabrication of the stent used in these studies were detailed in Chapter 2. The stent employed in all of these experiments had a length of 7mm, a diameter of 1.5 mm, and 1.5mm solid ring structures on the proximal and distal end of the stent. The stent was also genipin crosslinked.

Catheter Fabrication

The catheters were fabricated by covering a 15mm length of precision 304 stainless steel tubing, that has an outer diameter of 254μm and an inner diameter of 176 μm, with silastic tubing (Down Corning Midland, MI), that had an inner diameter of 305μm and an outer diameter of 635μm. A 5mm section of silastic tubing was also attached to the tip of the stainless steel tubing. The balloon was formed by placing a 30mm section of the balloon material, (Advanced Polymer, Salem, NH) that is 6.35μm thick and has an outer diameter of 1.6mm, over the catheter. The balloon was twisted and cinched down to the silastic tubing, and the ends are secured with cyanoacrylate. The cinched ends of the balloon were covered with heat shrink tubing, with an outside diameter of 1.1 mm and thickness of 13μm. The heat shrink tubing was heated with a heat gun until it shrunk to a nominal diameter of 650μm. A blunt tip 27 gauge needle was inserted into the distal end of the silastic after it had been placed in toluene for 1 minute to swell the tubing. The toluene was than allowed to evaporate from the silastic tubing, providing a snug fit. A length of suture is then tied over the needle and silastic tubing.

Sheathing Components

The sheath was created from two components. The first was a 1.25mm outer diameter sheath that has a thickness of 6.35μm. This sheath was passed over the 0.96mm sheath that has a thickness of 13μm and they were attached via cyanoacrylate.

Stent Delivery

To prepare the catheter for crimping, the balloon was deflated and flattened. The stent was then placed over the flattened balloon and the stent was flattened. The stent is then manipulated with surgical tweezers to allow for the stent and the balloon to be crimped as seen in Figure 5.2C. The stent was then allowed to dry prior to sheath placement. The loaded stent catheter system was traveled to the site of deployment. The sheath was removed, and the balloon was inflated to 3 atm using an inflator (Boston Scientific, Natick, Massachusetts) filled with sterile phosphate buffered saline. The inflated balloon was maintained for 1 minute, and then the balloon was deflated and withdrawn from the system.

Determination of Physical Parameters of Delivery System

The best practice in stent fabrication is discussed in Chapter 3. For these calculations, we used the same techniques that were used to determine stent thickness. The pre and post expanded stent thicknesses and diameters were measured by examining the proximal and distal ends of the stent. Once an image was taken, the stents were measured at eight points every 45º. The stent was always aligned so the attachment point was centered on 0º. The wall thickness would be characterized by measuring the thickness at all eight points. Crimped profile was determined by examining the proximal and distal end of the stent after the crimping process. The

crimping ratio was determined by subtracting the initial surface area of the uncrimped stent from the crimped stent and then dividing that difference by the uncrimped surface area. The void volume of the crimped stents was calculated by subtracting the surface area of the stent from the surface area of the crimped structure. The stent was then examined along the length and measured using image J. The radius of curvature was determined by placing the catheter system with stent on a template with a bending point and two movable assists, which were used to bend the stent. The diameter of the bending point was decreased until the system started to kink.

Collapse Pressure Setup

The same collapse pressure setup as described in Chapter 2 was utilized to quantify the collapse pressure of stents before and after the crimping process.

Video Acquisition Setup

The video acquisition system was used to monitor the deployment and expansion of the stent, as well as the stent delivery process.

Radiopaque Marker Incorporation

Radiopacity in the stent was achieved by adding tantalum to the construct. This was accomplished in two ways. The first way was to incorporate the tantalum into the mold before the elastin was cast in the mold. A suspension of ethanol and tantalum at a concentration of 1 gram/ml was used. The radiopaque doped elastin mimetic stent was then imaged using fluoroscopy.

Drug Incorporation

Drug incorporation was detailed in Chapter 4. In brief, the drug was mixed with the polymer solution and solvent cast into molds.

Experimental Procedure to Implant Stents in Rats

In the rat procedure, all surgeries were performed using a dissecting microscope (VWR™). Once the animal was anesthetized with isoflurane, a vertical midline laparotomy incision was made. After appropriate retraction for exposure, the abdominal contents were displaced to the left upper quadrant and covered in saline moistened sterile gauze. The bladder and seminal vesicles were displaced deep into the pelvis and similarly held in place with moistened sterile gauze, allowing for adequate exposure. The retroperitoneum was dissected to expose the infrarenal abdominal aorta to the level of the aortic bifurcation. The dissection planes between the aorta and the IVC were established 3-5 mm below the level of the left renal vein and 3-5 mm above the common iliac bifurcation. Each was further delineated by careful dissection along these planes. A microvascular clamp was applied to control aortic inflow and outflow at the proximal and distal regions just described. A 19-gauge needle, bent at a right angle, was used to create an arteriotomy approximately 8-10 mm above the common iliac bifurcation. A tie was placed proximally to the arteriotomy. This tie prevented blood from coming out of the aorta once the clamp was removed. A 1mm sheathed balloon and stent was inserted intraluminally via the arteriotomy. The proximal microvascular clamp was removed to allow free passage of the sheathed catheter. The catheter, which had been previously marked at various points, was inserted to the level of the bifurcation and then drawn back 1 cm. The sheath was then removed and the balloon was inflated to 3 atm. The balloon was kept inflated for 1 minute before it was deflated and removed. Prior to complete removal of the catheter, the proximal clamp was replaced to regain inflow control. The arteriotomy was closed with 9-0 Nylon suture in a running fashion.

The proximal and distal micro-clamps were removed to restore anterograde blood flow (confirmed by pulsation along the length of the aorta). The abdominal contents were replaced with care taken to avoid intestinal torsion, and the abdomen was closed in two layers with running 4-0 vicryl suture.

5.3 Results and Discussion

In this chapter, we discussed the implementation of the stent platform refined in Chapter 2 along with the material modulation we discussed in Chapter 4. However, first we had to design and develop a stent delivery system that was capable of delivering and deploying these novel elastin mimetic stents in rat aortas. To achieve this end, elastin mimetic stents were fabricated with a 1.5mm diameter, a thickness of 100μm, and a length of 7mm. In order to develop, validate, and refine a delivery and deployment process capable of in vivo testing, several endpoints had to be achieved that were based on the in vivo model chosen, the rat aortic model(Table 5.1). The feasibility and reduction to practice of these endpoints was achieved by vetting the stent with a series of in vitro tests. In Chapter 2, we explored the design and development of stents that allowed us to achieve certain physical features. The current stent design reflects the design parameters that had to be satisfied to ensure this stent functions properly. However, in so doing we created a stent that cannot be deployed in the rat aorta with generic balloons and sheaths. Therefore, we had to develop a balloon catheter system to successfully deliver these stents into mock arteries and achieve the endpoints listed in Table 5.1. To develop the delivery system, a balloon catheter and sheathing system were developed.

Table 5.1 In Vitro Benchmarks

In Vitro Benchmarks	
Stent ID Pre Expansion	1.35 mm
Stent ID Post Expansion	1.50mm
Stent Length	7 mm
Stent Wall Thickness	100 μm
Crimped Stent Profile	900 μm
Sheathing Diameter	940 μm
Radius of Curvature	7mm
Balloon Catheter Pressure Rating	≥ 4 atm

Development of Catheter System

Balloon catheters are fairly common devices that have been used for decades to deliver and expand stents at the site of stenosis. Before stenting was common practice, angioplasty balloons were used to open vessels that were partially blocked with plaque. A standard balloon catheter is composed of a balloon, tubing, and leurlocks to connect to an inflator. The problem with current commercially available balloon catheters is that the dimensions have not been optimized for our stent. The protein based stent's inability to be crimped with the standard processes created a higher cross sectional area, creating a radial profile that was too large for the rat aorta. Therefore, based on both our stent design and the animal model chosen, a complete redesign of the current balloon catheter setup had to be investigated.

The focus of the new catheter design was to maintain the reliability and functionality of current balloon catheters while minimizing their void volume and radial profile. Limiting the radial profile of the balloon catheters was achieved by replacing the plastic components of the catheter with low profile metallic components that achieved the same flexibility and trackability of the current catheters. The differences between standard balloon catheters and the new catheter system that was developed are illustrated in Figure 5.1. Current catheters have a larger diameter plastic tube, on which the system is placed. In our catheters, we reduced the diameter of this tubing from 780μm to 240μm and changed it from plastic to metal.

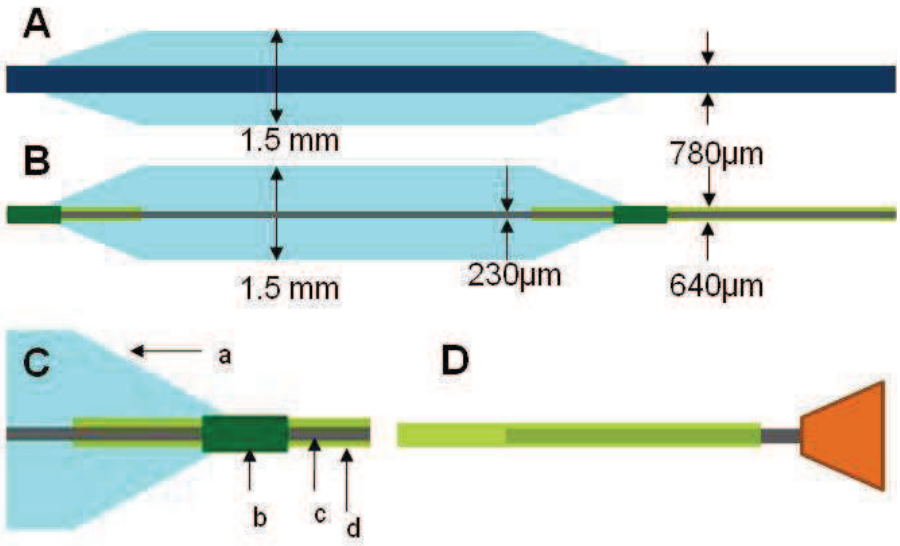

Figure 5.1 (A) Standard catheter design, (B) Experimental catheter design, (C) Zoomed in portion of B, a denoted balloon, b denotes attach mend point, c is inner lumen, d is outer lumen and (D) The distal end of the catheter

Initially the catheter tubing was replaced with concentric stainless steel tubing that allowed for a dual lumen and a small profile. However, this system was prone to kinking which would prevent the balloon from inflating. Thicker stainless steel that prevented kinking proved to lack the flexibility needed for the catheter to perform properly. Therefore, we removed the outer stainless steel tubing and replaced it with silastic tubing. This setup allowed for flushing the vessel with PBS and inflating the balloon, all while maintain the proper trackability of the system. Figure 5.1B shows differences in the radial profile of the existing catheters and the ones we developed. It should be noted that the portion of our catheter where the stent resides has a radial profile of 230μm, while the radial profile of the commercial catheter is 780μm.

Balloons were not commercially available at the 1.5mm size we needed. Therefore, we ordered thin walled tubing and cinched down the ends to create a balloon. The length, wall thickness, and material all affected the performance of the balloon. The balloon must be longer than the stent to ensure proper inflation. Initially we used a 25mm long balloon; however, when this procedure was transitioned to in vivo studies that length was too long so it was truncated down to 15mm. Two balloon thicknesses were studied. The first had thickness of 12μm and performed favorably upon inflation; however, it was too rigid to allow for proper crimping and deflation. The 6μm balloon thickness was more flexible, yet still provided the needed inflation force and could easily be crimped down and deflated.

One of the early limitations of our catheter was maintaining inflation pressures ≥ 4 atm. When the pressure would rise in the system, the PBS would leak from the proximal and distal ends of the balloon and from the attachment point of the needle and

silastic tubing. To address the leaks from the balloon, the cinched down portions of the balloon were covered with heat shrink tubing. The heat shrink tubing created a better seal and reinforced the attachment point of the balloon to the catheter allowing us to achieve higher pressures in the balloon. A 27 gauge blunt needle was inserted into the distal end of the silastic tubing. The 27 gauge needle was larger than the lumen of the silastic tubing so the silastic tubing was placed into toluene which swelled the tubing and allowed for the insertion of the needle. Upon evaporation of the toluene, the silastic tubing was contracted around the stent. Finally to prevent the tubing from moving on the needle, a suture was tied over the tubing needle interface.

Stent Insertion and Travel

The insertion of the stent and delivery of it to the site of deployment required a minimal radial profile, lubricious surface, prevention of stent migration, and sheath removal. A minimal radial profile was able to be achieved with the proper crimping strategy. The radial profile was minimized by selecting sheaths with small diameters and thicknesses in an effort to prevent damage to the vessel and to minimize the shear on the delivery device as it is traveled in the vessel. To aid in insertion, the tip of the sheath was crimped to be slightly tapered at the tip further decreasing the radial profile. The sheath was used to prevent the system from hydrating, which would increase the system radial profile. As previously demonstrated, the elastin mimetic stents can hydrate and begin to swell on very short time scales. The sheath also fixed the radial profile, which was important for insertion. On the unsheathed stents, the stent was getting stuck at the insertion point effectively increasing the stent diameter.

The sheath also prevented stent migration as the sheath created a uniform circumferential diameter that was subjected to the shear stress created during insertion. Preventing stent migration is important because stent migration off the back of the balloon would prevent expansion, but the stent should be able to be withdrawn on the catheter. If the stent migrated, off the front end of the balloon the stent would become separated from the catheter and retrieval could pose a life threatening condition.

Sheath Removal

As noted above, without the sheath, delivery of the elastin mimetic stent would be almost impossible. However, the sheath must be able to be removed to allow it to function properly. There were three places where sheath removal lead to problems. The first was the ability to uncrimp the sheath and retract it over the stent and balloon. The second was the interface between the sheath and the silastic tubing. The third was the ability to remove the sheath if the stent started to hydrate.

These first two limitations were overcome by changing the thicknesses of the sheath. When 6μm sheaths were used, their flexibility allowed the catheter to open the proximal twisted end and expel the stented catheter without moving the stent on the catheter. The next problem overcome by changing the thickness of the sheath was the interface between the silastic tubing and the sheath. The thin sheaths, 6μm, were flimsy and crumpled on the silastic tubing, preventing the sheath from being able to be pulled back. When the distal portion of the sheath was replaced with a 12μm thick section, the sheath was allowed to move freely on the catheter.

It should also be noted that even with the tip of the sheath crimped, stent hydration problems still plagued the delivery of the stent. With the small tubing, capillary

forces sucked in a large amount of the PBS that was in the mock vessel, causing the stent to swell and get stuck in the sheath. In previous studies with patterned stents, this was not a problem as the sheaths were not as tight as the current sheaths needed for rat aorta model. The crimped tip prevents the hydration as noted previously; however, once the sheath started to be removed, the solution rushed into the sheath. Even at shorter time scales, the stent swelled enough to cause the stent to get stuck in the 940μm sheath. This premature hydration led to a large amount of stress on the stent which ultimately lead to the failure of the stents in the in vitro system and was further exacerbated in the in vivo studies. To overcome this problem, a larger sheath was used that has a inner diameter of 1.25mm and a thickness of 6μm. Since the stent was still crimped down to a diameter of 900μm, the stent had plenty of room, and the sheath was compliant enough to allow for insertion and delivery.

In Vitro Testing and Design Revisions

In order to test the utility of the stent and delivery system in vivo, several test parameters had to be cleared in vitro. The in vitro system we developed used thin walled tubing that served as a mock artery as well as PBS flow that served as the fluid in the system. The mock vessel was clear to allow us to visualize the delivery and deployment of the stent as well as the expansion, deflation and removal of the balloon, and mechanical testing.

Stent Crimping, Delivery, and Deployment

To ensure that the catheters we developed in house were able to be crimped with the methodology explored in Chapter 2, we revisited the crimping of the stent. In all of these cases the crimping of the stent took place on the balloon, and the stent was

pleated with surgical tweezers. Crimping the stent on the balloon eliminated the wasted spaced that was formed when the two entities were crimped in progression and allowed for more uniform expansion of the stent.

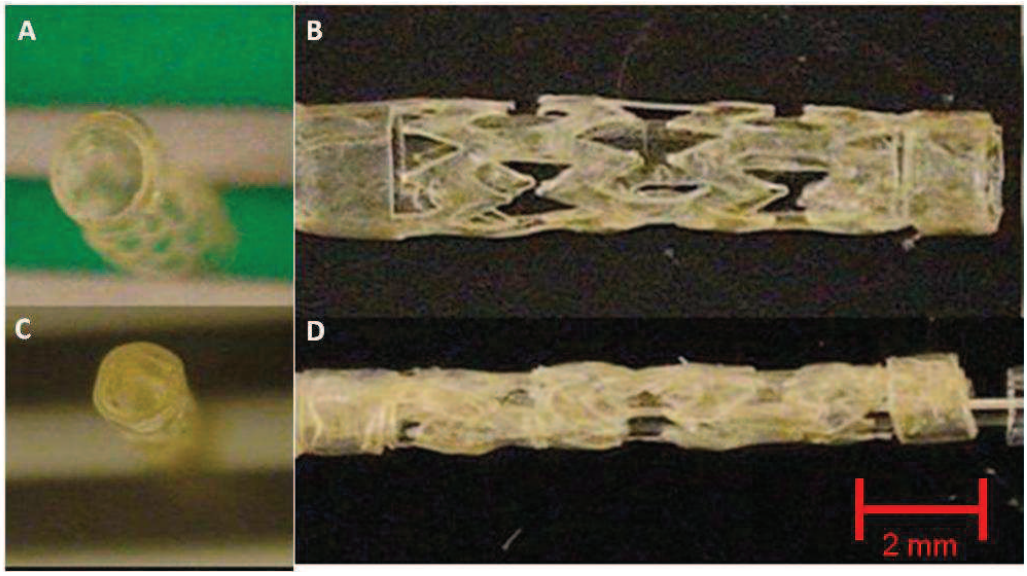

Figure 5.2 (A and B) Uncrimped Stent (C and D) Crimped Stent

Once the stent was traveled to the deployment site the sheath was removed. The sheath was retracted 25mm, to ensure the sheath is completely clear of the balloon there are markings on the sheath and catheter that must be aligned. The balloon was then inflated with PBS to 3atm with an inflator. To prevent some of the initial elastic recoil, the balloon was kept inflated for 1 minute after stent expansion allowing any stresses built up in the stent during the crimping and expansion process to relax.

The catheter has been tested to ensure that the balloon would inflate and deflate properly. We monitored the deflation of the balloon to ensure that it did not affect the diameter of the stent. Once the balloon was deflated, it was withdrawn from the vessel,

and it was noted that the thicker balloons, ≥10μm, affected both the ability to deflate the balloon and withdraw the balloon without moving the stent.

Ensure Proper Deployment

Once the stent was expanded it was examined to determine proper stent deployment, including uniform expansion and radial profile. The mechanical properties of the stent were then tested to ensure the delivery process did not affect the mechanical properties of the stent. Stent recoil was monitored at both short and long time points, and there was no change in size. To ensure there was no recoil stents were expanded in PBS, and their inner diameters was measured over time.

Expansion

For the elastin mimetic stent to be successful, it needs to have reliable uniform expansion so clinicians can size appropriately. Also, from a mechanical standpoint, the expansion of the stent was critical as defects in the expansion will compromise the mechanical integrity of the stent and create weak points that could lead to collapse. Failure to achieve predicted final stent diameter is a common problem, related to balloon under expansion and stent recoil, with commercial stents. In fact, the final stent minimal lumen diameter is only 73% of the expected diameter, irrespective of vessel size[170]. In order for the balloon expansion to perform optimally, three things are required: proper stent placement, uncompromised balloons, and proper catheter function.

To ensure proper expansion, we examined the balloon and the stent and ensured that the stent did not migrate off the balloon. Stents that did migrate had poor

expansion because part of the stent was not expanded by the balloon. Stent migration on the balloon was eliminated by addressing the sheathing issues discussed above in the sheath design section. It was also aided by the crimping process's ability to intertwine the stent with the balloon.

The other problem that we noted was a failure for the balloon to expand. This was a result of the crimping process. If the balloon was punctured during the crimping process, it did not inflate properly. This limitation of stent expansion was corrected by taking more precautions during the crimping process. The early catheter designs led to shaft crimping, which prevented the PBS from inflating the stent. When the outer lumen was changed from stainless steel to silastic tubing, this limitation was mostly overcome.

Stent Recoil

A study of the standard recoil for several metallic stents showed a standard stent recoil between 2.18% and 6.40%[171]. However, fabricating the stent in the expanded form allowed us to minimize this limitation as detailed in Chapter 2. Successfully deployed stents had recoil of 1.3±0.7%. This lack of recoil follows the hypothesis that stents fabricated in the expanded form and then crimped down would experience less recoil than stents expanded from a nominal diameter. Once a stent had been expanded it was monitored for elastic recoil. As discussed in the design rationale section this property was not seen as much in self expanding stents as balloon expandable stents. Elastic recoil was seen more in polymeric stents that were fabricated in the crimped diameter size and then expanded.

Expanded Integrity

Since the stent was crimped by folding, the inner profile of the stent was examined to ensure the lumen was still round and not deformed from the crimping. One of the concerns was the pleating and folding of these stents would impart some irrecoverable deformation that would cause the stent to lose round when deployed. We investigated this at both short-term and long-term time points, 1hour and 1 week. There was some deformation that occurred as the stent does not recover its entire shape after hydration, however, the stent does recover most of its initial shape. The fact that we dried the stent could aid in the process as the mechanical creep that the stent would experience is lessened because the polymeric chains lack flexibility in the dried state.

Mechanical Properties

Detailed mechanical testing on different stent designs and stent processing methods were discussed in detail in the stent design sections. However, to ensure that mechanical integrity of the stents was not compromised, through the crimping, delivery, storage, and expansion process, collapse pressure tests were performed. Stents were fabricated, hydrated, crimped down, dried, sheathed, stored for 1 week, tracked to the site of expansion, unsheathed, expanded for 1 minute, the balloon was removed and the stent was tested. These tests show that the crimping, storage and sheathing/unsheating processes do not affect the mechanical integrity of the stent(Figure 5.3).

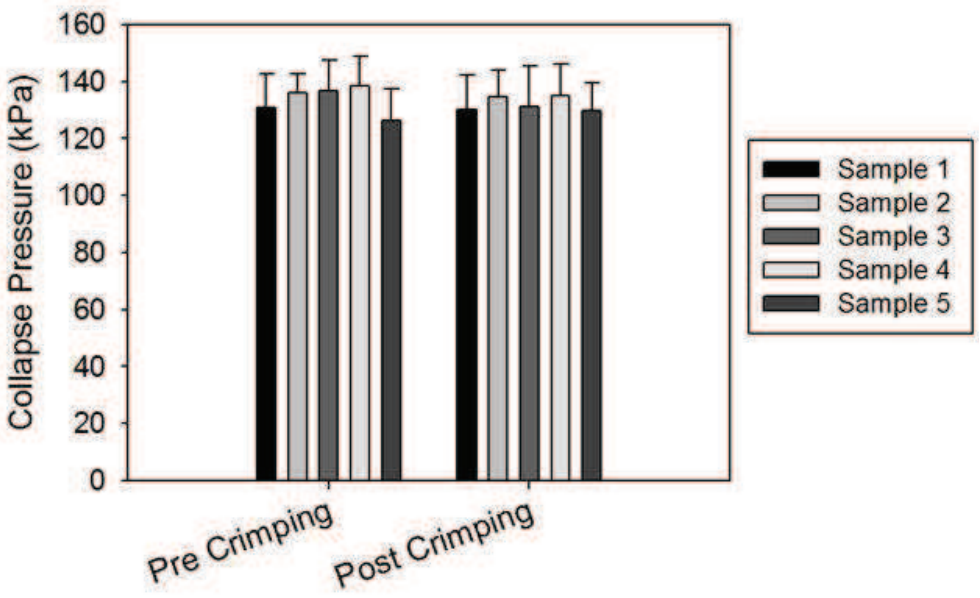

Figure 5.3 Collapse Pressure Before and After Stent Loading

Incorporation of Radiopaque Markers

Stents are an endovascular device and, as such, require fluoroscopy to allow clinicians to visualize the stent and ensure proper delivery and deployment. Radiopacity is a material property that obstructs the passage of x-rays, thereby giving objects such as metallic stents good contrast in the vessel. Some of the thinner metallic stents and self expanding stents fabricated from nitinol have had limited radiopacity, which limited their utility. To overcome this property, gold or tantalum markers were added to their the proximal and distal ends[172]. Imparting radiopacity into the elastin mimetic stent was crucial to allow for their endovascular deployment. The radiopacity of the elastin mimetic stent was also increased with the addition of tantalum microparticles.

Microparticles allowed for easy incorporation of the tantalum into the elastin mimetic stent through several different processing steps. The easiest way to incorporate

the tantalum material was to suspend the tantalum in TFE and syringe the solution into the proximal and distal ring reservoirs in the stent mold. Once the TFE evaporated, the tantalum was left in the mold and elastin mimetic solutions were cast into the mold. It should be noted that the tantalum was confined to the ring sutures to allow for determination of the proximal and distal ends of the stent, as well as for prevention of tantalum incorporation into a section that has to be ablated with the excimer laser.

Microparticles were also selected for their potential for being excreted from the body. Since the elastin mimetic stent can ultimately be degraded and absorbed back into the body, tantalum microparticles were selected instead of larger radiopaque markers. The particle size of the tantalum allows for it to be excreted by the body and not clog the vasculature.

Figure 5.4A shows different quantities of tantalum in the ring components of the stent design. The weight of tantalum ranged from 10μg, 25μg, 50μg, 75μg, and 100μg. Figure 5.4B shows the stents under fluoroscopy with a 3mm nitinol stent and a 6mm stainless stent. Finally Figure 5.4C shows the stent on a commercially available delivery catheter. There are three radiopaque markers on the sheath and one on the tip of the catheter. The sheath was then pulled back to reveal the proximal half of the stent and demonstrate the appearance of an unsheathed stent.

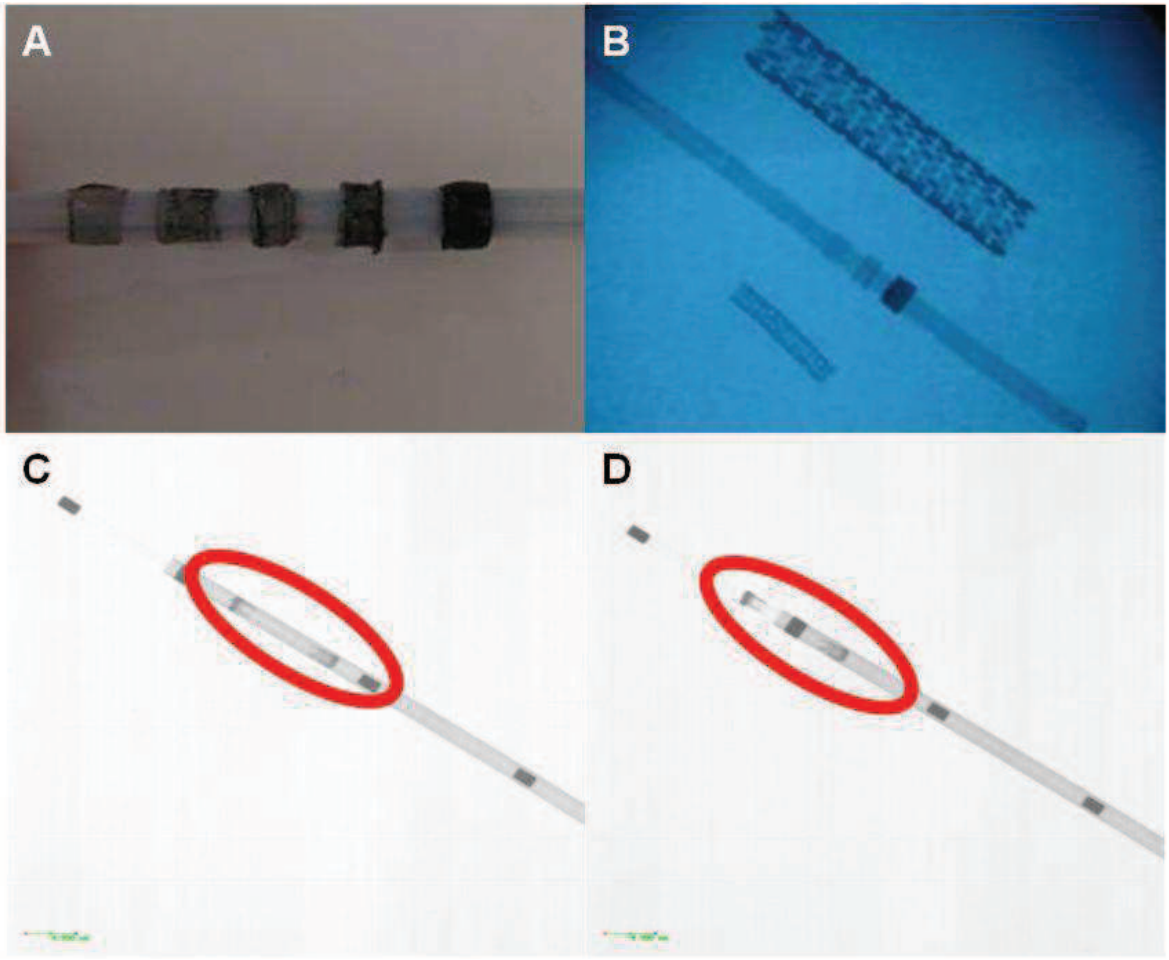

Figure 5.4 (A) Stent rings with different concentrations of tantalum(B) Stent rings examine through fluoroscopy with commercial stents above and below (C) Elastin mimetic stent doped with tantalum inside the delivery catheter (D) Stent half way out of the delivery catheter.

Pharmaceutical Incorporation

Drug eluting stents have shown to be effective at combating restenosis. To this end, we explored the ability to deliver drugs from the elastin mimetic stent platform. In these studies, rapamycin was used as a model drug because of its long documented history as an anti-restenotic drug incorporated into commercial stent platforms, such as the Cordis Cypher. The concentration of sirolimus on the surface of the Cordis Velocity

stent is 140 μg/cm^2[5]. This is the range that has been reported in the literature for other drug eluting stents, both coated metal and bioabsorbable stents, and will allow us to compare the elution rates of commercial stents and the elastin mimetic stent. The stent's drug delivery potential was studied in a release medium to allow for the generation of sink conditions. It should be noted that that in a PBS based system the drug would remain sequestered in the stent because of the low solubility of the drug in PBS[152].

In the first study, drug was incorporated throughout the stent, and differences between crosslinked and noncrosslinked stents were explored. We have previously demonstrated the potential for crosslinking to affect drug release(Chapter 4). Those results also held true in these full stent studies. Compared to the uncrosslinked stent, the crosslinked stent had a lower burst and a slower release rate coupled with extended release duration (Figure 5.5A). The burst release of the uncrosslinked stent was significantly higher than the crosslinked stent. Table 5.2 also shows that the duration that the drug remains in the stent was significantly higher for the crosslinked stent over the noncrosslinked stents. The crosslinked stent also had a lower burst release and a lower drug delivery rate. It should be noted that the crosslinking solution was measured to determine if any drug had eluted out of the stent, and no measurable drug elution from the stent into the crosslinking solution.

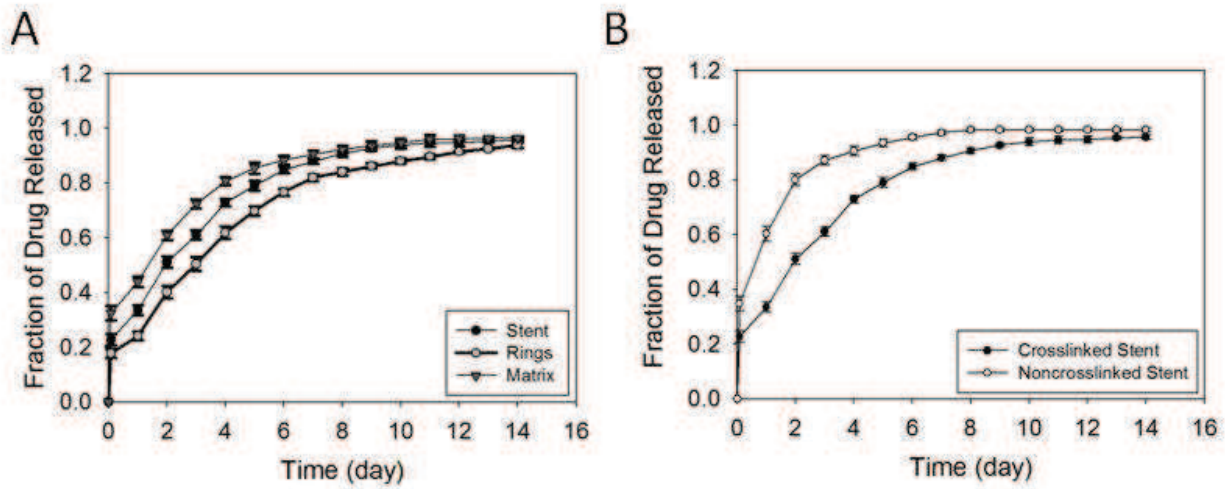

Figure 5.5. (A) Illustrates the potential for crosslinking to extend elution profiles. (B) Illustrates the elution profile for a crosslinked elastin based stent that has the drug located in discrete portions of the stent.

Table 5.2. Parameters from drug elution studies.

Elution Parameters	Uncrosslinked Stent	Crosslinked Stent	Stent Rings	Stent Matrix
Total Drug (ug)	105.00	105.00	105.00	105.00
Drug Concentration (µg/mm²)	2.79	2.79	5.81	5.38
Drug Surface Area of Vessel (µg/mm²)	1.74	1.74	5.81	2.49
Burst Amount (µg)	36.52 ± 2.77	23.85 ± 2.08	21.12 ± 1.67	34.06 ± 2.70
Rate (% days^{-1})	18.14 ± 1.15	12.83 ± 0.39	12.36 ± 0.33	14.20 ± 0.37
Duration (Days)	8.00 ± 0.71	13.20 ± 0.84	15.80 ± 0.84	10.80 ± 1.10
Cumulative Release 3 Day	87.00 ± 0.02	61.00 ± 0.02	50.00 ± 0.03	72.00 ± 0.02
Cumulative Release 7 Day	97.00 ± 0.01	88.00 ± 0.01	82.00 ± 0.01	90.00 ± 0.01

We then explored the potential of incorporating the drugs into discrete sections of the stent, namely the rings or the struts. The release profiles of the stents were dictated by the concentration and location of the drug in the stent(Figure 5.5B). The burst release of drug from the stent matrix was significantly higher than the ring portions. The

fact that the burst release increases more than 60% shows the potential to modulate drug release by incorporating the drug into discrete areas.

While it is obvious that the general release profiles for the different locations are similar, it should be noted that the initial burst release and the steady release thereafter are affected by the placement of the drug in the matrix. The ability to incorporate drugs in different portions of the stent appears to be an advantage of the molding fabrication process that can be leveraged to achieve longer drug delivery times and alter the burst release for the particular drug of interest. When comparing the stent rings and the struts, the two main variables are concentration of drug with regard to vessel area that the stent interacts with and the geometry. The weight by weight of the material and the drug are only slightly different. Therefore, the delayed drug release must be explained through the geometry. It should be noted that casting of the stent led to no measurable mixing between the two areas. Although the surface area of these two delivery platforms was almost identical, the geometry of the drug locations is quite different. In the matrix portion, the struts surface to thickness ratio was 5 to 1, whereas the rings have a ratio of 15 to 1. Therefore, the matrix could be losing a significant amount of drug through the sides perpendicular to the vessel wall.

All of the drug release profiles had a characteristic burst followed by a linear period of higher and then slower release rates as the remaining concentration of drug in the stent was lowered.

Biopharmaceutical Incorporation

One of the biggest drawbacks for drug eluting stents is late stage thrombosis[173], which can be overcome if the lumen of the stent can be fully endothelialized. The potential to endothelialize recombinant elastin mimetic materials has been previously documented [51, 53]. The elastin mimetic material has shown poor endothelialization without the addition of cell binding domains either along the protein backbone or via the incorporation of Fn[174]. In these studies, we were able to demonstrate the ability to obtain endothelialized stent surfaces with Fn passively adsorbed to the luminal surface of the stent. From a design point of view, the logical placement of biopharmaceuticals would be the luminal side of the stent to try and promote cell adhesion.

The potential to promote endothelial cell adhesion and proliferation was explored by passively adsorbing Fn to the control well and to the genipin crosslinked stent. Once the cells were seeded, they were harvested at two hours and a CyQuant assay was performed. The control well had an adhesion of 29.8±2.8%, while the stent construct had 22.1±3.8%(Figure 5.6A). The results of the CyQuant assays show that the adhesion rate for the stent construct was 73.3% when normalized to Fn. The cell number at 48 hours was 12487±456 for the control and 9245 ± 579 for the stent construct. The control had a 4.93 fold increase from 2 to 48 hours, while the stent had a 4.61 fold increase. These results show that the HUVECs can adhere and proliferate on the stent surface, which provides the framework for an endothelialized stent.

The cellularized stent sections were imaged to show the morphology and concentration of cells on the surface of the stent construct(Figure 5.6B and C). It was

apparent that 2 hours after seeding, cells are spreading and only a small fraction of the stent was cellularized(Figure 5.6B). After 48 hours, the HUVECs are forming a confluent layer; however, there are some sections that are bare and this could be a result of the nonuniform adhering of the cells after the cell seeding step(Figure 5.6C). The ability to seed stent constructs shows that these materials are capable of modification, and this modification was much easier than the incorporation of cell binding motifs into the protein backbone, as has been accomplished by our lab[162] and others[48, 175].

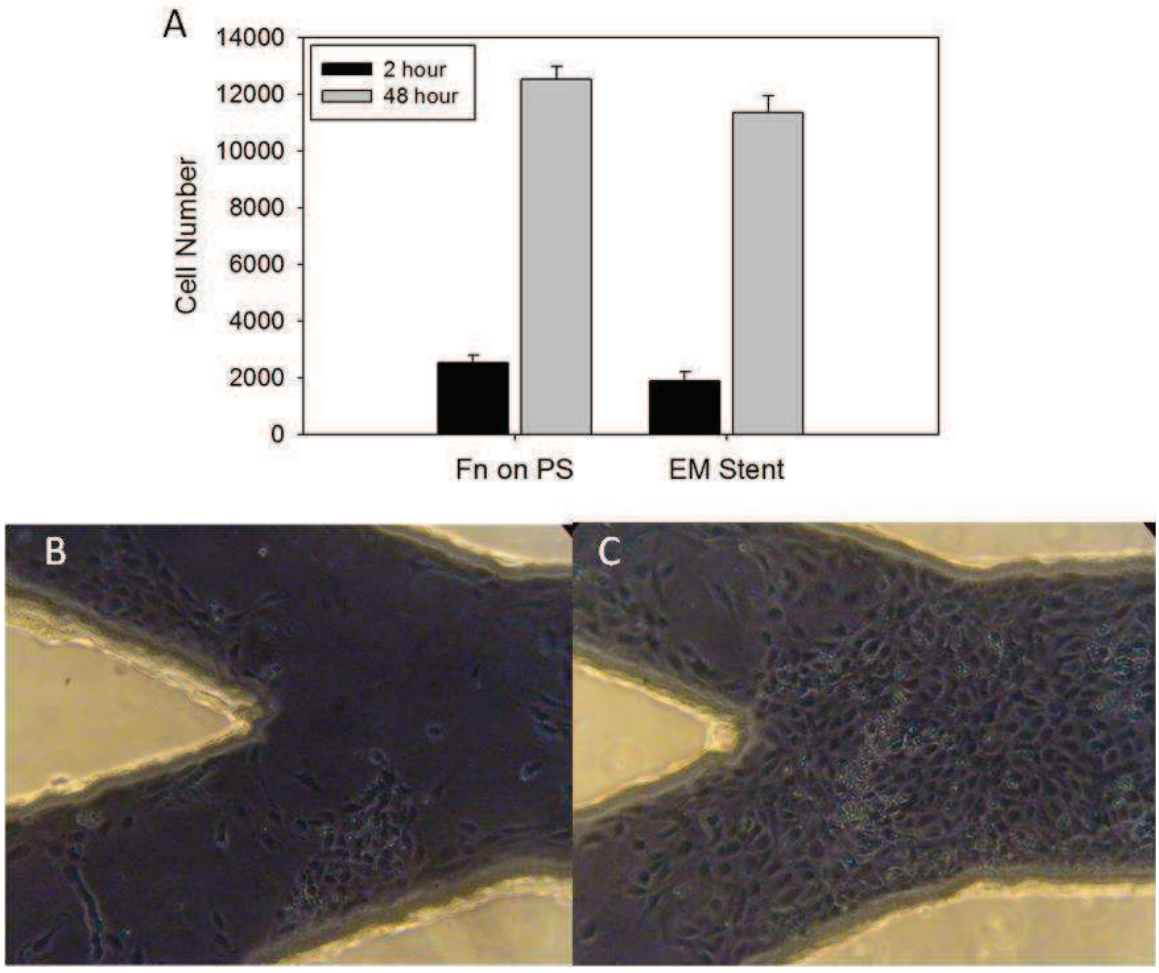

Figure 5.6. (A) Cell adhesion and proliferation on Fn polystyrene and Fn on stent section. (B) Genipin crosslinked stent after 2 and (C)48 hours post seeding.

In Vivo Model

Deploying the elastin mimetic stent in an animal model was the next logical step after the system was vetted with in vivo tests. In vivo models for stenting often focus on the rabbit iliac and porcine coronary models. However, the rat model has shown increasing promise over the past couple of years because of it low cost and high throughput[168, 176-182]. Researchers have also documented similar vascular responses in the rat aorta model to more benchmarked models such as the porcine and rabbit models[168, 169, 183]. Of importance to our drug delivery studies was the ability of the rat model to demonstrate reliable and reproducible in stent restenosis formation following stenting of the rat aorta[184]. It should also be noted that a couple of groups have explored novel drug delivery studies using the rat model [179, 185].

We were successfully able to deploy a 1.5mm stent which was in the range of stents previously deployed in this vessel[178]. The elastin mimetic stents were implanted in the aorta below the renals of the rat(Figure 5.7) following the standard procedure established previously. The experimental protocols were approved and performed in compliance with the proper review boards.

The rat aorta model allowed us to perform initial studies on implanting the stents in an animal test bed. The ability to use a model where the entire process can be visualized allowed us to see potential problems with the delivery system and stent deployment and work to eliminate them. We were able to implant stents in eight rats and had a 100% survival rate at two weeks. This was very promising as the literature has a referenced a much higher mortality rate than we experienced. Inserting and deploying the stent through the aorta lead to a mortality rate of 57% for Oyamada et al.

[186]. They had a lower mortality rate, 11% when the stent was inserted through the iliac and expanded in the aorta, but still high compared to our enrollment. Onuta et al. had a mortality rate of 17%[181].

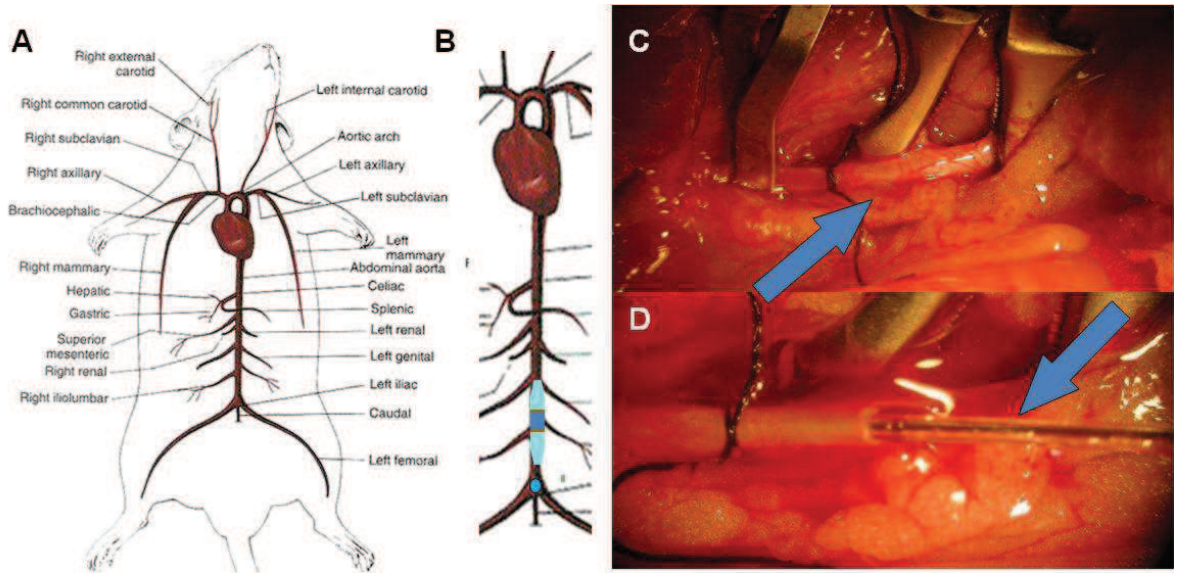

Figure 5.7 Diagram of rat circulatory system (http://www.biologycorner.com) (B) Site of Deployment (C) exposed ligated aorta, and (D) catheter loaded into the aorta

We were able to demonstrate stent deployment in the rat aorta(Figure 5.8). The animals were sacrificed at two weeks and at that time there was no signs of stent failure, which was usually reported in the literature as hind leg ischemia. While there is much more work that needs to be done, this is a significant step in translating the protein based stent from a design to a feasible device.

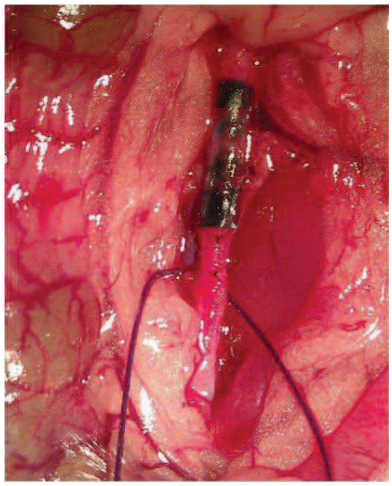

Figure 5.8 Elastin mimetic stent deployed in the rat aorta distal to renals.

5.4 Conclusions

The completed in vitro experiments were able to produce a delivery system that eliminated many of the failure points that would have been experienced in vivo. We were also able to demonstrate the potential to modulate drug delivery form the stent platform and endothelialization of stent constructs. The potential to use these protein based stents has several advantages over current platforms, and the delivery and expansion of these stents in an animal model provides the framework to study these stents further. As discussed in the preceding chapters, the chief advantage of these stents resides in the ability to modulate various mechanical and biological properties ranging from stiffness to endothelialization. The elastin mimetic stent has emerged as potentially powerful platform technology.

CHAPTER 6

Conclusions and Future Directions

Cardiovascular stenting as a means to open occluded vessels will be a necessary treatment for the foreseeable future. However, it will be necessary for the stents to be able to overcome the deleterious side effects that have plagued stenting over the past decade. To exploit the full clinical potential of stents they will need to be able to be tuned to specific lesion and patient characteristics. These can be achieved by incorporating pharmaceutical and bio pharmaceuticals to enhance stent performance. Also the potential for stents to perform their task and then adsorb back into the body provides a way forward that eliminates some of the chronic concerns of stenting.

The work encompassed in this thesis provides the foundation for the long-term goal of designing a protein based stent platform. A great number of endpoints have been achieved, however, several recommendations for future investigators have been proposed for each research chapter.

Chapter 2 Stent Design and Development: The current stent design that we selected has shown promising mechanical attributes. However, future designs should look at minimizing the overall ring length and potentially incorporating several thinner rings throughout the construct. The ratcheting stent ideal should also be explored in further detail to see if the mechanism can be worked out. This kind of design would save a great deal of time and energy in crimping down the stent to an acceptable radial profile as well as prevent the need to attach planar sheets.

The crimping process must also be enhanced to prevent the laborious task of crimping the stent and the potential for nonuniformities that arise when something is performed manually.

Chapter 3 Fabrication of Protein Based Materials: As the knowledge on protein based materials continues to expand and the barriers to produce these material lessen I believe there will be further implementation of these materials into medical devices. When these materials are adopted by the medical device community there will be a demand to fabricate these materials into a wide range of constructs.

The ability to machine protein based materials with the excimer laser has been known for a couple of decades in the medical field, however, it has been slow to be adopted by the research field. In fact no publications could be found that fabricated three dimensional mechanically robust patterned films. The ability to fabricate these films allow for more translation into the medical device space. This technique is already being looked into by collaborators to pattern biomaterials for tissue engineered blood vessels and brain tissue for nerve cell engineering. I believe that this technique on protein fabrication will be explored further and refined.

Finally, we have shown the potential to fabricate thin walled tubes. However, we have not had the capacity to laser ablate the fenestrations directly on these thin walled tubes. This creates a lot of problem with attaching the stent as shown in Chapter 3. Therefore, I believe that a top priority for stent fabrication should be acquiring the potential to fabricate stent form thin walled tubing.

Chapter 4 Advancing the Biological and Physical Properties of the Elastin Mimetic Material: One of the biggest driving forces in the use of recombinant protein engineering is the ability to tailor the proteins to a specific need. However, this process is time intensive and not always possible. Therefore, the ability to reengineer existing protein sequences with exogenous materials decrease the research and development time and cost to obtain enhanced materials.

We have explored three crosslinkers and three crosslinking systems. The ability for these systems to modulate the properties of the film will be further explored with other crosslinking agents. The ability to create more crosslinking sites on the protein backbone will also be utilized as a way to enhance crosslinking or as a handle to bind other compounds of interest.

While we were able to modulate the drug release from our films the time scales were not adequate for most applications. Therefore, other methods to retard drug elution should be explored. The easiest way to increase diffusion time would be the incorporation of drug loaded films or microspheres. The second aim would be to increase the dissolution time of the drug. This could be accomplished by crystallizing the drug or creating predefined drug reservoirs on the stent where the drug is heavily concentrated. The final aspect of delivery would be to release drugs based on degradation. This is seen in the bioabsorable stent literature where a top coat can dissolve releasing the drug as it degrades.

The ability to endothelialize the constructs should also be explored in greater detail. It was noted in our research that the Fn would wash out if it was adsorbed prior to

construct crosslinking. Further work needs to be done to ensure we can maintain Fn on the surface for several weeks. Also other cell binding sequences that are specific for endothelial cells or antibodies capable of binding CD34+ cells should be incorporated into the lumen of the stent.

Chapter 5 In Vitro and In Vivo Stent Deployment: The deployment of elastin mimetic stents into the rat aorta was a huge milestone for us to achieve. However, that is only the beginning of studies that need to be explored to examine the different properties of the stent. Future, stent studies will be explored to further determine the potential for the elastin mimetic stents to prevent thrombosis formation, combat restenosis and endothelialize to prevent late stage thrombosis.

References

1. Daemen, J., et al., *Early and late coronary stent thrombosis of sirolimus-eluting and paclitaxel-eluting stents in routine clinical practice: data from a large two-institutional cohort study.* Lancet, 2007. **369**(9562): p. 667-678.
2. Bhargava, B., et al., *A novel paclitaxel-eluting porous carbon-carbon nanoparticle coated, nonpolymeric cobalt-chromium stent: Evaluation in a porcine model.* Catheterization and Cardiovascular Interventions, 2006. **67**(5): p. 698-702.
3. Ye, Y.W., et al., *Bioresorbable microporous stents deliver recombinant adenovirus gene transfer vectors to the arterial wall.* Ann Biomed Eng, 1998. **26**(3): p. 398-408.
4. Wessely, R., et al., *Inhibition of neointima formation by a novel drug-eluting stent system that allows for dose-adjustable, multiple, and on-site stent coating.* Arterioscler Thromb Vasc Biol, 2005. **25**(4): p. 748-53.
5. Hausleiter, J., et al., *Prevention of restenosis by a novel drug-eluting stent system with a dose-adjustable, polymer-free, on-site stent coating.* Eur Heart J, 2005. **26**(15): p. 1475-81.
6. Mehilli, J., et al., *Randomized trial of three rapamycin-eluting stents with different coating strategies for the reduction of coronary restenosis.* Eur Heart J, 2008. **29**(16): p. 1975-82.
7. Wieneke, H., et al., *Synergistic effects of a novel nanoporous stent coating and tacrolimus on intima proliferation in rabbits.* Catheterization and Cardiovascular Interventions, 2003. **60**(3): p. 399-407.
8. Kollum, M., et al., *Particle debris from a nanoporous stent coating obscures potential antiproliferative effects of tacrolimus-eluting stents in a porcine model of restenosis.* Catheter Cardiovasc Interv, 2005. **64**(1): p. 85-90.
9. Rajtar, A. and K. G.L., *Hydroxyapatite-coated cardiovascular stents.* EuroIntervention, 2006. **2**: p. 113-115.
10. Costa, J.R., Jr., et al., *1-year results of the hydroxyapatite polymer-free sirolimus-eluting stent for the treatment of single de novo coronary lesions: the VESTASYNC I trial.* JACC Cardiovasc Interv, 2009. **2**(5): p. 422-7.
11. Blindt, R., et al., *A novel drug-eluting stent coated with an integrin-binding cyclic Arg-Gly-Asp peptide inhibits neointimal hyperplasia by recruiting endothelial progenitor cells.* Journal of the American College of Cardiology, 2006. **47**(9): p. 1786-1795.
12. Klugherz, B.D., et al., *Gene delivery from a DNA controlled-release stent in porcine coronary arteries.* Nature Biotechnology, 2000. **18**(11): p. 1181-1184.
13. Lin, P.H., et al., *Heparin-coated balloon-expandable stent reduces intimal hyperplasia in the iliac artery in baboons.* J Vasc Interv Radiol, 2003. **14**(5): p. 603-11.
14. Hong, Y.J., et al., *Effect of abciximab-coated stent on in-stent intimal hyperplasia in human coronary arteries.* American Journal of Cardiology, 2004. **94**(8): p. 1050-1054.
15. Meyers, S.R., D.J. Kenan, and M.W. Grinstaff, *Enzymatic release of a surface-adsorbed RGD therapeutic from a cleavable peptide anchor.* ChemMedChem, 2008. **3**(11): p. 1645-8.
16. Matsuno, H., et al., *Inhibition of Integrin Function by a Cyclic Rgd-Containing Peptide Prevents Neointima Formation.* Circulation, 1994. **90**(5): p. 2203-2206.
17. Pypen, C.M.J.M., et al., *Characterization of microblasted and reactive ion etched surfaces on the commercially pure metals niobium, tantalum and titanium.* Journal of Materials Science-Materials in Medicine, 1997. **8**(12): p. 781-784.
18. Palmaz, J.C., A. Benson, and E.A. Sprague, *Influence of surface topography on endothelialization of intravascular metallic material.* Journal of Vascular and Interventional Radiology, 1999. **10**(4): p. 439-444.

19. Lu, J., et al., *Improved endothelial cell adhesion and proliferation on patterned titanium surfaces with rationally designed, micrometer to nanometer features.* Acta Biomaterialia, 2008. **4**(1): p. 192-201.
20. Jing Lu, a.T.J.W. *Endothelial Cell Adhesion on highly Controllable Compared to Random Nanostuctured Titanium Surface Features*. in *Materials Research Society Symposium*. 2007.
21. Choudhary, S., K.M. Haberstroh, and T.J. Webster, *Enhanced functions of vascular cells on nanostructured Ti for improved stent applications.* Tissue Engineering, 2007. **13**(7): p. 1421-1430.
22. Samaroo, H.D., J. Lu, and T.J. Webster, *Enhanced endothelial cell density on NiTi surfaces with sub-macron to nanometer roughness.* International Journal of Nanomedicine, 2008. **3**(1): p. 75-82.
23. Choudhary, S., et al., *Increased endothelial and vascular smooth muscle cell adhesion on nanostructured titanium and CoCrMo.* International Journal of Nanomedicine, 2006. **1**(1): p. 41-49.
24. Khang, D., et al., *The role of nanometer and sub-micron surface features on vascular and bone cell adhesion on titanium.* Biomaterials, 2008. **29**(8): p. 970-983.
25. De, S., et al., *Enhancement of blood compatibility of implants by helium plasma treatment.* Conference Record of the 2004 Ieee Industry Applications Conference, Vols 1-4 - Covering Theory to Practice, 2004: p. 932-936.
26. Parker, E.R., et al., *Inductively coupled plasma etching of bulk titanium for MEMS applications.* Journal of the Electrochemical Society, 2005. **152**(10): p. C675-C683.
27. Yeh, H.I., et al., *Comparison of endothelial cells grown on different stent materials.* Journal of Biomedical Materials Research Part A, 2006. **76A**(4): p. 835-841.
28. Yin, Y.B., et al., *Covalent immobilisation of tropoelastin on a plasma deposited interface for enhancement of endothelialisation on metal surfaces.* Biomaterials, 2009. **30**(9): p. 1675-1681.
29. Yin, M., et al., *Development of mussel adhesive polypeptide mimics coating for in-situ inducing re-endothelialization of intravascular stent devices.* Biomaterials, 2009. **30**(14): p. 2764-2773.
30. Walter, D.H., et al., *Local gene transfer of phVEGF-2 plasmid by gene-eluting stents: an alternative strategy for inhibition of restenosis.* Circulation, 2004. **110**(1): p. 36-45.
31. Swanson, N., et al., *In vitro evaluation of vascular endothelial growth factor (VEGF)-eluting stents.* International Journal of Cardiology, 2003. **92**(2-3): p. 247-251.
32. Aoki, J., et al., *Endothelial progenitor cell capture by stents coated with antibody against CD34: the HEALING-FIM (Healthy Endothelial Accelerated Lining Inhibits Neointimal Growth-First In Man) Registry.* J Am Coll Cardiol, 2005. **45**(10): p. 1574-9.
33. Rossi, M.L., et al., *The first report of late stent thrombosis leading to acute myocardial infarction in patient receiving the new endothelial progenitor cell capture stent.* Int J Cardiol, 2009.
34. Trabbic-Carlson, K., L.A. Setton, and A. Chilkoti, *Swelling and mechanical behaviors of chemically cross-linked hydrogels of elastin-like polypeptides.* Biomacromolecules, 2003. **4**(3): p. 572-580.
35. Welsh, E.R. and D.A. Tirrell, *Engineering the extracellular matrix: A novel approach to polymeric biomaterials. I. Control of the physical properties of artificial protein matrices designed to support adhesion of vascular endothelial cells.* Biomacromolecules, 2000. **1**(1): p. 23-30.
36. Nowatzki, P.J. and D.A. Tirrell, *Physical properties of artificial extracellular matrix protein films prepared by isocyanate crosslinking.* Biomaterials, 2004. **25**(7-8): p. 1261-7.
37. Di Zio, K. and D.A. Tirrell, *Mechanical properties of artificial protein matrices engineered for control of cell and tissue behavior.* Macromolecules, 2003. **36**(5): p. 1553-1558.
38. Nagapudi, K., et al., *Protein-based thermoplastic elastomers: Properties and applications in tissue engineering.* Cell Transplantation, 2003. **12**(2): p. 170-171.

39. Nakayama, Y., et al., *Development of high-performance stent: gelatinous photogel-coated stent that permits drug delivery and gene transfer.* Journal of Biomedical Materials Research, 2001. **57**(4): p. 559-566.
40. Yuan, J.Q., et al., *Intravascular local gene transfer mediated by protein-coated metallic stent.* Chinese Medical Journal, 2001. **114**(10): p. 1043-1045.
41. Chen, M.C., et al., *A novel drug-eluting stent spray-coated with multi-layers of collagen and sirolimus.* Journal of Controlled Release, 2005. **108**(1): p. 178-189.
42. Shirota, T., H. Yasui, and T. Matsuda, *Intralumenal tissue-engineered therapeutic stent using endothelial progenitor cell-inoculated hybrid tissue and in vitro performance.* Tissue Engineering, 2003. **9**(3): p. 473-485.
43. Liu, W.E., et al., *Tumor accumulation, degradation and pharmacokinetics of elastin-like polypeptides in nude mice.* Journal of Controlled Release, 2006. **116**(2): p. 170-178.
44. Herrero-Vanrell, R., et al., *Self-assembled particles of an elastin-like polymer as vehicles for controlled drug release.* Journal of Controlled Release, 2005. **102**(1): p. 113-122.
45. Barnes, M.J. and D.E. MacIntyre, *Platelet-reactivity of isolated constituents of the blood vessel wall.* Haemostasis, 1979. **8**(3-5): p. 158-70.
46. Jordan, S.W., et al., *The effect of a recombinant elastin-mimetic coating of an ePTFE prosthesis on acute thrombogenicity in a baboon arteriovenous shunt.* Biomaterials, 2007. **28**(6): p. 1191-1197.
47. Woodhouse, K.A., et al., *Investigation of recombinant human elastin polypeptides as non-thrombogenic coatings.* Biomaterials, 2004. **25**(19): p. 4543-4553.
48. Girotti, A., et al., *Design and bioproduction of a recombinant multi(bio)functional elastin-like protein polymer containing cell adhesion sequences for tissue engineering purposes.* Journal of Materials Science-Materials in Medicine, 2004. **15**(4): p. 479-484.
49. Heilshorn, S.C., et al., *Endothelial cell adhesion to the fibronectin CS5 domain in artificial extracellular matrix proteins.* Biomaterials, 2003. **24**(23): p. 4245-4252.
50. Liu, J.C., S.C. Heilshorn, and D.A. Tirrell, *Comparative cell response to artificial extracellular matrix proteins containing the RGD and CS5 cell-binding domains.* Biomacromolecules, 2004. **5**(2): p. 497-504.
51. Costa, R.R., et al., *Stimuli-Responsive Thin Coatings Using Elastin-Like Polymers for Biomedical Applications.* Advanced Functional Materials, 2009. **19**(20): p. 3210-3218.
52. Liu, J.C. and D.A. Tirrell, *Cell Response to RGD Density in Cross-Linked Artificial Extracellular Matrix Protein Films.* Biomacromolecules, 2008. **9**(11): p. 2984-2988.
53. Heilshorn, S.C., J.C. Liu, and D.A. Tirrell, *Cell-binding domain context affects cell behavior on engineered proteins.* Biomacromolecules, 2005. **6**(1): p. 318-323.
54. Richman, G.P., D.A. Tirrell, and A.R. Asthagiri, *Quantitatively distinct requirements for signaling-competent cell spreading on engineered versus natural adhesion ligands.* Journal of Controlled Release, 2005. **101**(1-3): p. 3-12.
55. Ito, S., S. Ishimaru, and S.E. Wilson, *Application of coacervated alpha-elastin to arterial prostheses for inhibition of anastomotic intimal hyperplasia.* Asaio Journal, 1998. **44**(5): p. M501-M505.
56. De Beule, M., et al., *Finite element stent design: Parametric modeling of braided wirestents using pyformex.* Proceeding of the Amse Summer Bioengineering Conference - 2007, 2007: p. 719-720 1075.
57. Lally, C., F. Dolan, and P.J. Prendergast, *Cardiovascular stent design and vessel stresses: a finite element analysis.* Journal of Biomechanics, 2005. **38**(8): p. 1574-1581.

58. Rogers, C., et al., *Balloon-artery interactions during stent placement - A finite element analysis approach to pressure, compliance, and stent design as contributors to vascular injury.* Circulation Research, 1999. **84**(4): p. 378-383.
59. Agrawal, C.M., et al., *Evaluation of Poly(L-Lactic Acid) as a Material for Intravascular Polymeric Stents.* Biomaterials, 1992. **13**(3): p. 176-182.
60. Eberhart, R.C., et al., *Bioresorbable polymeric stents: current status and future promise.* Journal of Biomaterials Science-Polymer Edition, 2003. **14**(4): p. 299-312.
61. Yamawaki, T., et al., *Intramural delivery of a specific tyrosine kinase inhibitor with biodegradable stent suppresses the restenotic changes of the coronary artery in pigs in vivo.* J Am Coll Cardiol, 1998. **32**(3): p. 780-6.
62. Venkatraman, S., et al., *Collapse pressures of biodegradable stents.* Biomaterials, 2003. **24**(12): p. 2105-11.
63. Schrader, S.C. and R. Beyar, *Evaluation of the compressive mechanical properties of endoluminal metal stents.* Catheterization and Cardiovascular Diagnosis, 1998. **44**(2): p. 179-187.
64. SCHMITZ, K.P.B., D. BEHRENS, P. SCHMIDT, P., *Comparative Studies of Different Stent Designs.* Progress in Biomedical Research, 1999: p. 52-58.
65. W. SCHMIDT, R.A., P. BEHRENS, K.-P. SCHMITZ. *Comparison of mechanical properties of peripheral self-expanding nitinol and balloon-expandable stainless-steel stents*. in *Annual Meeting and Postgraduate Course of the Cardiovascular and Interventional Radiological Society of Europe (CIRSE)*. 2004. Barcelona, Spain.
66. Creel, C.J., M.A. Lovich, and E.R. Edelman, *Arterial paclitaxel distribution and deposition.* Circulation Research, 2000. **86**(8): p. 879-884.
67. Hwang, C.W. and E.R. Edelman, *Arterial ultrastructure influences transport of locally delivered drugs.* Circulation Research, 2002. **90**(7): p. 826-832.
68. Levin, A.D., et al., *Specific binding to intracellular proteins determines arterial transport properties for rapamycin and paclitaxel.* Proceedings of the National Academy of Sciences of the United States of America, 2004. **101**(25): p. 9463-9467.
69. Hwang, C.W., D. Wu, and E.R. Edelman, *Physiological transport forces govern drug distribution for stent-based delivery.* Circulation, 2001. **104**(5): p. 600-605.
70. Balakrishnan, B., et al., *Strut position, blood flow, and drug deposition - Implications for single and overlapping drug-eluting stents.* Circulation, 2005. **111**(22): p. 2958-2965.
71. Kim, B.K., et al., *Are There Differences in Clinical Outcomes after Target Lesion Revascularization for Restenosis According to the Type of Restenosed Drug-Eluting Stent? Comparisons between Sirolimus-versus Paclitaxel-Eluting Stent Restenosis.* American Journal of Cardiology, 2009. **103**(9A): p. 62b-62b.
72. Finn, A.V., et al., *Differential response of delayed healing and persistent inflammation at sites of overlapping sirolimus- or paclitaxel-eluting stents.* Circulation, 2005. **112**(2): p. 270-278.
73. Finn, A.V., et al., *Delayed healing and persistent inflammation at sites of overlapping sirolimus and paclitaxel drug-eluting stents.* Journal of the American College of Cardiology, 2005. **45**(3): p. 13a-13a.
74. Wessely, R., A. Schomig, and A. Kastrati, *Sirolimus and paclitaxel on polymer-based drug-eluting stents - Similar but different.* Journal of the American College of Cardiology, 2006. **47**(4): p. 708-714.
75. Wessely, R., et al., *Comparative characterization of cellular and molecular anti-restenotic profiles of paclitaxel and sirolimus - Implications for local drug delivery.* Thrombosis and Haemostasis, 2007. **97**(6): p. 1003-1012.

76. Ranade, S.V., et al., *Physical characterization of controlled release of paclitaxel from the TAXUS(TM) Express(2TM) drug-eluting stent.* Journal of Biomedical Materials Research Part A, 2004. **71A**(4): p. 625-634.
77. Drachman, D.E., et al., *Neointimal thickening after stent delivery of paclitaxel: Change in composition and arrest of growth over six months.* Journal of the American College of Cardiology, 2000. **36**(7): p. 2325-2332.
78. Carter, A.J., et al., *Long-term effects of polymer-based, slow-release, sirolimus-eluting stents in a porcine coronary model.* Cardiovasc Res, 2004. **63**(4): p. 617-24.
79. Zilberman, M., N.D. Schwade, and R.C. Eberhart, *Protein-loaded bioresorbable fibers and expandable stents: Mechanical properties and protein release.* Journal of Biomedical Materials Research Part B-Applied Biomaterials, 2004. **69B**(1): p. 1-10.
80. Alexis, F., et al., *In vitro study of release mechanisms of paclitaxel and rapamycin from drug-incorporated biodegradable stent matrices.* Journal of Controlled Release, 2004. **98**(1): p. 67-74.
81. Prabhu, S. and S. Hossainy, *Modeling of degradation and drug release from a biodegradable stent coating.* Journal of Biomedical Materials Research Part A, 2007. **80**(3): p. 732-41.
82. Mehilli, J., et al., *Randomized trial of three rapamycin-eluting stents with different coating strategies for the reduction of coronary restenosis.* European Heart Journal, 2008. **29**(16): p. 1975-1982.
83. Finkelstein, A., et al., *Local drug delivery via a coronary stent with programmable release pharmacokinetics.* Circulation, 2003. **107**(5): p. 777-84.
84. Stoeckel, D., C. Bonsignore, and S. Duda, *A survey of stent designs.* Minimally Invasive Therapy & Allied Technologies, 2002. **11**(4): p. 137-147.
85. Sallach, R.E., et al., *Long-term biostability of self-assembling protein polymers in the absence of covalent crosslinking.* Biomaterials, 2010. **31**(4): p. 779-91.
86. Yaszemski, M.J., in *Tissue engineering and novel delivery systems*. 1997.
87. Sallach, R.E., et al., *Elastin-mimetic protein polymers capable of physical and chemical crosslinking.* Biomaterials, 2009. **30**(3): p. 409-422.
88. Stack, R.S. and R.M.e.a. Califf, *Interventional cardiac catherization at duke medical center: new interventional technology.* Am J Cardiol, 1988. **2 F**: p. 3F-24F.
89. Tamai, H., et al., *Initial and 6-month results of biodegradable poly-l-lactic acid coronary stents in humans.* Circulation, 2000. **102**(4): p. 399-404.
90. Chen, M.-C., et al., *Mechanical properties, drug eluting characteristics and in vivo performance of a genipin-crosslinked chitosan polymeric stent.* Biomaterials, 2009. **30**(29): p. 5560-5571.
91. Ormiston, J.A. and P.W. Serruys, *Bioabsorbable coronary stents.* Circ Cardiovasc Interv, 2009. **2**(3): p. 255-60.
92. Tanimoto, S., et al., *Late stent recoil of the bioabsorbable everolimus-eluting coronary stent and its relationship with plaque morphology.* J Am Coll Cardiol, 2008. **52**(20): p. 1616-20.
93. Chen, M.C., et al., *Rapidly self-expandable polymeric stents with a shape-memory property.* Biomacromolecules, 2007. **8**(9): p. 2774-80.
94. Yong Chae, J., S. Hyang Hwa, and C. Jae Whan, *Water-Responsive Shape Memory Polyurethane Block Copolymer Modified with Polyhedral Oligomeric Silsesquioxane.* Journal of Macromolecular Science: Physics, 2006. **45**(4): p. 453-461.
95. Grenacher, L., et al., *In vitro comparison of self-expanding versus balloon-expandable stents in a human ex vivo model.* Cardiovascular and Interventional Radiology, 2006. **29**(2): p. 249-254.
96. W. SCHMIDT1, R.A., P. BEHRENS1, K.-P. SCHMITZ1, *Comparison of mechanical properties of peripheral self-expanding Nitinol and balloon-expandable stainless-steel stents*, in *Electronic Poster at the Annual Meeting and Postgraduate Course of the Cardiovascular and Interventional*.

97. Su, S.H., et al., *Expandable bioresorbable endovascular stent. I. Fabrication and properties.* Annals of Biomedical Engineering, 2003. **31**(6): p. 667-677.
98. Tan, L.P., et al., *Collapse pressures of bilayered biodegradable stents.* J Biomed Mater Res B Appl Biomater, 2006. **79**(1): p. 102-7.
99. Rieu, R., et al., *Radial force of coronary stents: A comparative analysis.* Catheterization and Cardiovascular Interventions, 1999. **46**(3): p. 380-391.
100. Grabow, N., et al., *Mechanical Properties of a Biodegradable Balloon-expandable Stent From Poly(L-lactide) for Peripheral Vascular Applications.* Journal of Medical Devices, 2007. **1**(1): p. 84-88.
101. Timmins, L.H., et al., *Effects of Stent Design and Atherosclerotic Plaque Composition an Arterial Wall Biomechanics.* Journal of Endovascular Therapy, 2008. **15**(6): p. 643-654.
102. Nagapudi, K., et al., *Protein-based thermoplastic elastomers.* Macromolecules, 2005. **38**(2): p. 345-354.
103. Kathuria, Y.P., *Biocompatible metallic stent for medical therapy.* Window on the Laser Medicine World, 2003. **5287**: p. 52-61180.
104. Aguilar, C.A., et al., *Direct micro-patterning of biodegradable polymers using ultraviolet and femtosecond lasers.* Biomaterials, 2005. **26**(36): p. 7642-7649.
105. Li, M., et al., *Nanostructuring in submicron-level waveguides with femtosecond laser pulses.* Optics Communications, 2002. **212**(1-3): p. 159-163.
106. Li, C.D., S. Nikumb, and F. Wong, *An optimal process of femtosecond laser cutting of NiTi shape memory alloy for fabrication of miniature devices.* Optics and Lasers in Engineering, 2006. **44**(10): p. 1078-1087.
107. Heublein, B., et al., *Biocorrosion of magnesium alloys: a new principle in cardiovascular implant technology?* Heart, 2003. **89**(6): p. 651-6.
108. Xia, M. and Y.L. Tu, *An investigation of femtosecond laser micromachining.* 2005 International Conference on MEMS, NANO and Smart Systems, Proceedings, 2005: p. 296-300479.
109. Grabow, N., et al., *A biodegradable slotted tube stent based on poly(L-lactide) and poly(4-hydroxybutyrate) for rapid balloon-expansion.* Ann Biomed Eng, 2007. **35**(12): p. 2031-8.
110. Grabow, N., et al., *Mechanical properties of laser cut poly(L-lactide) micro-specimens: implications for stent design, manufacture, and sterilization.* J Biomech Eng, 2005. **127**(1): p. 25-31.
111. Lootz, D., et al., *Laser cutting: influence on morphological and physicochemical properties of polyhydroxybutyrate.* Biomaterials, 2001. **22**(18): p. 2447-52.
112. Tonshoff, H.K., et al., *Micro-machining using femtosecond lasers.* 1St International Symposium on Laser Precision Microfabrication, 2000. **4088**: p. 136-139410.
113. Kathuria, Y.P., *Laser microprocessing of metallic stent for medical therapy.* Journal of Materials Processing Technology, 2005. **170**(3): p. 545-550.
114. Takahata, K. and Y.B. Gianchandani, *A planar approach for manufacturing cardiac stents: Design, fabrication, and mechanical evaluation.* Journal of Microelectromechanical Systems, 2004. **13**(6): p. 933-939.
115. Takahata, K., Y.B. Gianchandani, and K.D. Wise, *Micromachined antenna stents and cuffs for monitoring intraluminal pressure and flow.* Journal of Microelectromechanical Systems, 2006. **15**(5): p. 1289-1298.
116. *SMST-2000: proceedings of the International Conference on Shape Memory and Superelastic Technologies*. in *Shape Memory and Superelastic Technologies*. 2000. Pacific Grove, California, USA: SMST, The International Organization on Shape Memory and superelastic Technology.

117. Craig, C.H., et al., *Development of a platinum-enhanced radiopaque stainless steel (PERSS (R))(7).* Stainless Steels for Medical and Surgical Applications, 2003. **1438**: p. 28-38 276.

118. Kuribayashi, K., et al., *Self-deployable origami stent grafts as a biomedical application of Ni-rich TiNi shape memory alloy foil.* Materials Science and Engineering a-Structural Materials Properties Microstructure and Processing, 2006. **419**(1-2): p. 131-137.
119. de Miranda, R.L., C. Zamponi, and E. Quandt, *Fabrication of TiNi thin film stents.* Smart Materials & Structures, 2009. **18**(10): p. -.
120. Rumpf, H., et al., *Near net-shape fabrication of superelastic NiTi devices by sputtering and photoetching.* Materials Transactions, 2006. **47**(3): p. 523-526.
121. Tolken, S., *Firms Investing in angio-plastics solution.* Plastics News, 2005. **16**(46).
122. Park, J.H., et al., *Micromachined biodegradable microstructures.* Mems-03: Ieee the Sixteenth Annual International Conference on Micro Electro Mechanical Systems, 2003: p. 371-374 711.

123. Armani, D.K. and C. Liu, *Mircofabrication technology for polycaprolactone, a biodegradable polymer.* Journal of Micromechanics and Microengineering, 2000. **10**(1): p. 80-84.
124. Lafont, A., et al., *PLA stereocopolymers as sources of bioresorbable stents: Preliminary investigation in rabbit.* Journal of Biomedical Materials Research Part B-Applied Biomaterials, 2006. **77B**(2): p. 349-356.
125. Grayson, A.C.R., et al., *Multi-pulse drug delivery from a resorbable polymeric microchip device.* Nature Materials, 2003. **2**(11): p. 767-772.
126. Ryu, W., et al., *Microfabrication technology of biodegradable polymers for interconnecting microstructures.* Journal of Microelectromechanical Systems, 2006. **15**(6): p. 1457-1465.
127. Chen, M.C., et al., *Mechanical properties, drug eluting characteristics and in vivo performance of a genipin-crosslinked chitosan polymeric stent.* Biomaterials, 2009. **30**(29): p. 5560-5571.
128. Yamada, A., F. Niikura, and K. Ikuta, *A three-dimensional microfabrication system for biodegradable polymers with high resolution and biocompatibility.* Journal of Micromechanics and Microengineering, 2008. **18**(2): p. -.
129. Han, D.W., et al., *Development of epigallocatechin gallate-eluting polymeric stent and its physicochemical, biomechanical and biological evaluations.* Biomedical Materials, 2009. **4**(4).
130. Vogt, F., et al., *Long-term assessment of a novel biodegradable paclitaxel-eluting coronary polylactide stent.* European Heart Journal, 2004. **25**(15): p. 1330-1340.
131. Blindt, R., et al., *Development of a new biodegradable intravascular polymer stent with simultaneous incorporation of bioactive substances.* International Journal of Artificial Organs, 1999. **22**(12): p. 843-853.
132. Vogel, A. and V. Venugopalan, *Mechanisms of pulsed laser ablation of biological tissues.* Chem Rev, 2003. **103**(2): p. 577-644.
133. Doi, K., Y. Nakayama, and T. Matsuda, *Novel compliant and tissue-permeable microporous polyurethane vascular prosthesis fabricated using an excimer laser ablation technique.* J Biomed Mater Res, 1996. **31**(1): p. 27-33.
134. Rajaraman, S., et al., *Microfabrication technologies for a coupled three-dimensional microelectrode, microfluidic array.* Journal of Micromechanics and Microengineering, 2007. **17**(1): p. 163-171.
135. Reiersen, H. and A.R. Rees, *Trifluoroethanol may form a solvent matrix for assisted hydrophobic interactions between peptide side chains.* Protein Engineering, 2000. **13**(11): p. 739-743.
136. Roccatano, D., et al., *Mechanism by which 2,2,2-trifluoroethanol/water mixtures stabilize secondary-structure formation in peptides: A molecular dynamics study.* Proceedings of the National Academy of Sciences of the United States of America, 2002. **99**(19): p. 12179-12184.

137. Strawhecker, K.E., et al., *The critical role of solvent evaporation on the roughness of spin-cast polymer films.* Macromolecules, 2001. **34**(14): p. 4669-4672.
138. Virmani, R., et al., *Localized Hypersensitivity and Late Coronary Thrombosis Secondary to a Sirolimus-Eluting Stent.* Circulation, 2004. **109**(6): p. 701-705.
139. Yao, C.-H., et al., *Preparation of networks of gelatin and genipin as degradable biomaterials.* Materials Chemistry and Physics, 2004. **83**(2-3): p. 204-208.
140. Butler, M.F., Y.F. Ng, and P.D.A. Pudney, *Mechanism and kinetics of the crosslinking reaction between biopolymers containing primary amine groups and genipin.* Journal of Polymer Science Part a-Polymer Chemistry, 2003. **41**(24): p. 3941-3953.
141. K . Inam Park , J.U.C., and H . Aesun Park *Chapter 10. Superporous Hydrogel CompositesA New Generation of Hydrogels with Fast Swelling Kinetics,High Swelling Ratio and*, in *Polymeric Drugs and Drug Delivery Systems*, R.M.O.a.S.W. Kim, Editor. 2000, CRC Press.
142. Chang, W.H., et al., *A genipin-crosslinked gelatin membrane as wound-dressing material: in vitro and in vivo studies.* Journal of Biomaterials Science-Polymer Edition, 2003. **14**(5): p. 481-495.
143. Carew, E.O., J.E. Barber, and I. Vesely, *Role of Preconditioning and Recovery Time in Repeated Testing of Aortic Valve Tissues: Validation Through Quasilinear Viscoelastic Theory.* Annals of Biomedical Engineering, 2000. **28**(9): p. 1093-1100.
144. Humphrey, J.D., *Cardiovascular solid mechanics: cells, tissues, and organs*. 2002: Springer.
145. Gosline, J., et al., *Elastic proteins: biological roles and mechanical properties.* Philosophical Transactions of the Royal Society of London Series B-Biological Sciences, 2002. **357**(1418): p. 121-132.
146. Lillie, M.A. and J.M. Gosline, *THE EFFECTS OF HYDRATION ON THE DYNAMIC MECHANICAL-PROPERTIES OF ELASTIN.* Biopolymers, 1990. **29**(8-9): p. 1147-1160.
147. Li, B., et al., *Hydrophobic hydration is an important source of elasticity in elastin-based biopolymers.* Journal of the American Chemical Society, 2001. **123**(48): p. 11991-11998.
148. Nicolas, F.L. and C.H. Gagnieu, *Denatured thiolated collagen .2. Cross-linking by oxidation.* Biomaterials, 1997. **18**(11): p. 815-821.
149. Thakur, G., et al., *Crosslinking of gelatin-based drug carriers by genipin induces changes in drug kinetic profiles in vitro.* Journal of Materials Science-Materials in Medicine, 2011. **22**(1): p. 115-123.
150. Nicolas, F.L. and C.H. Gagnieu, *Denatured thiolated collagen .1. Synthesis and characterization.* Biomaterials, 1997. **18**(11): p. 807-813.
151. Ormiston, J.A., et al., *A bioabsorbable everolimus-eluting coronary stent system for patients with single de-novo coronary artery lesions (ABSORB): a prospective open-label trial.* Lancet, 2008. **371**(9616): p. 899-907.
152. Simamora, P., J.M. Alvarez, and S.H. Yalkowsky, *Solubilization of rapamycin.* International Journal of Pharmaceutics, 2001. **213**(1-2): p. 25-29.
153. Balakrishnan, B., et al., *Intravascular drug release kinetics dictate arterial drug deposition, retention, and distribution.* Journal of Controlled Release, 2007. **123**(2): p. 100-108.
154. Edelman, E.R. and C. Rogers, *Pathobiologic responses to stenting.* Am J Cardiol, 1998. **81**(7A): p. 4E-6E.
155. Kamath, K.R., J.J. Barry, and K.M. Miller, *The Taxus (TM) drug-eluting stent: A new paradigm in controlled drug delivery.* Advanced Drug Delivery Reviews, 2006. **58**(3): p. 412-436.
156. Canal, T. and N.A. Peppas, *CORRELATION BETWEEN MESH SIZE AND EQUILIBRIUM DEGREE OF SWELLING OF POLYMERIC NETWORKS.* Journal of Biomedical Materials Research, 1989. **23**(10): p. 1183-1193.

157. Ganguly, S. and A.K. Dash, *A novel in situ gel for sustained drug delivery and targeting.* International Journal of Pharmaceutics, 2004. **276**(1-2): p. 83-92.
158. Fan, H.Y. and A.K. Dash, *Effect of cross-linking on the in vitro release kinetics of doxorubicin from gelatin un-plants.* International Journal of Pharmaceutics, 2001. **213**(1-2): p. 103-116.
159. Young, S., et al., *Gelatin as a delivery vehicle for the controlled release of bioactive molecules.* Journal of Controlled Release, 2005. **109**(1-3): p. 256-274.
160. Zhao, P., et al., *Biodegradable fibrous scaffolds composed of gelatin coated poly(ϵ-caprolactone) prepared by coaxial electrospinning.* Journal of Biomedical Materials Research Part A, 2007. **83A**(2): p. 372-382.
161. Peppas, N.A., et al., *Hydrogels in pharmaceutical formulations.* European Journal of Pharmaceutics and Biopharmaceutics, 2000. **50**(1): p. 27-46.
162. Ravi, S., *RECOMBINANT ELASTIN ANALOGS AS CELL-ADHESIVE MATRICES*, in *Biomedical Engineering*. 2010, Georgi Institute of Technology: Atlanta, GA.
163. Discher, D.E., P. Janmey, and Y.-l. Wang, *Tissue Cells Feel and Respond to the Stiffness of Their Substrate.* Science, 2005. **310**(5751): p. 1139-1143.
164. Xi-xun, Y., et al., *In vitro study in the endothelial cell compatibility and endothelialization of genipin-crosslinked biological tissues for tissue-engineered vascular scaffolds.* J Mater Sci Mater Med, 2010. **21**(2): p. 777-85.
165. Sung, H.W., et al., *Stability of a biological tissue fixed with a naturally occurring crosslinking agent (genipin).* J Biomed Mater Res, 2001. **55**(4): p. 538-46.
166. Tsai, C.L., S.H. Hsu Sh, and W.L. Cheng, *Effect of different solvents and crosslinkers on cytocompatibility of Type II collagen scaffolds for chondrocyte seeding.* Artif Organs, 2002. **26**(1): p. 18-26.
167. Kantor, B., et al., *The experimental animal models for assessing treatment of restenosis.* Cardiovascular Radiation Medicine, 1999. **1**(1): p. 48-54.
168. Langeveld, B. and A.J.M. Roks, *Rat restenosis models: Means for thorough restenosis research.* Journal of Endovascular Therapy, 2005. **12**(3): p. 343-345.
169. Langeveld, B., et al., *Rat abdominal aorta stenting: A new and reliable small animal model for in-stent restenosis.* Journal of Vascular Research, 2004. **41**(5): p. 377-386.
170. Aziz, S., et al., *Stent expansion: a combination of delivery balloon underexpansion and acute stent recoil reduces predicted stent diameter irrespective of reference vessel size.* Heart, 2007. **93**(12): p. 1562-1566.
171. Schmitz, K.-P.S., W. Behrens, P. Behrend, D. Lootz, D. Graf, B. , *In-Vitro Examination of Clinically Relevant Stent Parameters.* PROGRESS IN BIOMEDICAL RESEARCH, 2000. **5**(3): p. 197-203
172. Stoeckel, D., A. Pelton, and T. Duerig, *Self-expanding nitinol stents: material and design considerations.* Eur Radiol, 2004. **14**(2): p. 292-301.
173. Finn, A.V., et al., *Pathological Correlates of Late Drug-Eluting Stent Thrombosis.* Circulation, 2007. **115**(18): p. 2435-2441.
174. Urry DW, N.A., Gowda DC, Hoban LD, McKee A, and O.D. Williams T, Cox BA, *Medical Applications of bioelastic materials*, in *Biotechnological polymers: medical, pharmaceutical, and industrial applications*, C.G. Gebelein, Editor. 1993, Technomic Pub.
175. Panitch, A., et al., *Design and biosynthesis of elastin-like artificial extracellular matrix proteins containing periodically spaced fibronectin CS5 domains.* Macromolecules, 1999. **32**(5): p. 1701-1703.
176. Lowe, H.C., C.N. Chesterman, and L.M. Khachigian, *Rat aortic stenting: toward a simple model of in-stent restenosis.* The American journal of cardiology, 2001. **88**(6): p. 720-721.
177. Onuta, G., et al., *Long-Term Type 1 Diabetes Enhances In-Stent Restenosis after Aortic Stenting in Diabetes-Prone BB Rats.* Journal of Biomedicine & Biotechnology, 2011: p. Article No.: 396734.

178. Ma, X., et al., *Paclitaxel/sirolimus combination coated drug-eluting stent: In vitro and in vivo drug release studies.* Journal of Pharmaceutical and Biomedical Analysis, 2011. **54**(4): p. 807-811.
179. Deuse, T., et al., *Introducing the first polymer-free leflunomide eluting stent.* Atherosclerosis, 2008. **200**(1): p. 126-134.
180. Deuse, T., et al., *Imaging In-Stent Restenosis: An Inexpensive, Reliable, and Rapid Preclinical Model.* J Vis Exp, 2009(31): p. e1346.
181. Onuta, G., et al., *Long-term type 1 diabetes enhances in-stent restenosis after aortic stenting in diabetes-prone BB rats.* J Biomed Biotechnol, 2011. **2011**: p. 396734.
182. Langeveld, B., W.H. Van Gilst, and F. Zijlstra, *A simple, inexpensive, rapid, and accurate preclinical model for in-stent restenosis.* J Am Coll Cardiol, 2005. **45**(8): p. 1310-.
183. Finn, A.V., et al., *A novel rat model of carotid artery stenting for the understanding of restenosis in metabolic diseases.* J Vasc Res, 2002. **39**(5): p. 414-25.
184. Lowe, H.C., B. James, and L.M. Khachigian, *A novel model of in-stent restenosis: rat aortic stenting.* Heart, 2005. **91**(3): p. 393-5.
185. Kwon, J.S., et al., *Comparison of bare metal stent and paclitaxel-eluting stent using a novel rat aorta stent model.* J Vet Sci, 2011. **12**(2): p. 143-149.
186. Oyamada, S., et al., *Trans-Iliac Rat Aorta Stenting: A Novel High Throughput Preclinical Stent Model for Restenosis and Thrombosis.* Journal of Surgical Research, 2011. **166**(1): p. e91-e95.